

INFILTRATION UNDER TWO CONTRASTING HYDROLOGIC SCENARIOS IN  
TEXAS

A Thesis

by

SURAJIT DASGUPTA

Submitted to the Office of Graduate Studies of  
Texas A&M University  
in partial fulfillment of the requirements for the degree of

MASTER OF SCIENCE

May 2005

Major Subject: Rangeland Ecology and Management

INFILTRATION UNDER TWO CONTRASTING HYDROLOGIC SCENARIOS IN  
TEXAS

A Thesis

by

SURAJIT DASGUPTA

Submitted to Texas A&M University  
in partial fulfillment of the requirements  
for the degree of

MASTER OF SCIENCE

Approved as to style and content by:

---

Binayak P Mohanty  
(Chair of Committee)

---

Bradford Wilcox  
(Member)

---

Kevin McInnes  
(Member)

---

Steve Whisenent  
(Head of Department)

May 2005

Major Subject: Rangeland Ecology and Management

## ABSTRACT

Infiltration under Two Contrasting Hydrologic Scenarios in Texas.

(May 2005)

Surajit Dasgupta, B.E., Kuvempu University

Chair of Advisory Committee: Dr. Binayak P Mohanty

Investigation of infiltration provides insights about the flow of water and transport of contaminants through the vadose zone. Infiltration is governed by prevailing environmental conditions like soil characteristics, plant cover and geologic settings. The main objective was to study preferential flow dominated infiltration at two contrasting hydrologic settings in Texas. For the first study, artificial rainfall was simulated within a plot covered with juniper trees at a karst region of the Edwards Plateau and sub-surface flow was monitored using TDR probes. Sub-surface flow was simulated using HYDRUS-2D. Results demonstrated that sub-surface flow occurred in a tri-modal manner, consisting of flow in karst conduits, planar fractures in the limestone, and soil matrix. Both fracture and matrix flow responses increased with increase in rainfall intensity. During large rainfall events, water exchange was observed between the fractures and matrix. Dye studies indicated that fractures and juniper roots were primary pathways for preferential flow occurring within the plot. The model simulated flow characteristics like exchange processes and differentiated between preferential and conduit flow besides determining approximate van Genuchten parameters for each geologic unit.

For the second study, tension infiltrometers were used to conduct infiltration experiments at six soil water pressures ( $\Psi = -0.2$  to  $0$  m) in an agricultural field near College Station over a 21 month period. The aim was to determine steady infiltration rate,  $i_f$ , saturated hydraulic conductivity,  $K_{sat}$ , unsaturated hydraulic conductivity,  $K(\Psi)$  and unsaturated flux density  $\Phi(\Psi)$ . Moreover, the effect of varying disc diameters on steady state infiltration rates ( $i_f$ ) was also studied. Results demonstrated that infiltration occurred in a bi-modal fashion consisting of preferential flow and matrix flow. Macropores and roots present in the soil resulted in gravity dominated flow at  $\Psi = -0.05$  to  $0$  m for all experiments. Statistical analysis suggested that the soil did not exhibit spatial variability within the plot and the five different disc diameters had no effect on  $i_f$ . Statistically significant differences in  $i_f$  were observed between  $0.2$  and  $0.24$  m disc diameters at saturation over the 21 month period. The  $i_f$  values illustrated strong temporal variations based on natural conditions over the 21 month period.

To my parents, whose love, blessings and support have been a constant motivation for my work throughout my life.

## ACKNOWLEDGEMENTS

I would like to take this opportunity to thank each and everyone who has had an immense contribution in my work.

I would like to extend my gratitude to my guide and mentor, Dr. Binayak P. Mohanty for all of his suggestions and advice. He was always present to support me throughout my tenure as a student. A special note of thanks goes out to Dr. Maximilian J. Köhne whose invaluable support has enabled me to complete my studies at Texas A&M. His guidance and advice has played a vital role in my research work. I would also like to thank Dr. Bradford Wilcox and Dr. Kevin McInnes for their guidance and support during my research work and their help for conducting the field experiments. Furthermore, Dr. Clyde Munster and Dr. Keith Owens have also been very helpful with their suggestions and guidance for the studies conducted at Honey Creek. I would also like to thank Andrew Weichert, Philip Traucer, Gary Nolan, Lucas Gregory, Shane Porter and Josh Sorensen for their help in conducting the rainfall experiments at Honey Creek. I would like to acknowledge the assistance I received from Xavier Maillard and Narendra Das in conducting the tension infiltration experiments. Special thanks to Shibani Datta for her love and encouragement throughout my student life at Texas A&M University. Lastly, I would like to express my appreciation and gratefulness to my parents and my sister without whom, I would not have been able to accomplish my studies.

## TABLE OF CONTENTS

	Page
ABSTRACT .....	iii
DEDICATION .....	v
ACKNOWLEDGEMENTS .....	vi
TABLE OF CONTENTS .....	vii
LIST OF TABLES .....	ix
LIST OF FIGURES.....	x
CHAPTER	
I    GENERAL INTRODUCTION .....	1
II   SUB-SURFACE FLOW PROCESSES IN A JUNIPER PLOT IN A KARST REGION OF THE EDWARDS PLATEAU..	3
Introduction .....	4
Geographic and hydro-geologic characteristics of site	8
Rainfall simulation and data collection.....	15
Data analysis .....	22
Modeling assumptions.....	22
Results .....	30
Discussions.....	47
Conclusions .....	49
III  SOIL HYDRAULIC PROPERTIES AND THEIR SPATIO- TEMPORAL VARIATIONS IN TEXAS VERTISOLS .....	52
Introduction .....	53
Site description and methodology .....	56
Data analysis .....	62
Results and discussions .....	67
Conclusions .....	81

CHAPTER	Page
IV GENERAL CONCLUSIONS .....	83
REFERENCES .....	85
APPENDIX	
A TDR RESPONSES FOR VARIOUS SIMULATIONS .....	90
B WATER BALANCE CALCULATIONS USING MODEL.	99
VITA .....	101



## LIST OF TABLES

TABLE	Page
II-1 Spatial locations of the TDR probes before and after the adjustments were made. ‘Unit’ indicates the layer in which the probes were located and ‘Depth’ indicates the depth of each probe from the top surface of the trench face.....	17
II-2 Details of various simulations carried out at the plot. Each simulation contained a succession of runs with gaps in between. The average intensity and total rainfall amount for each simulation were calculated .....	18
II-3 Initial hydraulic parameters for each geologic material.....	28
II-4 First response times and average response times for all TDR probes for each simulation event.....	38
II-5 Final van Genuchten parameters for different geologic units for model domain with fractures.....	47
III-1 Details of infiltration experiments over 21 month period.....	62
III-2 Results of one way analysis of variance (ANOVA) test for comparing the means of Log $i_f$ values between four sites within the plot. Each soil water pressure range has been classified as a separate group for the comparison. ‘df’ denotes degrees of freedom, ‘F’ denotes the statistic value and ‘Sig’ denotes the significance ‘p’ value for the test for $\alpha=0.5$ .....	70
III-3 Results of one way analysis of variance (ANOVA) test for comparing the means of Log $i_f$ values between varying disc diameters within the plot. Each soil water pressure range has been classified as a separate group for the comparison. ( $\alpha = 0.5$ ) .....	71
III-4 Results of one way analysis of variance (ANOVA) test for comparing the means of $i_f$ values between 0.2 and 0.24 m disc diameters. Each soil water pressure range has been classified as a separate group .....	73
III-5 Soil hydraulic parameters of five different infiltration disc diameters at six soil water pressures during the 12 day period .....	80

## LIST OF FIGURES

FIGURE	Page
II-1 The study area was the Honey Creek State Natural Area located in Comal County TX. Also shown are the various hydrologic zones of the Edwards aquifer .....	9
II-2 Honey creek experimental plot with spatial locations of juniper trees, rainfall simulator masts and the trench. Application bands of three dyes during dye-tracer studies are also illustrated in the layout.....	10
II-3 Schematic sketch of trench cross section illustrating the stratification of the trench face; (a) illustrates the older TDR probe locations (October to mid-December, 2003) and (b) illustrates the newer ones (mid-December, 2003 to May, 2004) .....	12
II-4 Photograph showing cross-section of trench face beside the plot.....	13
II-5 Dye sampling points within the trench face .....	21
II-6 Two-dimensional model profile with fractures. The lower limestone unit and the Marl layer were assumed to have similar hydraulic characteristics. The upper limestone unit has the highest density of conduits followed by the lower limestone unit. This differentiates between the two based on the actual fracture density observed at the trench face. The marl layer does not have any conduit as we did not observe any fractures in this layer at the trench .....	25
II-7 Two-dimensional model profile without fracture network. One observation node has been placed in each material type.....	27
II-8 The response time for the first onset of outflow from various sampling locations at the trench face. Refer to Fig. II-4 for spatial locations of the sampling points. The sampling locations are arranged by increasing depth; for Run 15 and 17, C2 was the upper most point at the trench and A1 was the lowermost point and for Run 16 and 18, B4 was the uppermost point and A1 the lowermost. Run 15 and 17 were low intensity long duration events while Run 16 and 18 were high intensity long duration events.....	31

FIGURE	Page
II-9 Response time of dyes at various sampling points within the trench face for the second dye-tracer test. Numbers beside the bars indicate peak concentration times as registered by the Spectrofluoro-photometer. (Red indicates the times for Phloxin B and blue indicates that of Eosin.....	33
II-10 Relationship between response time and boundary conditions ((a) total rainfall and (b) rainfall intensity) .....	34
II-11 Relationship between rainfall intensity and initial moisture content with first response times for various TDR probes during different simulations .....	35
II-12 Relationship between total sub-surface flow and (a) rainfall intensity and (b) total rainfall from various rainfall simulations .....	39
II-13 Simulated sub-surface flow at different times for domain with fracture network .....	40
II-14 Simulated sub-surface flow at different times for domain without fracture network .....	41
II-15 Water flux at seepage face for (a) domain with fractures and (b) domain without fractures .....	44
II-16 Water flux at the bottom boundary for (a) domain with fractures and (b) domain without fractures .....	45
II-17 Measured and simulated flow responses for first dye-tracer test for a 7 hour period for a domain with fractures. The table provided below the graph lists each observation and their corresponding sensor numbers node used when the model was run in inverse mode .....	46
III-1 Location of experimental plot near College Station, TX.....	57
III-2 Vegetation and surface cracks in soil within the experimental plot .	58
III-3 Infiltration disc placed on the soil. A thin layer of contact sand was applied for good contact between the disc and soil. The disc was surrounded by a metal disc to prevent any lateral flow.....	60

FIGURE	Page
III-4 The 20 m x 16 m experimental plot divided into four (7 m x 5 m) sites with 2 m spacings from all sides. The circles in each site denote the different infiltration disc diameters used for the experiments. A typical experimental layout for May 2003 is illustrated .....	61
III-5 Flow chart adapted for running the one way analysis of variance (ANOVA) test .....	66
III-6 Box plots of steady state infiltration rates ( $i_f$ ) at different pressures for varying disc diameters .....	68
III-7 Temporal variability of $i_f$ [ $\text{ms}^{-1}$ ] and antecedent moisture content $\theta$ at varying pressures	74
III-8 Statistical correlation between $i_f$ and $\theta$ at $\Psi = -0.2, -0.15, -0.1$ and $-0.02$ m .....	75
III-9 Temporal variability of $i_f$ and $\theta$ at saturation for 0.2 and 0.24 m disc diameters .....	77
III-10 Statistical correlation between $i_f$ and $\theta$ at saturation for 0.2 and 0.24 m disc diameters .....	78

## CHAPTER I

### GENERAL INTRODUCTION

Infiltration plays a vital role in the determination of the water balance of a particular area. The laminar flow of water in a saturated media is defined by Darcy's law and that in an unsaturated media is defined by Richard's equation. It is a well established fact that the infiltration of water in the vadose zone is enhanced by preferential flow (Logsdon and Jaynes, 1996; Mohanty et al., 1997, 1998, Shouse and Mohanty, 1998). Preferential flow refers to the rapid movement of water through soils. This type of flow usually bypasses the soil matrix, which increases the chances of groundwater and surface water contamination (DiCarlo et al., 1999). Preferential flow usually occurs through macropores which might be created by three main reasons; biological activities (worm-holes and root decay), agricultural activities and natural phenomena like erosion or fractured rocks. Thus, the process of infiltration of water through the soil is strongly influenced by the natural/environmental conditions.

This study investigates the process of infiltration at two contrasting hydrologic settings in Texas. The first study deals with the sub-surface flow processes occurring in a karst environment dominated by juniper trees on the Edwards Plateau, TX. It essentially addresses the eco-hydrologic and geo-hydrologic impacts on the process of infiltration. The second study is based on the determination of soil hydraulic parameters and their

---

This thesis follows the style of Vadose Zone Journal.

spatial and temporal variations within an agricultural field in the floodplains of the Brazos River near College Station, TX. In this case, it is the spatio-temporal variations of the soil hydraulic parameters influenced by macropore flow, that affect the infiltration process. The overall goal is to compare and contrast the processes that govern the infiltration of water at such varying hydrologic and eco-hydrologic settings.

## CHAPTER II

### SUB-SURFACE FLOW PROCESSES UNDER A JUNIPER PLOT IN A KARST REGION OF THE EDWARDS PLATEAU

The impacts of juniper trees on the water cycle at the Edwards plateau with karst geology have been the focus of active research for several years. The objective of this paper is to gain a comprehensive insight about the sub-surface flow processes occurring at a site on the Edwards Plateau (Honey Creek) containing juniper trees. A 2.3 m deep trench was excavated at the downslope end of the plot and TDR probes were installed at various locations within the trench face to measure volumetric water contents. A rainfall simulator consisting of 6 individual (15 m high) telescopic masts was set up to provide artificial rainfall on the plot. Six rainfall simulations (with different intensities and durations) and two dye-tracer tests were conducted on the plot during a 7 month period. Sub-surface interflow was visually inspected at various locations on the trench face and monitored by TDR probes. The total volume of sub-surface flow was also recorded after each rainfall simulation. A variably-saturated flow model HYDRUS-2D was used to simulate the sub-surface flow processes occurring within the plot. The results demonstrated that sub-surface flow occurred in a tri-modal manner, consisting of flow in karst conduits, planar fractures in the limestone, and soil matrix. Preferential flow at the trench increased with increase in rainfall. Matrix flow response time decreased with high rainfall and low initial moisture content. During large rainfall events, water exchange was observed between the fractures and matrix which was absent during smaller rainfall

events. The dye studies indicated that fractures and juniper roots are primary pathways for preferential flow occurring within the plot. The HYDRUS-2D model simulated the exchange processes and differentiated between conduit and preferential flow. It also provided approximate van Genuchten parameters for each geologic unit within the trench face. The incorporation of fracture/root network within the model domain enhanced conduit flow as observed in the field when compared to a domain with limestone without fractures.

### **Introduction**

Nearly 20% of the United States is underlain by karst aquifers and 40% of the groundwater that is used for drinking purposes comes from karst aquifers (USEPA, 1998). The Edwards Aquifer as part of the Edwards Plateau is a karst aquifer system that covers a distance of 265 kilometers across South-central Texas. The Edwards Aquifer is the major source of water supply for 1.5 million people in San Antonio and parts of Austin. Water from this aquifer is used primarily for drinking purposes besides being used for agricultural, industrial and military purposes (Loaiciga et al., 2000). One of the primary concerns in this region is that the total (municipal + agricultural + industrial) demand for water is exceeding the rate at which water is recharged into the aquifer (Edwards Aquifer Bibliography, 2003). This poses a threat to the supply of drinking water as well as the availability of water for agricultural and industrial purposes. For achieving sustainable water resource management, it is imperative to gain a proper



understanding of the hydro-geologic and eco-hydrologic processes occurring in this region.

From the eco-hydrologic perspective, an important issue in trying to understand and predict the water budget within the Edwards region is to gain a comprehensive insight into the role played by plants in the water cycle. Ashe juniper (*Juniperus ashei*) is by far, the most dominant species of trees found within the Edwards aquifer region. This species has encroached this area in the last century and has replaced the native grass species like Indian grass, Little bluestem and Switch grass. This phenomenon may be a result of a multitude of factors including changing patterns of herbivory and fire frequencies and/or changes in climate and CO<sub>2</sub> concentrations (Archer 1994; Wilcox 2002). Review of studies/experiments, related to juniper-water interactions, indicated the existence of contradicting hypotheses. Some experiments indicated that juniper removal reduces overland flow (Richardson et al., 1979; Dugas et al., 1998) while others suggested that overland flow actually increases after junipers have been removed by burning (Wright et al., 1976). Juniper roots act as macropores and preferential flow paths for water that infiltrates the soil surface and thus increases sub-surface flow as water moves very rapidly through these preferential flow paths in both lateral and/or vertical directions (Jackson et al., 2000). In contrast, the presence of junipers lowers the infiltration capacity of the adjacent locations. Since the grass patches are absent, the capture of runoff is less and there is more free flowing water which ultimately results in higher run off rates (Wilcox et al., 2002). Junipers have a higher interception and transpiration capacity throughout the year as compared to other shrubs because they are

evergreen and have a high leaf-area density (Dugas et al., 1998). Hence, based on this concept, juniper removal would decrease the amount of water intercepted, thus increasing the availability of water for infiltration into the soil and/or surface run off. From the above mentioned studies with contrasting results, it can be concluded that the relationship between junipers and components of the water budget are complex and are not well understood. Hence, detailed experiments need to be carried out to accurately predict the effect of junipers on the water cycle.

Besides the eco-hydrology, the hydro-geologic characteristics of the underlain aquifer play a vital role in determining the hydrology of such regions. Karstic aquifers like the Edwards Aquifer are unique because unlike other aquifers, they are characterized by a three fold porosity/permeability. Pore spaces formed within the rocks by minerals, form the primary or matrix porosity, the joints and fractures produced by orogenic processes, form the secondary or fracture porosity (mm-scale) and the cavities and integrated conduits which are a characteristic feature of karst regions, form the tertiary or conduit porosity (cm to m scale) (White, 1998). Thus, a sound knowledge of the hydrology of such triple porosity/permeability media entails an understanding of the rate of recharge into the various components of the permeability and the exchange of water between these components (White, 2002). Martin et al., (2001) considered the matrix and fracture flow as laminar flow and the conduit flow as turbulent flow and mentioned that exchange of water takes place between the matrix and the fractures and vice versa in such karst media. Scanlon et al., (2003) suggested that several approaches have been adapted for modeling groundwater flow in karst systems. Some incorporated

the lumped parameter model (Barrett and Charbeneau, 1996) while others used the equivalent porous media distributed parameter models. The latter can be divided into a single continuum approach (Greene et al., 1999; Keeler and Zhang, 1997) and a double continuum approach (Teutsch, 1993). These modeling studies simulated recharge rates into the aquifer for time intervals ranging from 10 to 5000 years, which were based on watershed scales.

This study reports results of an experiment on a single plot for analyzing the sub-surface flow patterns that exist in the juniper dominated karst region. Furthermore, the flow processes occurring within a 7 hour time-scale on the plot, were simulated using a two-dimensional variably-saturated numerical flow model HYDRUS-2D (Simunek et al, 1999).

The objectives of this study are: 1. to obtain a comprehensive understanding of the nature and origin of sub-surface flow processes occurring in a juniper dominated karst plot, 2. to analyze the effects of initial and boundary conditions on the onset, rate and spatio-temporal patterns of sub-surface flow as observed in a trench beside the plot, 3. to simulate the sub-surface flow within a 4 m section of the plot with fractures using the variably-saturated flow model HYDRUS-2D and determine the hydraulic properties of each geologic unit as observed within the trench face and 4. to compare flow responses between a 4 m section with fractures and one without fractures to determine the role played by fractures in enhancing sub-surface flow processes.

A series of rainfall simulations were carried out in the plot and the sub-surface flow processes were monitored. A dye tracer study was used to assist in the

understanding of the flow mechanisms. Finally, the flow processes that were observed and recorded were simulated using the numerical flow model HYDRUS-2D.

### **Geographic and hydro-geologic characteristics of site**

The study area was located within the Honey Creek State Natural Area (29°44'N, 98°26'W) of 9 km<sup>2</sup>, which is part of the Guadalupe River State Park, located in the western part of Comal County (Fig. II-1). The climate in this region can be classified as sub-humid, subtropical with mean annual rainfall of approximately 800 mm (Kuniansky et al., 2001). The experimental plot (Fig. II-2) was rectangular with dimensions 14m x 7 m. The edges of the plot were marked with strips of aluminum sheets inserted 5 cm into the grooves made on the rocks. The soil surface was characterized by a black colored litter/organic soil layer. Ash juniper and live oak were the most dominant species around the plot along with occasional patches of cacti. Below this litter layer lay the bedrock (limestone) layer. At certain locations, the bedrock was exposed to the surface. The surface of the plot was characterized by several mild depressions of few meter-scale.

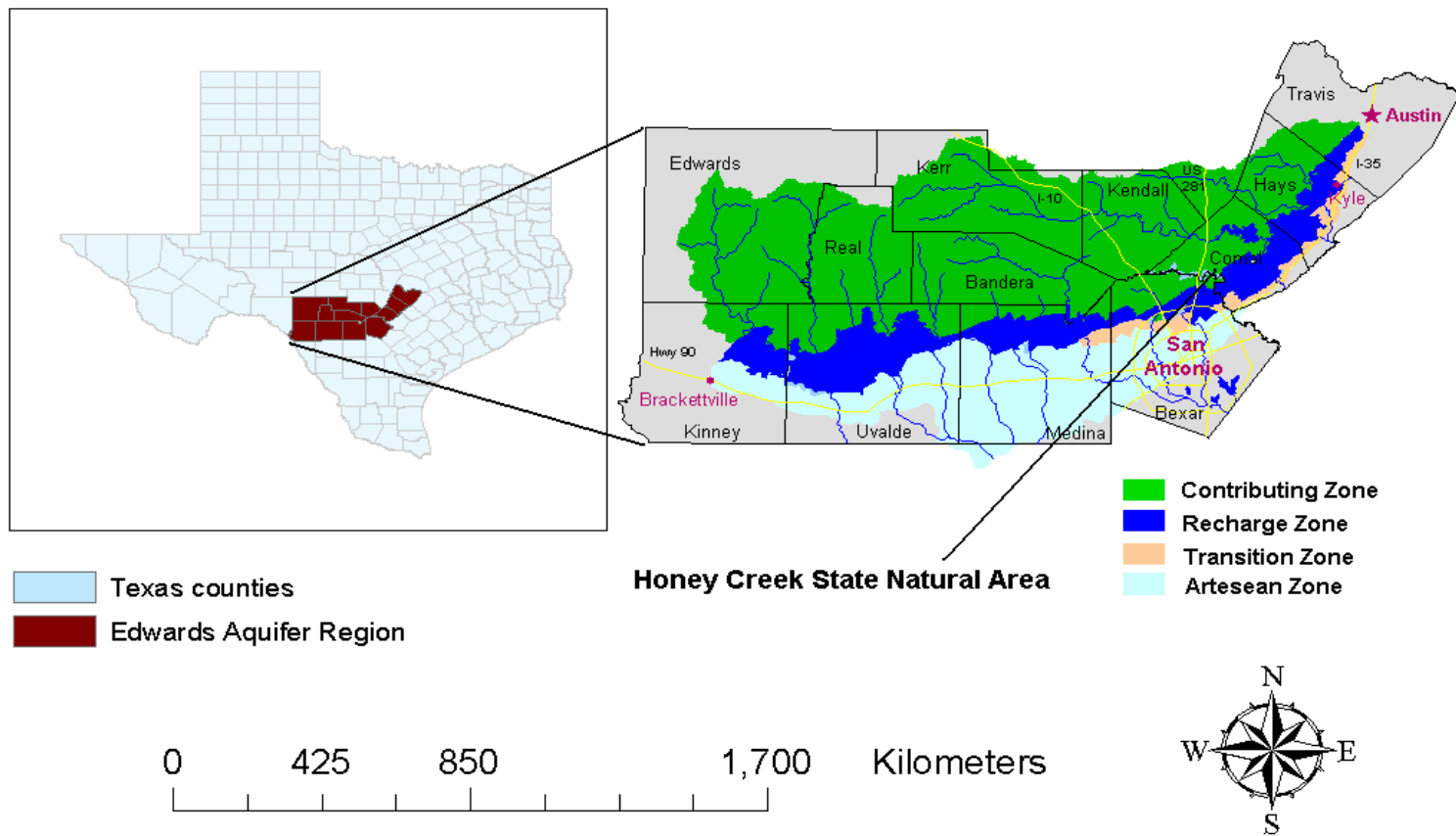


Fig. II-1. The study area was the Honey Creek State Natural Area located in Comal County TX. Also shown are the various hydrologic zones of the Edwards aquifer.

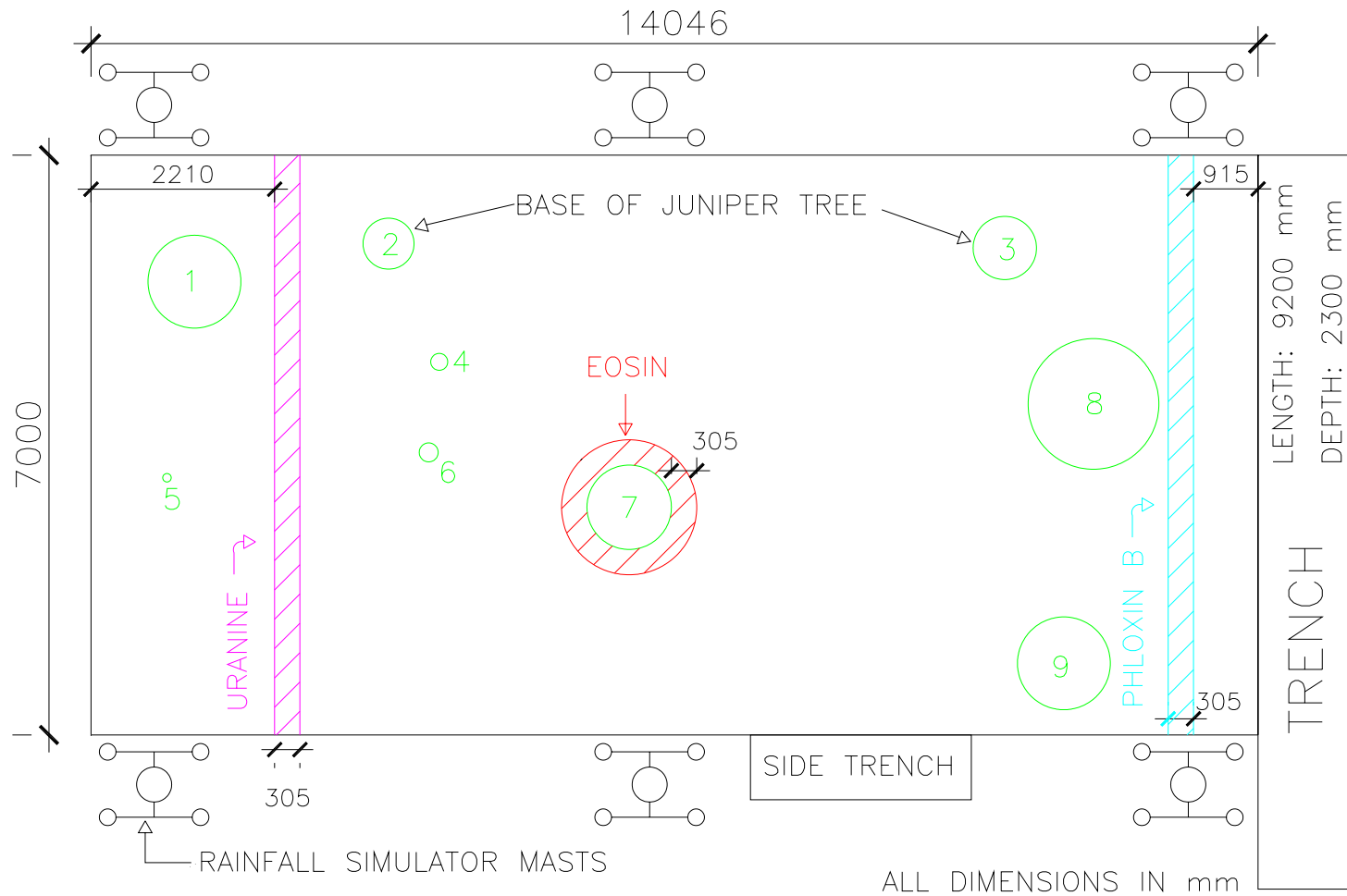
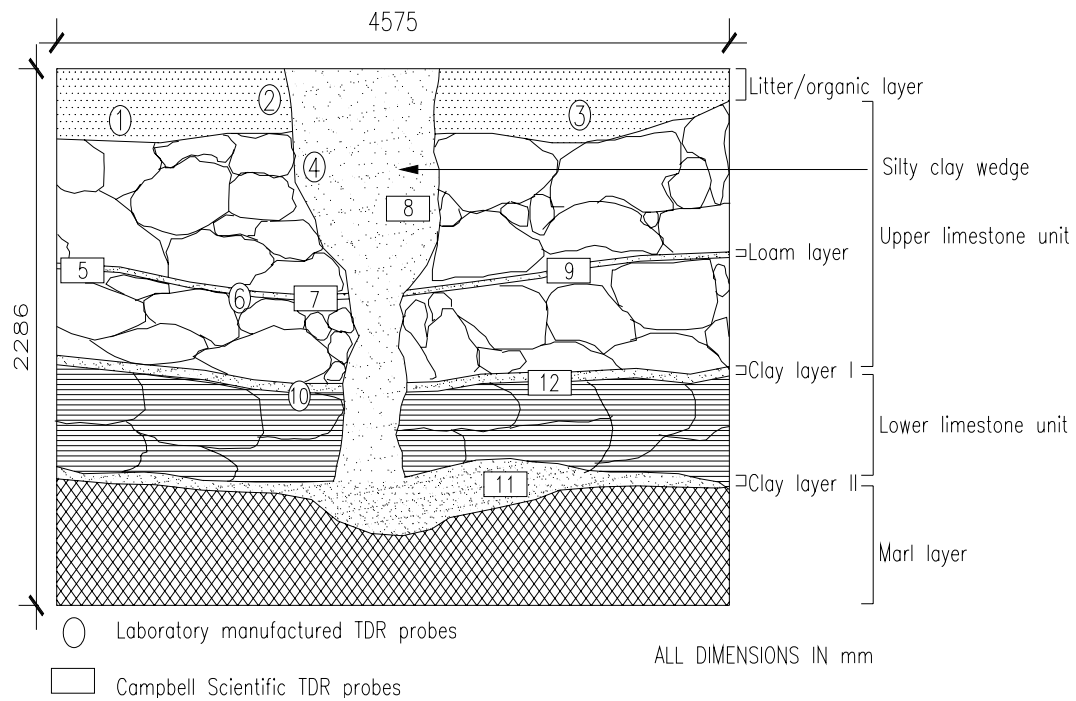
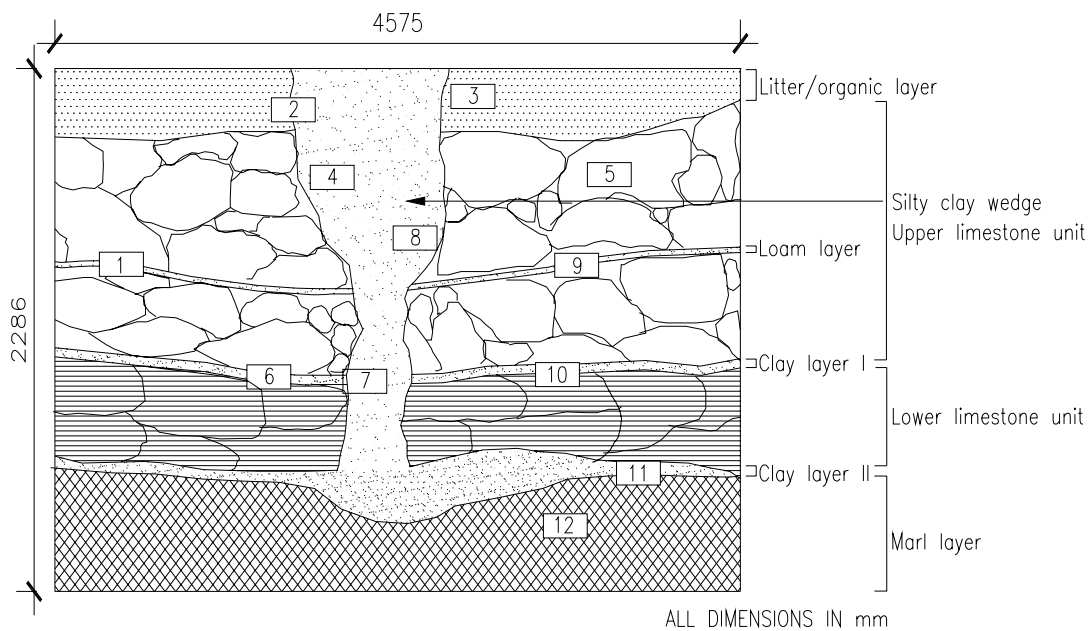


Fig. II-2. Honey creek experimental plot with spatial locations of juniper trees, rainfall simulator masts and the trench. Application bands of three dyes during dye-tracer studies are also illustrated in the layout.

The plot contained nine juniper trees inside it. The trees had variable basal diameters ranging from 0.05 to 0.56 m. A trench (9.2 m long and 2.3 m deep) was excavated at the downslope end of the plot for monitoring the sub-surface flow processes of the karst system. At the trench, the soil/rock profile consisted of parallel layers that were assumed as representative of the whole plot. Fig. II-3 provides a schematic diagram of the trench cross section. It also shows the spatial locations of 12 Time Domain Reflectometry (TDR) probes which were used to determine the volumetric water contents. Note that a representative fraction of 4.5 m of the total length of 9.2 m of the trench has been illustrated in Fig. II-3. Fig. II-4 shows a photograph of the trench face with the different layers. The upper horizon of the trench at the site was divided into two regions. The upper region, which primarily consisted of litter, was of variable depth ranging between 0.04 and 0.1 m. This litter was composed of fallen leaves and debris from past few years that had not yet been broken down. The lower layer, which extended up to 0.6 m into the soil wedge (Fig. II-3 and Fig. II-4), was characterized by an organic rich, black colored clay. The high organic content was a result of leaching. This region contained juniper roots protruding out at the trench face along with some fragments of limestone. The upper limestone unit, located just below the soil layer, was characterized by a prodigious layer of limestone intersected by horizontal and vertical fractures. Some of the fractures had roots protruding out of them. This upper limestone unit, whose depth varied from about 0.38 to 0.56 m, was highly brittle and was characterized by a dense network of fractures all along the trench face.



(a)



(b)

Fig. II-3. Schematic sketch of trench cross section illustrating the stratification of the trench face; (a) illustrates the older TDR probe locations (October to mid-December, 2003) and (b) illustrates the newer ones (mid-December, 2003 to May, 2004).



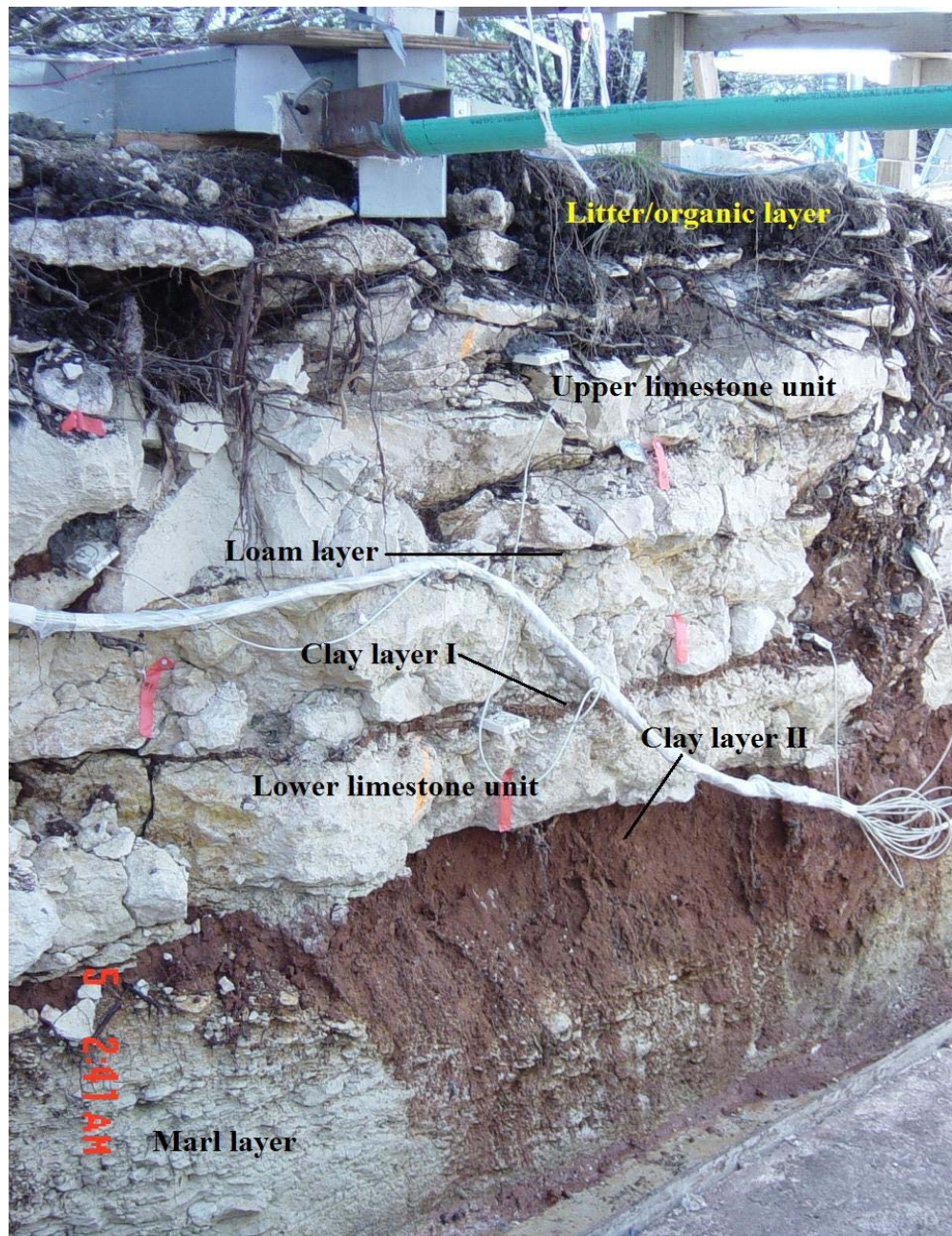


Fig. II-4. Photograph showing cross-section of trench face beside the plot.

There existed a thin band (0.01 to 0.04 m) of a loam (33% Sand, 47% Silt and 20% Clay) layer across the face of the trench that cut across the upper limestone unit. Small roots (root-lets) protruded out at certain locations from this layer. The first clay layer (13% Sand, 36% Silt and 51% Clay) extended across the trench profile in between the upper and lower limestone units with a varying depth between 0.03 and 0.07 m. The lower limestone unit whose depth, varied between 0.4 and 0.46 m across the trench, was less brittle as compared to the upper limestone unit and featured a lower density of fracture network. This lower layer extended as one complete unit and exhibited micro-cracks that extended all along the length of the trench. The 'marl' layer that existed at the lowermost horizon of the trench was a clay-rich limestone zone whose depth varied from 1.02 m at the extreme left to 0.63 m at the extreme right portion of the trench. The second clay layer (8% Sand, 34% Silt and 58% Clay) located within the marl layer, existed as a thin strip (0.05 m) at the left and right portions of the trench with a maximum depth of 0.50 m at the center of the trench just below the silty-clay pocket. The silty-clay (11% Sand, 44% Silt and 45% Clay) wedge existed as a vertical strip of soil that ran from the upper litter layer to the second clay layer. This layer contained a few plant roots along with some minor limestone fragments. Unlike the other horizontal layers, the silty clay wedge was only a superficial layer that extended up to 20-50 mm perpendicular to the trench face and did not contribute to the hydrology of the system. The soil samples from the trench face were analyzed by the (ASTM, 1961) texture analysis method in Texas A&M University soil hydrology laboratory.

### **Rainfall simulation and data collection**

A rainfall simulator set was installed to provide artificial rainfall within the plot. It consisted of six telescopic masts having a height of 15 m. Three masts were set up on either side along the length of the plot, making a total of six (Fig. II-2). Each mast had four sprinkler heads individually controlled by manually operated valves. The masts were connected via a (Honda WP-20 X) pump, Flow meter and Pressure gauge to a 5000 gallon collapsible water tank. The simulator was capable of delivering rainfall intensities varying from 25.4 mm (1") to 152.4 mm (6"). Eight different rainfall simulations were carried out at the site between October 2003 and May 2004. The surface component of the water budget was monitored by the following devices: Plastic rain gauges (140 ml capacity) were placed inside and outside the plot for measuring the total rainfall falling inside as well as outside the plot. They were arranged inside the plot in a rectangular grid (14 x 5) with a spacing of 1 m and 14 others were placed around the plot. Throughfall was measured using throughfall funnels, which were placed within the juniper canopy inside the plot to capture the amount of water falling through the canopy cover on the plot. Stemflow was measured using a stemflow collar, which measured the amount of water that was diverted by the stems. Runoff was measured by a 150 mm H-flume that was placed at the downslope end of the plot. A sump was created within the trench to collect total volume of sub-surface flow. The sump contained a submersible pump connected to a tipping bucket device which was in turn connected to a Datalogger (CR-10 X, Campbell Scientific) for continuously monitoring the sub-surface flow rate into the trench.

The sub-surface flow processes were thoroughly investigated using two separate methods. The fast flowing component of the flow was visually inspected at the end of each simulation. We noted down the time it took for the first flow to occur within the trench from the start of a particular simulation and termed it the ‘response-time’ of the flow. We also calculated the discharge of flow at various locations. The slow flowing component was measured at the trench face using Campbell Scientific’s Time Domain Reflectometry (TDR) system, which included the TDR 100 Time Domain Reflectometer, Campbell Scientific CR10-X Datalogger, SDMX50 co-axial multiplexers and TDR probes that were operated by the PCTDR software. The probes contained three stainless steel rods (diameter 4.8 mm) with a length of 300 mm. These rods were cut to a length of 150 mm so that they could penetrate and easily be placed within the fractures of the trench face. A pit on the left hand side of the plot was dug, and two probes were inserted in it to further our understanding of the sub-surface flow characteristics occurring within the plot. So, in total there were twelve probes in the main trench and two in the side trench (SI and S2). The datalogger was programmed to record data at intervals of 10 minutes. The first phase of data collection lasted from August to mid-December in 2003. During the second phase (mid-December 2003 to May 2004), the laboratory manufactured probes were replaced with Campbell scientific probes and some of the spatial locations of the probes within the trench face were altered to better monitor the flow processes (Fig. II-3(a) and II-3(b)). Table II-1. lists the details of the spatial locations of the old and new positions of each TDR probe.

Table II-1. Spatial locations of the TDR probes before and after the adjustments were made. ‘Unit’ indicates the layer in which the probes were located and ‘Depth’ indicates the depth of each probe from the top surface of the trench face.

Probe #	Old location		New location	
	Unit	Depth [m]	Unit	Depth [m]
1	Litter	0.25	Loam	0.61
2	Litter	0.15	Litter	0.40
3	Litter	0.22	Litter	0.22
4	Upper limestone	0.48	Upper limestone	0.40
5	Loam	1.12	Upper limestone	0.43
6	Loam	1.14	Clay I	1.14
7	Loam	0.91	Clay I	1.06
8	Upper limestone	0.68	Upper limestone	0.91
9	Loam	0.99	Loam	0.68
10	Clay I	1.78	Clay I	1.01
11	Clay II	2.17	Clay II	2.17
12	Clay I	1.44	Marl	2.35
S1	-	-	Litter	0.12
S2	-	-	Upper limestone	0.45

Table II-2. Details of various simulations carried out at the plot. Each simulation contained a succession of runs with time gaps in between. The average intensity and total rainfall amount for each simulation were calculated

Simulation	Date	Run #	Intensity per run [mm]	Duration [hr]	Time gaps [hr]	Average Intensity [mm]	Total rainfall [mm]
Sim 1	3-Oct-03	1	59.20	2.00	1.00	43.9	170.2
		2	58.90	0.88			
Sim 2	17-Oct-03	3	8.70	3.50	1.00	7.0	56.4
		4	7.40	3.50			
Sim 3	31-Oct-03	5	12.40	3.50	1.20	9.9	74.2
		6	11.00	2.80			
Sim 4	5-Dec-03	7	59.00	1.00	2.48	24.0	107.6
		8	48.60	1.00			
Sim 5	11-Dec-03	9	67.50	0.75	1.083 1.35	21.0	108.9
		10	44.80	1.00			
		11	13.50	1.00			
Sim 6	18-Dec-03	12	91.20	0.75	1.45 1.21	24.8	134.1
		13	52.00	1.00			
		14	13.70	1.00			
Dye-test 1	30-Jan-04	15	25.40	4.00	1.23	40.8	254.0
		16	152.40	1.00			
Dye-test 2	13-May-04	17	23.40	4.00	1.13	37.9	232.0
		18	138.45	1.00			

During two of the simulations, dye-tracer experiments were conducted (Table II-2). Each simulation consisted of either two or three separate runs with a particular intensity and duration, interrupted by time gaps. This time gap (between each run) was required to manually record the readings of all devices that measured the surface component of the water budget.

Consider any simulation event 's' ( $s = 1,2,3,\dots,n$ ) consisting of 'j' number of runs ( $j = 1,2,\dots,m$ ) and 'g' number of gaps ( $g = 1,2,\dots,p$ ). The average intensity for 's' was calculated based on the formula

$$I_s = \frac{\sum_{j=1}^m i_j d_j}{\sum_{j=1}^m d_j + \sum_{g=1}^p d_g} \quad [\text{II-1}]$$

In the above equation,  $I_s$  [mm] was the average rainfall intensity for simulation 's',  $i_j$  [mm] was the intensity of the  $j_{th}$  run,  $d_j$  [hr] was duration of the  $j_{th}$  run and  $d_g$  [hr] was the duration of the  $g_{th}$  gap between runs. The gaps were assumed to have zero intensity. The dye tracer experiments were conducted besides the simulation experiments to supplement our understanding of the sub-surface flow processes with special emphasis on their origin, and the nature of their flow paths (root macropores and or fractures). Three different dyes were used in these tests to enable us to differentiate between the sub-surface flow processes and their origin based on separate spatial locations (where they were applied) within the plot.

During the first dye-tracer test (30, January, 2004), three dyes Phloxin B (10.5 mg/l), Eosin (37.0 mg/l) and Uranine (42.2 mg/l) were applied. The locations of each dye are illustrated in Fig. II-2. After the application of the three dyes, two runs were carried out (Table II-2). Water samples were then collected from 15 outflow locations (Fig. II-5) within the trench face at 10 minute intervals. These samples were then taken back to the laboratory and analyzed for the tracers using a Spectrofluoro-photometer (Perkin Elmer™). The analysis revealed that the dye concentrations used were too low. Hence, a second dye-tracer experiment (13, May, 2004) was conducted and this time, the concentrations were increased by a factor of 100; Phloxin B (1.05 g/L), Eosin (3.7 g/L) and Uranine (4.22 g/L). The application, location and scheme of rainfall simulation were kept similar to the first test. We observed that after each run, outflow occurred at various point locations within the trench face. We assumed that this was the fast component of the sub-surface flow since it usually occurred within 3 hours from the start of each run. On the other hand, the TDR probes usually took much longer (23 – 30 hours) to respond to the rainfall patterns as compared to the outflow that occurred at the point locations on the trench face. Thus, we noted that the probes predominantly recorded the slow component of the sub-surface flow.



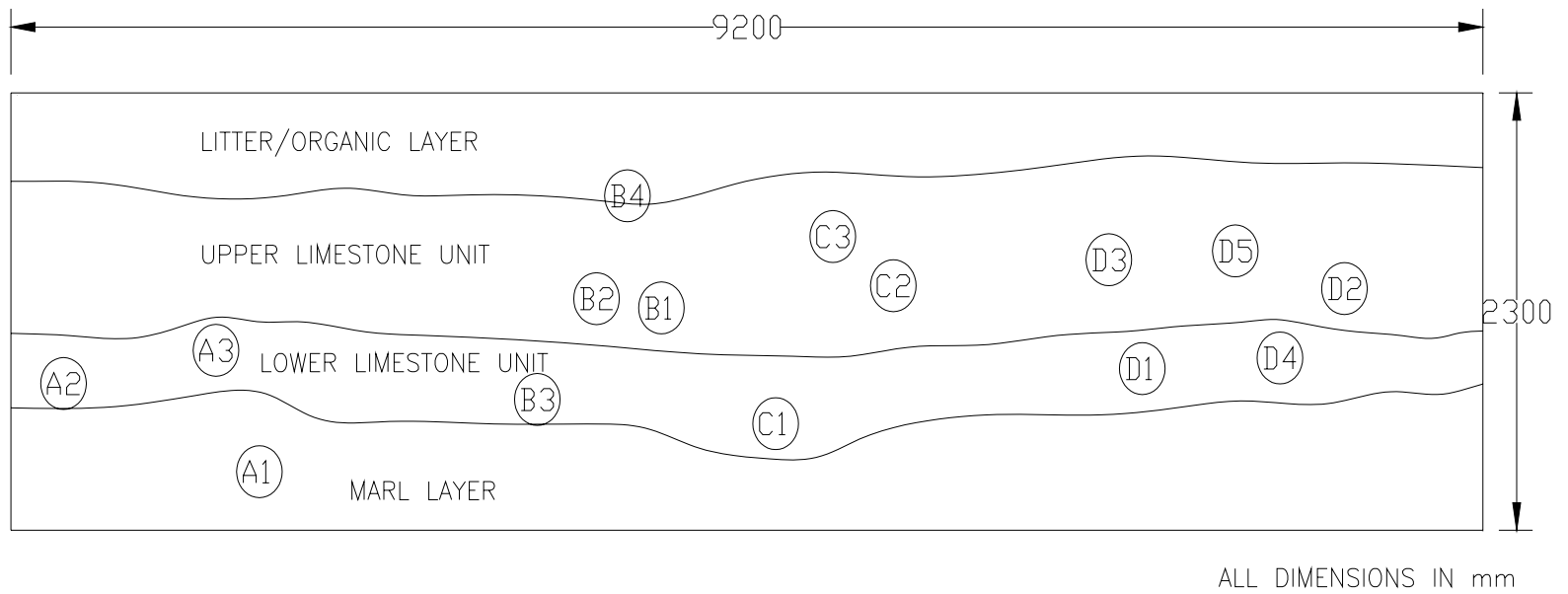


Fig. II-5. Dye sampling points within the trench face.

### Data analysis

Readings from each TDR probe were collected for each simulation event for 48 hours, starting from the onset of the first run of the simulation. The readings obtained from the probes were converted to volumetric water contents using the equation of Topp et al., (1980). The water content values were analyzed to determine significant parameters like response time, initial and final moisture contents. Statistical relationships were established between these parameters and the rainfall parameters (intensity and total rainfall amount) for each simulation event. The initial moisture content was taken as the arithmetic mean of the values recorded by the probes over a period of 15-20 hours before the probes registered a rise. The final moisture content was calculated by taking the arithmetic mean of the highest values recorded by the probes until the values started to decrease.

### Modeling assumptions

The numerical flow model HYDRUS-2D (Simunek et al, 1999) uses the Galerkin finite element method with linear basis functions to solve the Richards's equation for two-dimensional variably-saturated water flow. The transient two-dimensional isothermal Richards' equation governing the flow of water in a variably-saturated media:

$$\frac{\partial \theta}{\partial t} = \frac{\partial}{\partial x_i} [K (K_{ij}^A \frac{\partial h}{\partial x} + K_{iz}^A)] - S \quad [\text{II-2}]$$

where,  $\theta$  [ $\text{L}^3\text{L}^{-3}$ ] is the volumetric water content,  $h$  [L] is the pressure head,  $S$  [ $\text{T}^{-1}$ ] is a sink term,  $x_i$  ( $i = 1, 2$ ) [L] are the spatial coordinates,  $t$  [T] is time,  $K_{ij}^A$  are components of

a dimensionless anisotropy tensor  $K^A$ , and  $K$  [ $LT^{-1}$ ] is the unsaturated hydraulic conductivity which is given by

$$K(h, x, z) = K_s(x, z)K_r(h, x, z) \quad [\text{II-3}]$$

where,  $K_r$  is the relative hydraulic conductivity and  $K_s$  [ $LT^{-1}$ ] is the saturated hydraulic conductivity. In the model, the unsaturated soil hydraulic properties are implemented by van Genuchten (1980) to obtain an equation for predicting the unsaturated hydraulic conductivity function in terms of soil water retention parameters. The expressions obtained by van Genuchten are

$$\theta(h) = \theta_r + \frac{\theta_s - \theta_r}{[1 + (\alpha h)^n]^{1 - \frac{1}{n}}} \quad \text{for } h < 0 \quad \text{and}$$

$$\theta(h) = \theta_s \quad \text{for } h \geq 0 \quad [\text{II-4}]$$

where  $\theta(h)$  represents the water retention curve,  $\theta_r$  [ $L^3L^{-3}$ ] and  $\theta_s$  [ $L^3L^{-3}$ ] are residual and saturated water contents, respectively,  $\alpha$  [ $L^{-1}$ ] is the inverse of air-entry value and  $n$  is a pore distribution index.

$$K(h) = K_s S_e^l \{1 - [1 - S_e^{n/(n-1)}]^{1-1/n}\}^2 \quad [\text{II-5}]$$

where  $l$  is an empirical pore tortuosity/connectivity parameter.

It was difficult to determine the exact root and/or fracture network present below the plot unless further geologic studies were conducted using instruments like ground penetrating radar (GPR). Hence, the idea was to model the flow processes and determine the hydraulic properties of each geologic unit within a small section of the plot using a simplified root/fracture network and then consider a larger section of the plot and use

either stochastic or GPR techniques to ascertain the fracture network. This study was limited to using a simplified fracture network and simulating the sub-surface flow processes after applying rainfall events similar to Run 15 and 16 of the dye-tracer test (Table II-2) within a 4 m section of the plot. The whole profile consisted of 5 different materials similar to those observed at the trench face. The model domain was a two-dimensional profile of the actual experimental plot having a length of 4 m and depth of 2.3 m (Fig. II-6). The partial length of the plot assumed for simulation studies (4 m) was set based on the observations at the trench face during dye tracers experiment, and model calibration. Three vertical conduits were used within the upper limestone unit with a spacing of 1 m between them to represent a bundled/lumped fracture/root network. They were interconnected by horizontal conduits which allowed for lateral sub-surface flow. These conduits were assumed as a continuum with high conductivity value. The lower limestone unit had fewer vertical conduits because it was characterized by a lower fracture density than the upper limestone unit. The litter/organic clay and clay layers represent the actual zones as observed at the trench. The boundary conditions used on 4 sides of the domain are also illustrated in the figure. The top boundary condition (atmospheric) was based on the rainfall simulations conducted on the plot. We assumed the left portion of the model profile to have 'no-flow' boundary condition to treat the whole profile as a single and isolated hydro-geologic unit. The right portion of the profile had seepage face to represent the trench. The lower portion was assumed to have deep drainage. Six observation nodes were located within the profile which corresponded with actual spatial location of TDR probes within the trench.

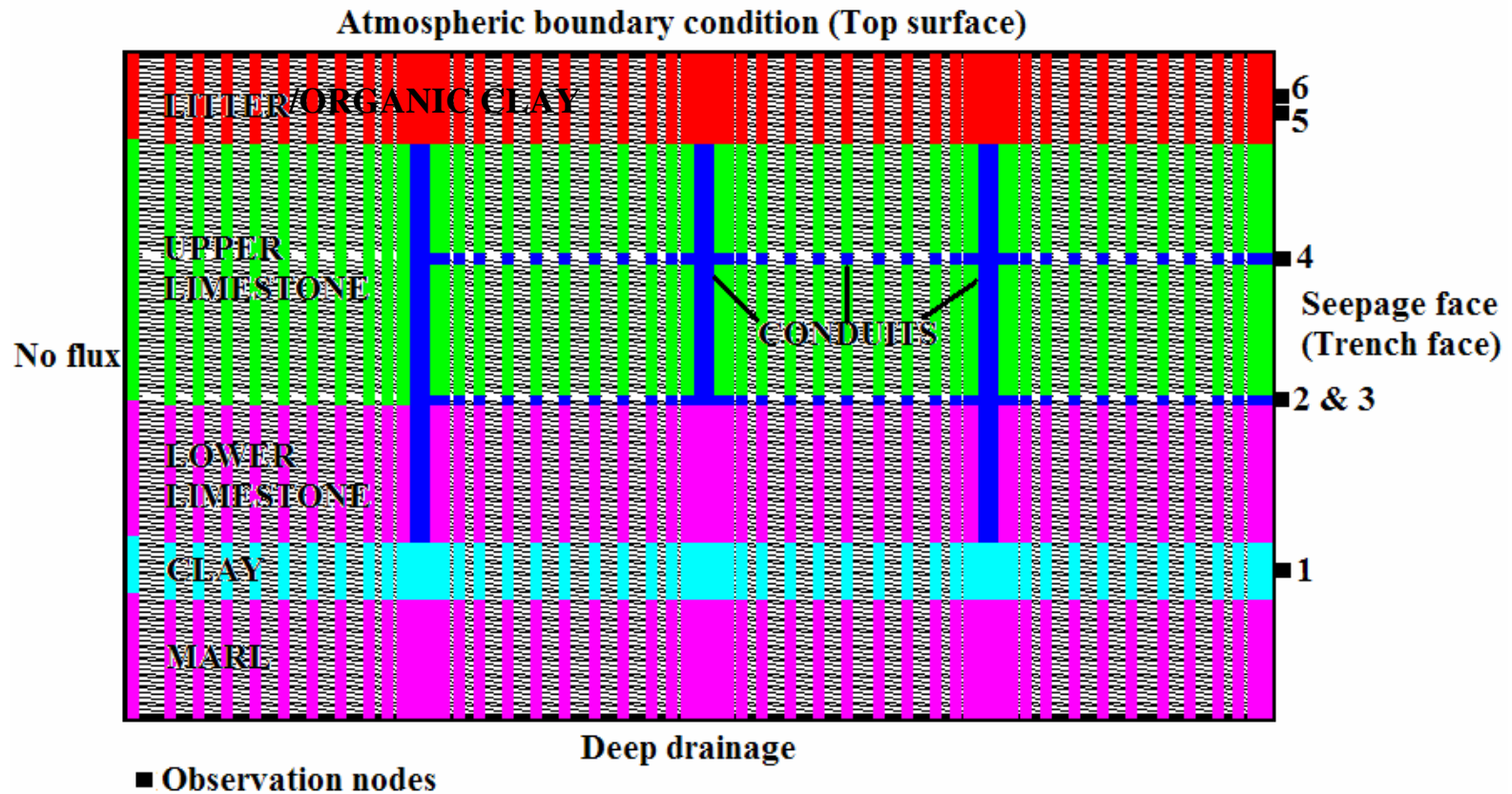


Fig. II-6. Two-dimensional model profile with fractures. The lower limestone unit and the Marl layer were assumed to have similar hydraulic characteristics. The upper limestone unit has the highest density of conduits followed by the lower limestone unit. This differentiates between the two based on the actual fracture density observed at the trench face. The marl layer does not have any conduit as we did not observe any fractures in this layer at the trench.

To investigate the role played by fractures/conduits in augmenting sub-surface flow, another 4 m section without any fracture network was used for model simulation (Fig. II-7). All other variables (material type and boundary conditions) were kept similar to the one with fractures. The fracture domain was used for determination of hydraulic parameters. Table II-3 lists the initial van Genuchten parameters that were used for the model for each geologic unit of the trench face. The  $\theta_r$  and  $\theta_s$  values for each material were obtained based on the TDR probe readings before and after the first dye-tracer test. The  $K_s$  values for the litter layer and the conduits were established by conducting infiltration experiments beside the plot using a tension infiltrometer. The neural network prediction option of the HYDRUS-2D software was used to determine the parameters the lower clay layer by providing the percentages of sand, silt and clay as determined by texture analysis. A constant value of 0.5 was assumed for  $l$  in all cases (Mualem, 1976). The parameters for the limestone units were obtained from literature review of hydraulic parameters of fractured rocks (Flint, 2003). After providing the initial values of the van Genuchten parameters for each layer, the model was then run in the inverse mode to determine the final parameters.

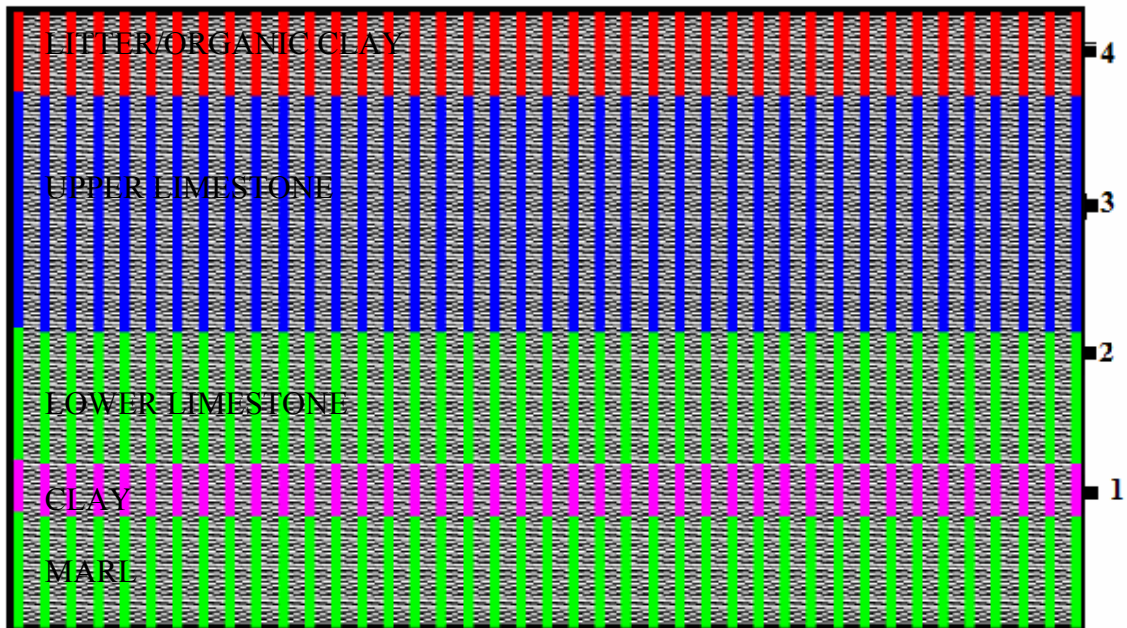


Fig. II-7. Two-dimensional model profile without fracture network. One observation node has been placed in each material type.

Table II-3. Initial hydraulic parameters for each geologic material.

Material	Geologic unit	$\theta_r$ [m <sup>3</sup> m <sup>-3</sup> ]	$\theta_s$ [m <sup>3</sup> m <sup>-3</sup> ]	$\alpha$ [m <sup>-1</sup> ]	$n$	$K_s$ [mhr <sup>-1</sup> ]	$l$
1	Litter/Organic	0.14†	0.61†	1.5‡	1.3‡	3.01‡	0.5
2	Conduit	0.18†	0.44†	10‡	3‡	12‡	0.5
3	Upper limestone	0.12†	0.17†	1.5§	1.3§	0.00091§	0.5
4	Lower limestone/Marl	0.12†	0.17†	1.5§	1.3§	0.00054§	0.5
5	Clay	0.31†	0.47†	1.7¶	1.25¶	0.012¶	0.5

† Measured from TDR probes

‡ Measured from infiltration experiments

§ Literature review of hydraulic parameters of fractured rocks

¶ Neural network predictions from HYDRUS-2D.



Water balance calculations were done using the predicted water fluxes from the HYDRUS-2D model. The model runs were made for the flow domain with fractures and the one without fractures. The water balance error was calculated using the equation given below:

$$\text{Water balance error [\%]} = \frac{I - O}{I} * 100 \quad [\text{II-6}]$$

where,  $I$  [ $\text{m}^2$ ] is the total amount of water entering the system and  $O$  [ $\text{m}^2$ ] is the total amount of water leaving the system.

$$I = A - E \quad [\text{II-7}]$$

$A$  [ $\text{m}^2$ ] is the atmospheric boundary flux and  $E$  [ $\text{m}^2$ ] is the evaporation flux.

$$O = SR + SF + DD + V \quad [\text{II-8}]$$

$SR$  [ $\text{m}^2$ ] is the total surface runoff,  $SF$  [ $\text{m}^2$ ] is the seepage flux,  $DD$  [ $\text{m}^2$ ] is the deep drainage flux and  $V$  [ $\text{m}^2$ ] is the total volume of water retained in the system.

$$V = \sum_{i=1}^n (\theta_f - \theta_i) * \text{Cross - sectional Area} \quad [\text{II-9}]$$

The total volume of water retained in the system is the summation of the water retained in each layer/material type ( $i = 1$  to  $5$ ).  $\theta_f$  is the final volumetric water content of each layer and  $\theta_i$  is the initial volumetric water content. A single number that best represented the  $\theta_f$  and  $\theta_i$  values that were observed from TDR measurements were selected for the calculations from the model. Area of each layer was calculated from the two-dimensional model profile (Fig. II-6). The values of atmospheric boundary flux, seepage face flux and deep drainage flux were obtained from the model. Surface runoff was assumed zero because we did not observe any runoff at the plot scale while

conducting the rainfall simulation experiments. The evaporation value was assumed a constant =  $2.5 \text{ mm day}^{-1}$  for the entire simulation period of 7 hours. A very low value was selected because of the high intensity and low duration of the rainfall event. For conditions with and without fractures, 5-10% mass balance errors were encountered in the simulation experiments. Detailed results are provided in Appendix B.

### **Results**

Fig. II-8 compares the response times of outflow at various sampling locations within the trench face for the two dye tracer studies. Runs 15 and 17 (with intensities of 25.4 mm and 23.4 mm, respectively) resulted in outflow from only 7 locations whereas Runs 16 and 18 (with intensities of 152.4 mm and 138.4 mm, respectively) resulted in outflow from 15 locations on the trench face. This demonstrated that a larger segment of the plot contributed to the outflow at the trench when the rainfall intensity was increased. As we move up along the Y axis of Fig. II-8 (which indicates the increasing depth of the sampling locations, see Fig.II-5); there is no evidence of a systematic change in response times for any of the four runs. It appears that the outflow occurring at the trench did not follow any specific preferred horizontal or vertical pathways. The comparison of the sequence of wetting up of the sampling points for each run, shows a (Pearson's ranked) sequence correlation coefficient of 0.78 for low intensity runs (15 and 17) and a sequence correlation of 0.81 for the high intensity runs (16 and 18). This signified that the sequence of outflow based on the spatial locations of the sampling points within the trench face was comparable for similar rainfall intensities.

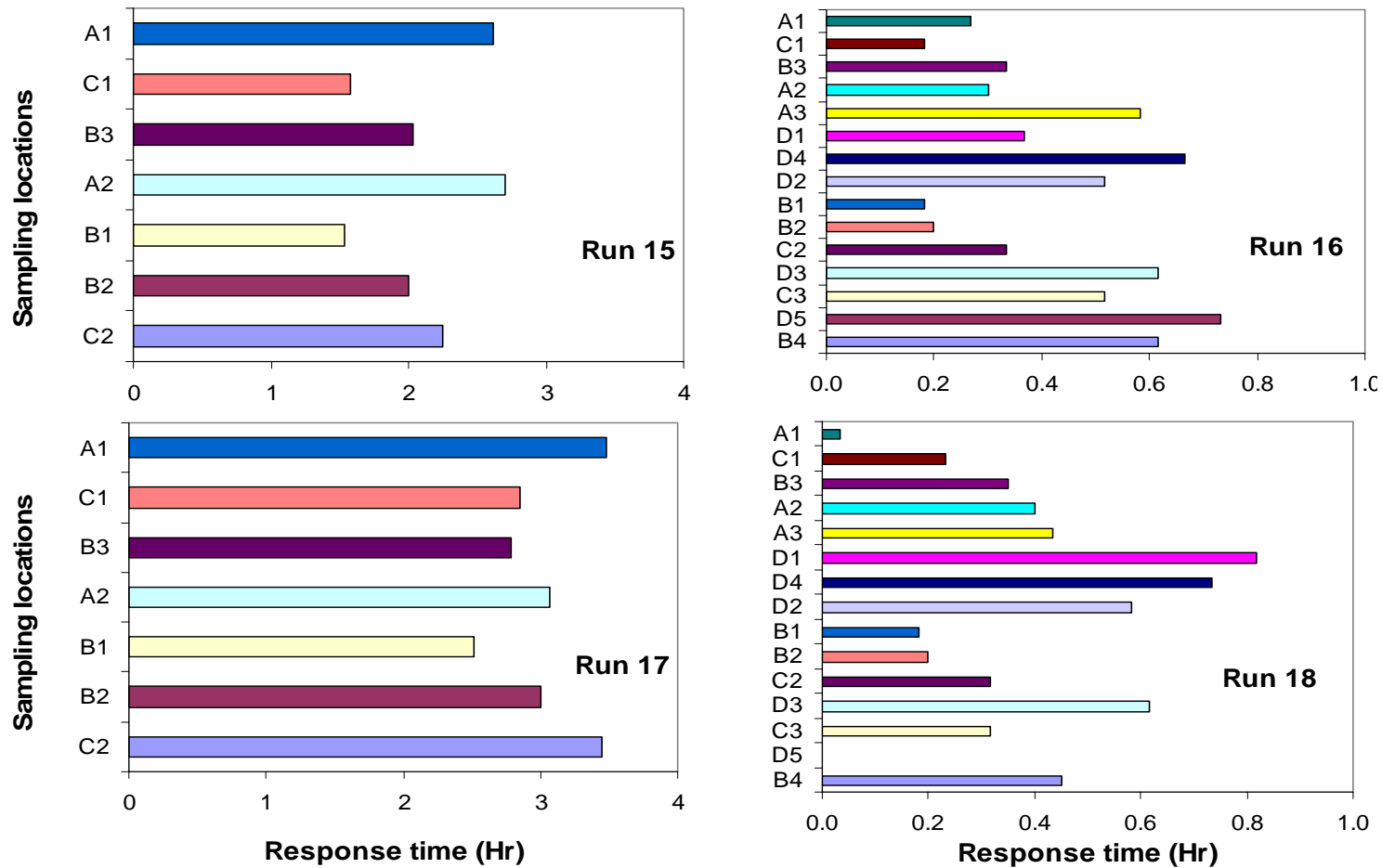


Fig. II-8 Response time for the first onset of outflow from various sampling locations at the trench face. Refer to Fig. II-5 for spatial locations for sampling points. The sampling locations are arranged by increasing depth; for Run 15 and 17, C2 was the upper most point at the trench and A1 was the lowermost point and for Run 16 and 18, B4 was the uppermost point and A1 the lowermost. Run 15 and 17 were low intensity long duration events while Run 16 and 18 were high intensity long duration events.

Fig. II-9 illustrates the responses of the dyes that were used in the second dye-tracer test. The response times indicate the time during which these dyes were first detected in the water samples collected during the test. The response times of the dyes are comparable to the responses of the fast flow component (comparison of Fig. II-9 and Fig. II-8). The response times of the dyes on an average, lag behind the response time of the fast flowing component at the trench by approximately 1 to 1.5 hours. Fig. II-9 shows us that there is uniform distribution of the two dyes along the entire trench face and that the response times of both dyes are also similar, which would suggest that transport via roots and fractures were inter-connected. Moreover, the sequence of appearance of the two dyes at the trench face were comparable, which is demonstrated by a (Pearson's ranked) correlation coefficient value of 0.89. Uranine (which was applied at the far end of the plot, with the largest concentration) did not appear at any of the 15 sampling locations of the trench face for the dye test. This could suggest that (seepage) outflow at the trench face was dominated by flow processes occurring within the front half section of the plot. This may further be related to our observation of the standing (ponding) water over the mild depression in the front portion of the plot during the rainfall simulations. We believe that this water eventually infiltrated through plot.

The analysis carried out based on the response times of outflow occurring at the trench and the dye studies yielded three main results: i) flow did not occur uniformly in either the vertical or the horizontal direction. Instead, the outflow locations were clustered at areas with fractures and root structures, ii) outflow at the trench enunciated

comparable characteristics for similar boundary conditions and iii) transport of dyes via roots and fractures were inter-connected and occurred only within the front half of the plot close to the trench.

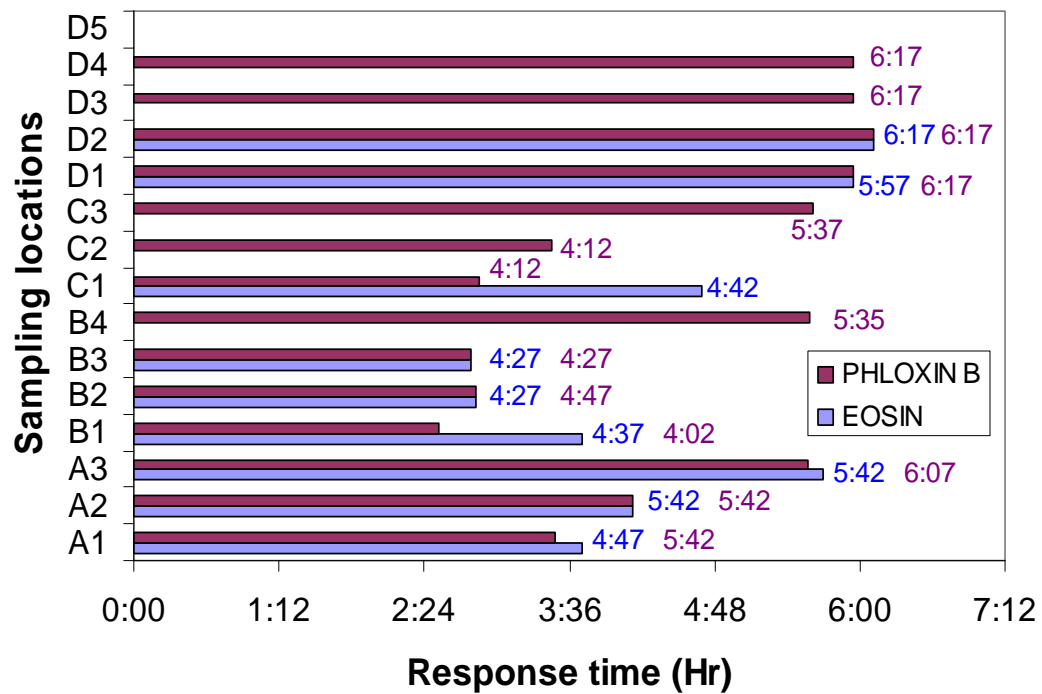
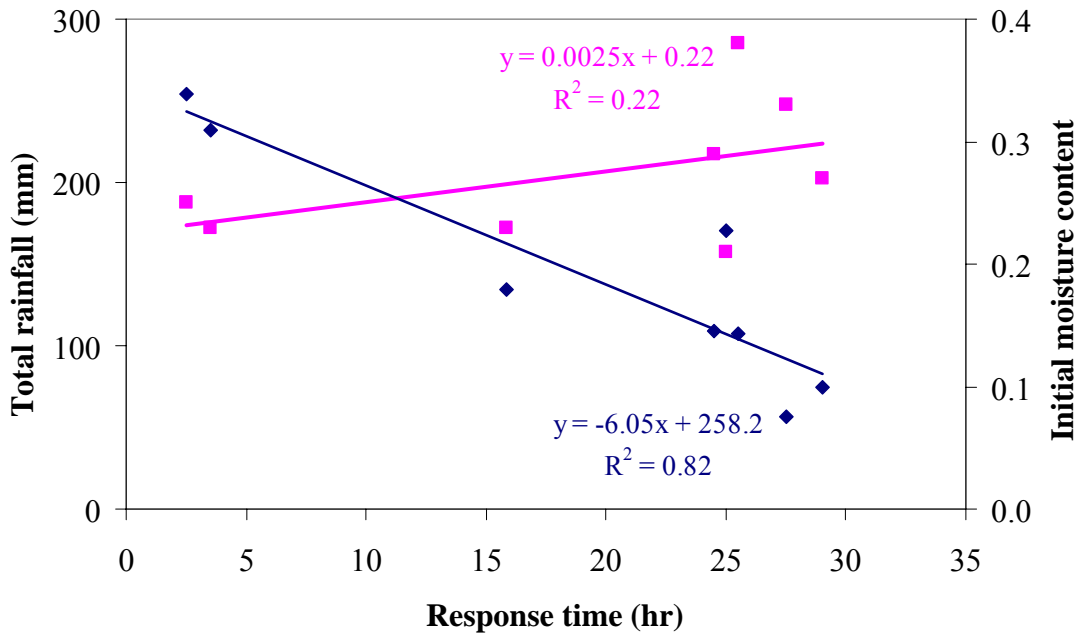
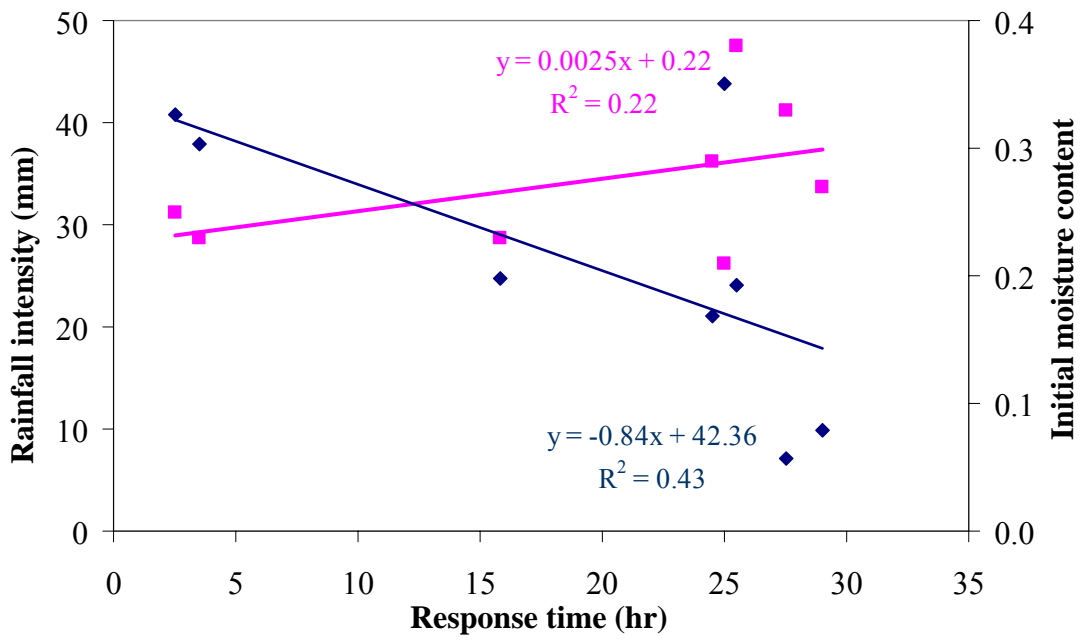


Fig. II-9. Response time of dyes at various sampling points within the trench face for the second dye-tracer test. Numbers beside the bars indicate peak concentration times as registered by the Spectrofluoro-photometer. (Red indicates the times for Phloxin B and blue indicates that of Eosin).



(a)



(b)

- ◆ Response time vs. Rainfall
- ◆ Response time vs. Initial moisture content

Fig. II-10. Relationship between response time and boundary conditions ((a) total rainfall and (b) rainfall intensity).

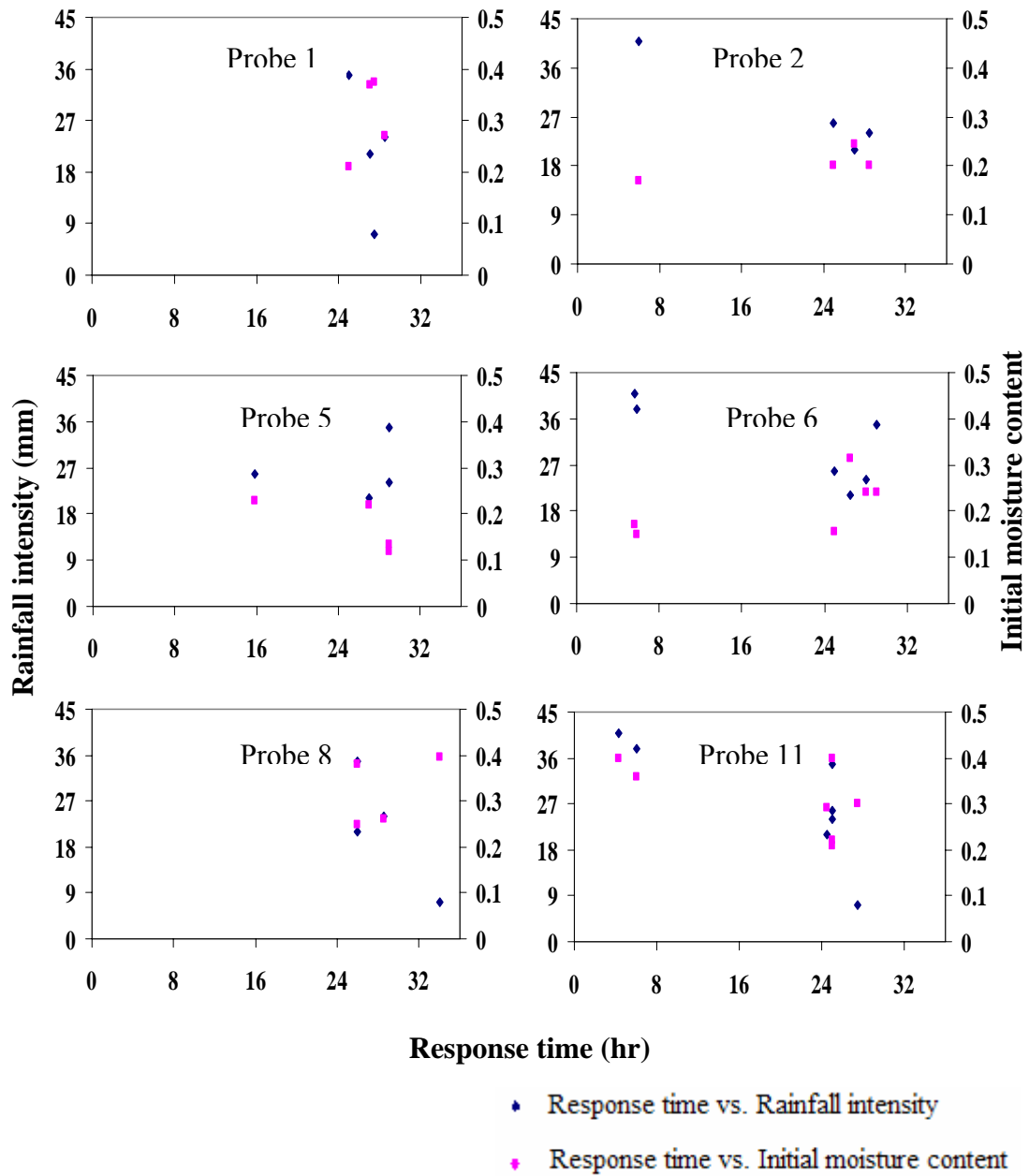


Fig. II-11. Relationship between rainfall intensity and initial moisture content with first response times for various TDR probes during different simulations.

Fig. II-10 shows the relationship of TDR response times with (a) total rainfall and initial moisture content and (b) rainfall intensity and initial moisture content. These responses were first response times as registered by various TDR probes for different simulations. These plots show the combined influence of rainfall and initial moisture content on the probe response times. Both figures demonstrate a negative linear relationship between rainfall (total amount of rainfall and rainfall intensity) and response time suggesting that water reached the probes faster when rainfall was increased. However, it is also seen that the response times increase with increase in initial/antecedent moisture content. So, it can be seen that both rainfall amount and antecedent moisture content govern the response time of the probes. Fig. II-11 illustrates the relationship of rainfall and initial moisture content with response time for individual probes for various simulations. Five out of the six probes show a negative relationship between rainfall intensity and response time. Furthermore, four out of the six probes show a positive relationship between initial moisture content and response time. These figures strengthened the observations of Fig. II-10. Detailed responses for each TDR probe for the different simulation events are provided in Appendix A.

The analysis carried out on the data recorded by the TDR probes yielded the following key findings: i) the response times of the TDR probes depended both on rainfall amount and initial moisture content, ii) since the TDR probes did not exhibit a uniform wetting process in either the vertical or the horizontal direction; it appeared that this slow flow component did not occur in any specific horizontal and vertical pathways



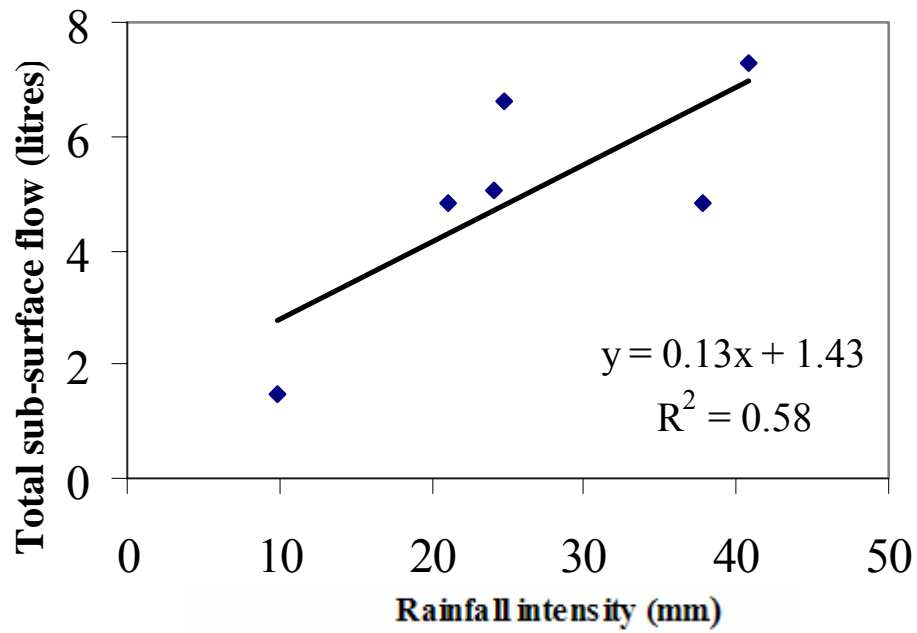
at the trench face and iii) the TDR response times were lower (indicating more flow) when rainfall intensity was high and antecedent moisture content was low.

Table II-4 shows us that the response times (average response time and first response time) registered by the TDR probes for the first 6 simulations, which fall within the 15 to 30 hour range. It is interesting to note that for the two dye tracer tests (with high rainfall intensities) the responses were very fast and comparable to the fast flow responses at the trench. This suggests that when rainfall amount is large ( $> 200$  mm) exchange occurs between the fast and slow components of the sub-surface flow. The difference in pressure head between the fractures and matrix rises during such high rainfall events and this causes water to flow from the fractures/root channels to the matrix. Fig. II-12 shows the relationship between boundary conditions like (a) rainfall intensity and (b) total rainfall and the total volume of sub-surface flow in. It can be observed that volume of sub-surface flow increases with the increase in amount of rainfall or rainfall intensity.

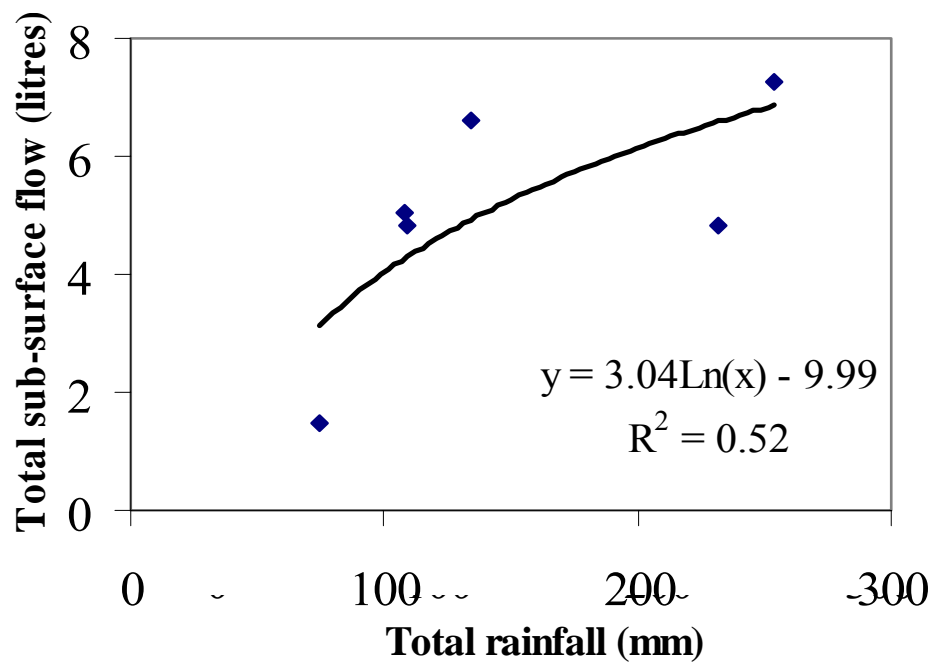
Table II-4. First response times and average response times for all TDR probes for each simulation event

Simulation	Total rainfall amount [mm]	TDR Probe Responses	
		First response time [Hr]	Average response time [Hr]
Sim 1	170.2	25.0	26.6
Sim 2	56.4	27.5	30.7
Sim 3	74.2	29.0	30.7
Sim 4	107.6	25.5	26.7
Sim 5	108.9	24.5	26.0
Sim 6	134.1	15.8	23.3
Dye-test 1	254.0	2.5†	4.6†
Dye-test 2	232.0	3.5†	5.1†

† Indicates fast TDR responses as a result of exchange between fast and slow components of flow



(a)



(b)

Fig. II- 12. Relationship between total sub-surface flow and (a) rainfall intensity and (b) total rainfall from various rainfall simulations.

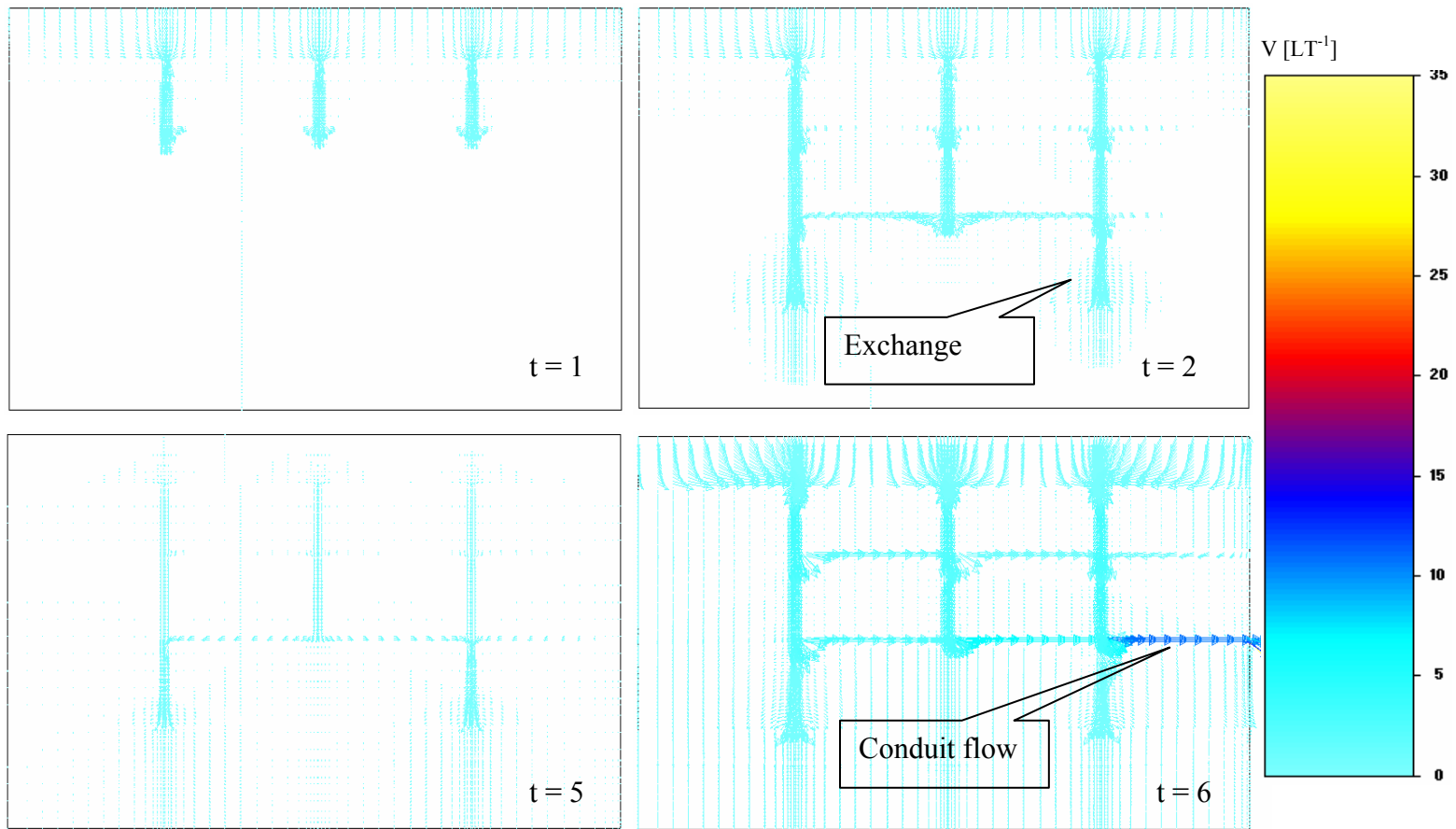


Fig. II-13. Simulated sub-surface flow at different times for domain with fracture network.

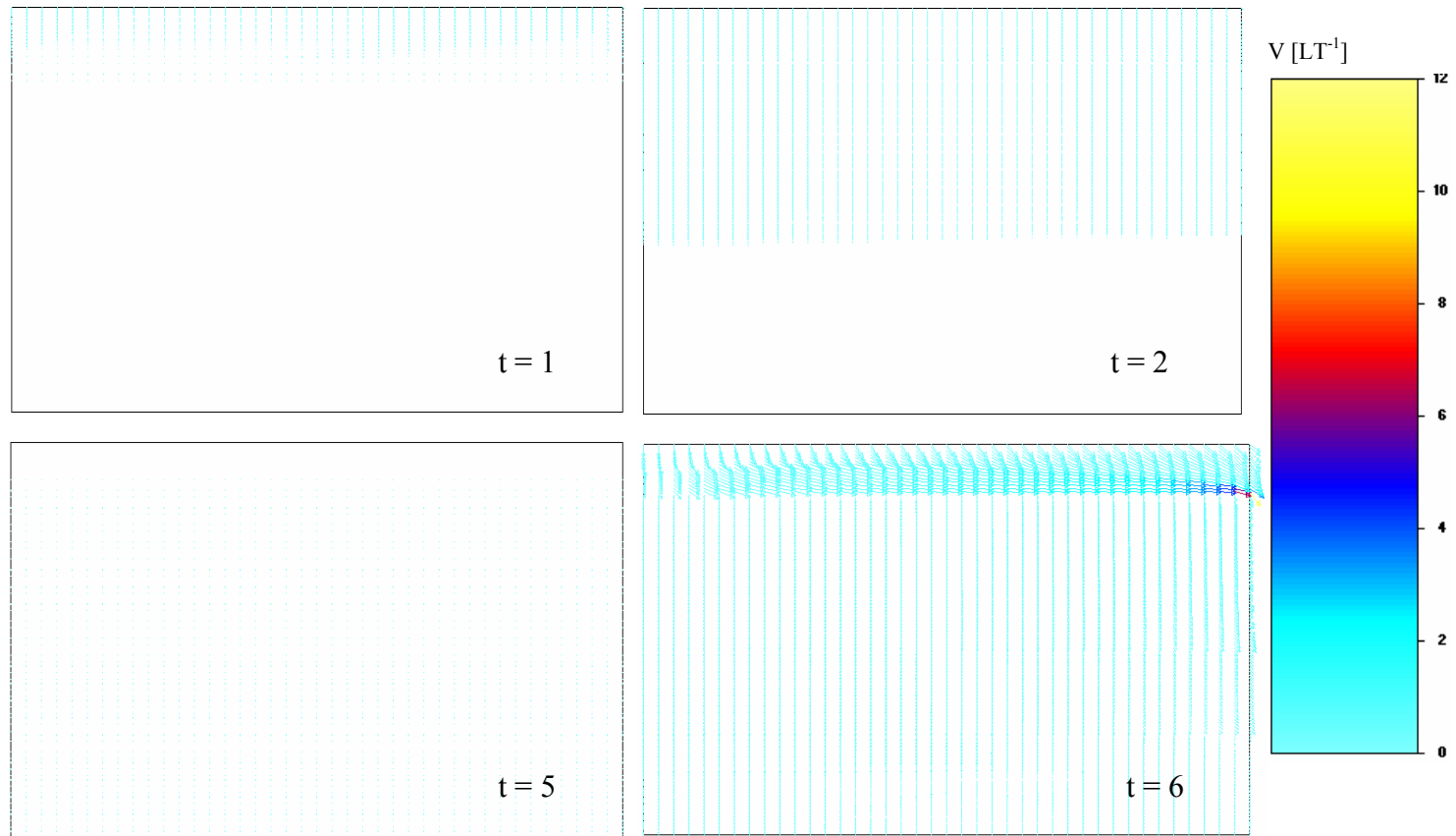


Fig. II-14. Simulated sub-surface flow at different times for domain without fracture network.

Fig. II-13 shows the simulated sub-surface flow processes using HYDRUS-2D at different times with fracture network. The flow vectors show the direction of flow and the color represents the velocity. The three important observations from this figure are: i) at time  $t = 2$  hours, we observe flow occurring through the upper limestone unit. This reflects the exchange process that was observed during the experiments. Although, the upper limestone unit has a much lower conductivity value as compared to the conduits, flow occurs due to the difference of pressure head, ii) at  $t = 5$  hours, we see that flow in the conduits has reduced. This is because of the one hour gap in rainfall event between the two runs during the first dye-tracer test and iii) at  $t = 6$  hours, a sharp rise in the flow velocity is observed at the lower horizontal conduit which is equivalent to the very fast outflow that was observed at the trench face during high rainfall events. Fig II-14 shows the simulated flow vectors without the fracture network in the model domain. In this case, most of the flow occurs at the seepage face within the top layer. When the two figures (Fig.II-13 and Fig. II-14) are compared, it is seen that the fracture network proliferates the sub-surface flow processes occurring within the two dimensional domain. Furthermore, water reaches the clay and marl layers much quicker due to fast/bypass flow via the fracture/conduit network. Fig. II-15 illustrates the water flux at the seepage face of (a) domain with fractures and (b) domain without fractures. It is seen that water flows out at the seepage face within the top layer earlier for the domain without fractures reflecting limited vertical flow to the deeper horizons as opposed to the observations during the field experiments. Furthermore, Fig. II-16 shows the water flux at the lower boundary of (a) domain with fractures and (b) domain without fractures.

This figure shows us that water reaches the lower boundary earlier for the model domain with fractures. This kind of comparison of various fluxes between the two model domains suggests that the fractures result in more water infiltrating vertically through the system. Fig. II-17 compares the measured vs. simulated flow responses for the domain with fractures when the model was run in inverse mode. N1 to N6 denote the simulated water contents ( $\theta$ ) and C13 to C23 denote the actual water contents as measured by the TDR probes after dye-tracer 1 test. The table given below the graph relates the actual TDR probes to the modeling observation nodes. It also lists the corresponding simulated and measured responses for each observation point. At observation node 1 which was within the clay layer, the measured and simulated responses were very similar. However, at nodes 2 and 3 which were directly on the conduits, it was seen that the simulated water contents increased with a sharp rise unlike the actual readings from the probes. The observed and simulated responses were closer at node 4. At nodes 5 and 6 which were within the litter/organic clay layer, the measured and simulated responses were very different. This discrepancy can be explained by the fact that the upper litter/organic clay layer within the plot, unlike the modeling domain consisted of several secondary structures like roots, stones, shrubs which reduced the volume of water infiltrating directly through the litter layer. Such vegetative features and rocks were not included in the model and hence, the rate of infiltration of water through the litter layer was much quicker than actually observed.

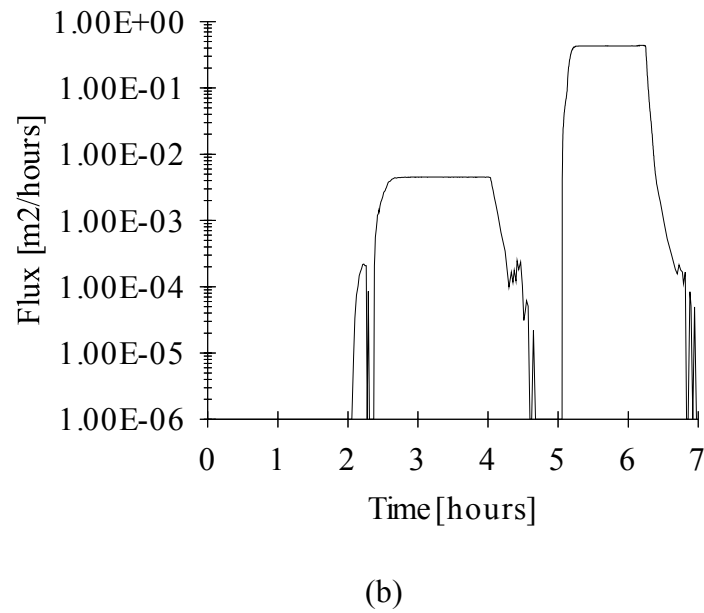
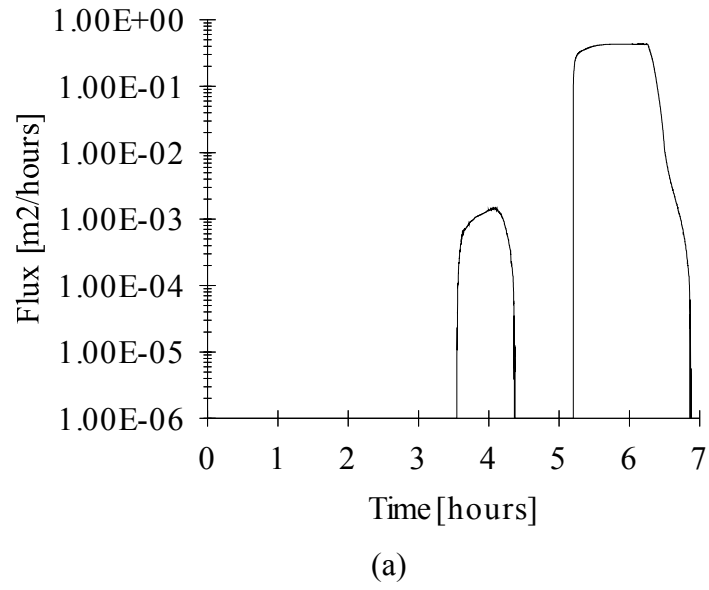
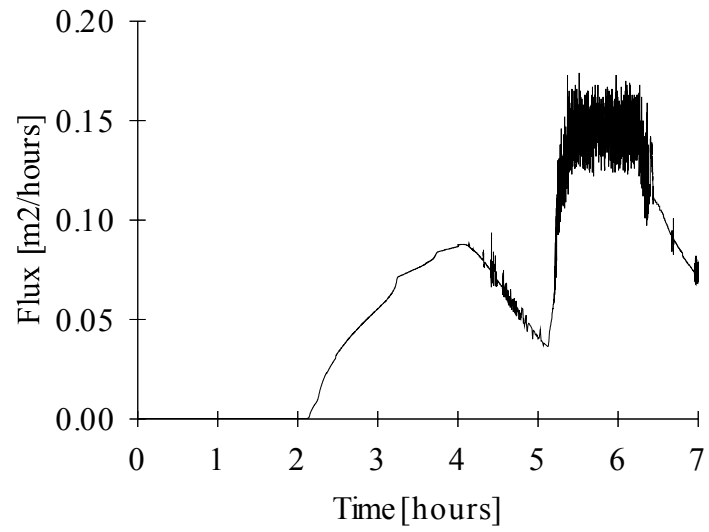
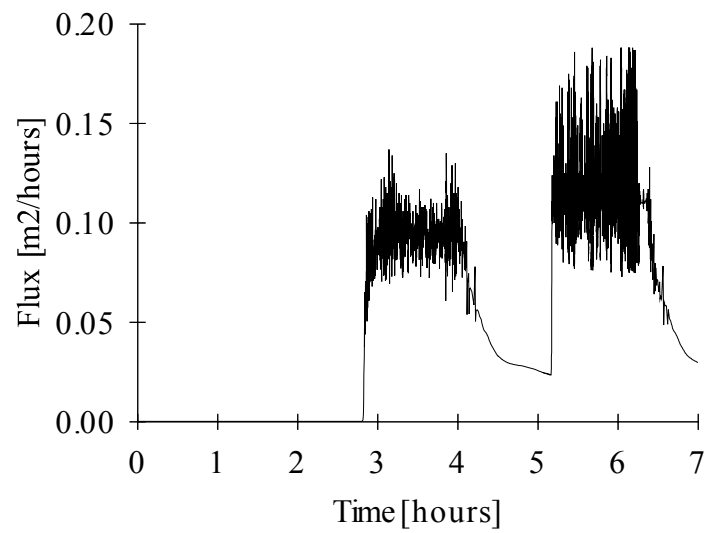


Fig. II-15. Water flux at seepage face for (a) domain with fractures and (b) domain without fractures.



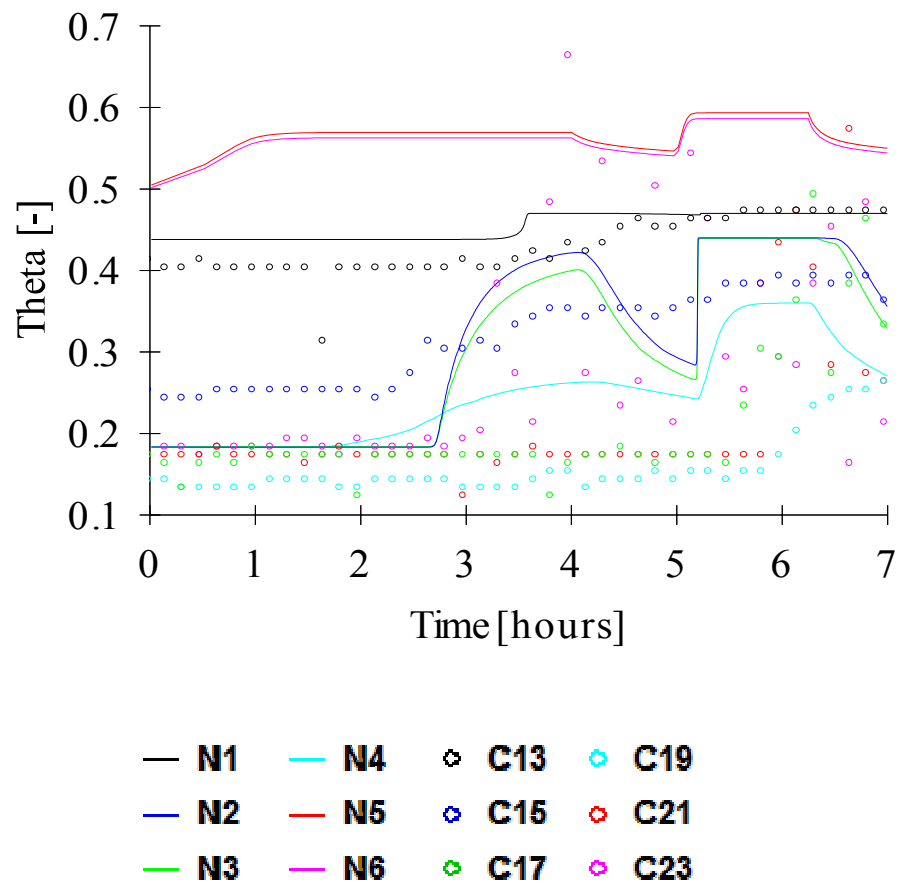


(a)



(b)

Fig. II-16. Water flux at the bottom boundary for (a) domain with fractures and (b) domain without fractures.



Observation node	TDR probe #	Simulated response	Measured response
1	11	N1	C13
2	7	N2	C15
3	6	N3	C17
4	9	N4	C19
5	2	N5	C21
6	3	N6	C23

Fig. II-17. Measured and simulated flow responses for first dye-tracer test for a 7 hour period for a domain with fractures. The table provided below the graph lists each observation and their corresponding sensor numbers node used when the model was run in inverse mode.

Table II-5 lists the final van Genuchten parameters that were used in the model domain with fractures. The  $K_s$  and  $\alpha$  values (for all materials except the clay layer) were obtained by inverse estimation. All parameters obtained by the neural network predictions for the clay layer were kept constant. The values of  $n$ ,  $l$ ,  $\theta_r$  and  $\theta_s$  for all other layers were also kept constant.

Table II-5. Final van Genuchten parameters for different geologic units for model domain with fractures

Material	Geologic unit	$\theta_r$ [m <sup>3</sup> m <sup>-3</sup> ]	$\theta_s$ [m <sup>3</sup> m <sup>-3</sup> ]	$\alpha$ [m <sup>-1</sup> ]	$n$	$K_s$ [mhr <sup>-1</sup> ]	$l$
1	Litter/Organic	0.14	0.61	2.37†	1.3	31.09†	0.5
2	Conduit	0.18	0.44	8.56†	3	40.5†	0.5
3	Upper limestone	0.12	0.17	5.16†	1.3	0.085†	0.5
4	Lower limestone/Marl	0.12	0.17	3.97†	1.3	0.049†	0.5
5	Clay	0.31	0.47	1.7	1.25	0.012	0.5

† Calibrated parameters by inverse modeling

## Discussion

For all the rainfall simulation events carried out at the plot, the sub-surface flow at the trench always occurred in two distinct modes. The fast flow (response time within 3 hours) occurred as outflow from the face of the trench, and the slow flow (response time within 15-30 hours) recorded by the TDR probes. During large rainfall events, some TDR probes responded similar to the fast flow, which indicated exchange between the two flow domains. Besides occurring mostly from the fractures of the upper limestone unit, the fast flow also occurred at 3-4 places from the tips of small roots that

protruded from the upper litter layer, loam layer and clay layers. We observed that the larger fractures within the upper limestone unit housed some large root structures while the loam and clay layers were characterized by small roots. We believe that the smaller roots of the invasive junipers are conveniently located in the clay layers so that they have access to adequate water supply. Moreover, the larger roots accentuate the larger fractures that exist in the upper limestone unit by ‘wedging’ or enlarging them. During the rainfall simulations, we also observed that rate of discharge of the fast flow at the trench varied at different locations of the trench. At some places, it occurred as drips from the small root tips and at other locations, the discharge was as high as 0.5 liters/second. The high flow usually occurred at large fracture openings (10 mm aperture) within the upper rock layer. Based on the fracture size, the Reynolds number for this particular flow event was 509, reflecting turbulent flow. The slow flow component usually occurred through the smaller fractures or pores present at the trench and its onset usually lagged behind the fast component by 20 to 25 hours for each simulation event.

The two-dimensional flow modeling used in this study provided further insights to the hydrology at the plot including: i) the two dimensional flow domain with fractures/conduits differentiated between preferential flow and conduit flow, the latter having a much higher flow velocity than the former, ii) the model effectively captured the exchange phenomenon that occurred between the conduits (with high conductivity) and limestone units/clay layers (having relatively low conductivities), iii) the model provided detailed hydrologic characterization of each geologic unit (van Genuchten

parameters for soil water retention and hydraulic conductivity functions) in a karst environment with juniper trees, iv) it also provided detailed information about water fluxes at the boundaries (seepage face and lower boundary) which provided valuable insights about the overall characteristics of sub-surface flow in such regions, v) the model demonstrated the role played by fractures/roots in enhancing vertical sub-surface flow and vi) the model assisted in water balance calculations. While this modeling effort provides these benefits, the main disadvantage of such a model is the over-simplified fracture network which does not accurately represent the real network of roots and fractures. Furthermore, water fluxes at the seepage face cannot be compared to the actual volume of water collected at the trench from the sump pump because the model uses a two-dimensional flow domain rather than a three-dimensional one.

### **Conclusions**

The fast outflow observed at various locations on the trench face was preferential flow through fractures of the limestone units and the juniper roots. The responses of the dyes at the trench indicate that juniper roots as well as fractures played a significant role in the proliferation of preferential flow processes that occurred in this region. The preferential flow occurred as a combination of laminar as well as turbulent flow. The responses of the preferential flow demonstrated comparable characteristics for similar boundary conditions. Furthermore, outflow responses at the trench face were a result of preferential flow processes occurring within the front half of the plot. When the fracture sizes were sufficiently large ( $> 10$  mm), preferential flow occurred in a turbulent (non-Darcian) mode and could be termed as conduit flow. The slow flow that was registered

by the probes was the matrix flow that occurred through the smaller fractures and pores. The matrix flow responses illustrated a negative linear relationship with rainfall intensity and a positive linear relationship with initial moisture content. The matrix flow responses were lowest during high rainfall events with low initial moisture content. Matrix flow usually lagged behind preferential flow; nevertheless, during large rainfall events, there was exchange of flow between the fractures/roots and matrix and the emulated responses similar to preferential flow.

At the study plot, sub-surface flow processes (affected by juniper roots and fractures in the rocks) occurred essentially in a tri-modal fashion (preferential flow + matrix flow + conduit flow), which was in accordance with the triple porosity models of flow through fractured media. This feature is well documented in previous studies by Ford and Williams (1989), White (1998), Martin et al. (2001), Spangler (2002), and Kaufmann (2003).

From the modeling perspective, it is evident that the hydraulic parameters need to be further calibrated to improve the modeling response based on the observed ones. In addition, the fracture network can be improved by using sophisticated characterization and modeling techniques. Nevertheless, this ecohydrologic experiment-modeling study does provide an introductory knowledge about various hydraulic parameters and the hydraulic responses in the shallow subsurface in the Edwards Aquifer region with karst geology and juniper cover. The model was useful in predicting the exchange processes as well as characterizing the difference between preferential and conduit flow. It also

demonstrated the role played by the fractures in increasing vertical sub-surface flow when compared to a domain without any fractures.

## CHAPTER III

SOIL HYDRAULIC PARAMETERS AND THEIR SPATIO-TEMPORAL  
VARIATIONS IN A TEXAS VERTISOL

The knowledge of soil hydraulic parameters and their spatio-temporal variation is crucial for estimating the rate of water and solute movement within the vadose zone. Tension infiltrometers are widely used for determining soil hydraulic parameters *in situ*. The objective of this paper is to determine soil hydraulic parameters (steady infiltration rate,  $i_f$ , saturated hydraulic conductivity,  $K_{sat}$ , unsaturated hydraulic conductivity,  $K(\Psi)$  and unsaturated flux density  $\Phi(\Psi)$ ) of a clay-dominated vertisol near College Station, Texas using tension infiltrometers. Moreover, the impact of varying disc diameters (measurement support) on the steady state infiltration rate ( $i_f$ ) and its spatio-temporal variations were also investigated. The experimental study was conducted within a 20 m X 16 m plot over a 21-month period to investigate the temporal variability of soil hydraulic parameters under varying environmental conditions.

Infiltration occurred in a bi-modal fashion consisting of preferential flow (occurring at  $\Psi = -0.05$  to 0 m) and matrix flow (occurring at  $\Psi = -0.2$  to  $-0.1$  m). Macropores and roots present in the soil resulted in gravity dominated flow near saturation ( $\Psi = -0.05$  to 0 m) for all experiments. Statistical analyses of  $i_f$  at varying soil water pressures suggested that  $i_f$  variability between different disc diameters and different sites was more enhanced for  $\Psi = -0.05$  to 0 m as compared to  $\Psi = -0.2$  to  $-0.1$



m. In addition, hydraulic parameters at four different locations within the experimental plot did not show significant spatial variability. However, statistically significant differences in  $i_f$  were observed between 0.2 and 0.24 m disc diameters at  $\Psi = 0$  m over the 21-month period. Furthermore, the  $i_f$  values demonstrated strong temporal variations over the 21 month period based on natural environmental conditions.

### **Introduction**

The investigation of soil hydraulic parameters is important for characterizing the rate of water flow and fate of contaminant transport through the vadose zone. Various studies (Clothier and White, 1981; White and Sully, 1987; 1988; Ankeny et al., 1991; Messing and Jarvis, 1993; Logsdon and Jaynes, 1993; Mohanty et al., 1994 a, Mohanty et al., 1994 b, Lin et al., 1996) have been conducted to determine *in situ* near saturated hydraulic conductivities of soils using tension infiltrometers. Near saturated hydraulic parameters are important in characterizing preferential flow processes (Mohanty et al., 1997, Mohanty, 1999). The *in situ* measurements of  $K(\Psi)$  using a tension infiltrometer provides a better representation of near saturated flow conditions as compared to those obtained from laboratory analysis of soil cores (Shouse and Mohanty, 1998). In addition, the popularity of using these devices for *in situ* measurements arises from the fact that tension infiltrometers are portable and use relatively small quantities of water (Mohanty et al., 1994 b; Jarvis and Messing, 1995). Furthermore, tension infiltrometers can be used to measure both saturated and unsaturated hydraulic properties at the same location which eliminates spatial variability between samples (Lin, 1995)

It is well known that infiltration of water and chemicals in many field soils are enhanced by macropores (Logsdon and Jaynes, 1996; Mohanty et al., 1997, 1998, Shouse and Mohanty, 1998). Thus, spatial variation, size and interconnectedness of macropores would play a key role in determining the rate of influx through soils. The shrink/swell characteristics of soils as a result of drying/wetting (Lin et al., 1998) along with annual tillage practices, give rise to temporal variations in the soil parameters as well. Hence, precise predictions of water flow and the fate of chemicals applied to soils would entail a comprehensive understanding of the spatio-temporal variations of soil hydraulic parameters. Such studies of the transport of water and chemicals through the vadose zone would support water balance calculations and easily quantify groundwater contamination processes. Several studies have been conducted in the past to study the spatial and temporal variations of saturated hydraulic conductivities  $K_{sat}$ . Cassel and Nelson (1985) demonstrated a large temporal variation in  $K_{sat}$  at different depths in a laboratory soil column. Jaynes and Hunsaker (1989) did not observe significant temporal patterns of  $K_{sat}$  in the fields where they conducted their experiments. Starr (1990) reported temporal variations of  $K_{sat}$  values because of agricultural practices. Few independent spatial (Mohanty et al., 1994 a) or temporal (Lin et al., 1998) variability studies have been conducted for unsaturated hydraulic conductivity parameters in the past. Messing and Jarvis (1993) and Logsdon and Jaynes (1996) investigated the temporal variation in unsaturated hydraulic properties due to agricultural operations.

Messing and Jarvis, (1993) carried out tension infiltrometer studies on ploughed and unploughed plots in a clay soil between June and October 1991 in Sweden to

monitor the spatio-temporal aspects of both saturated as well as unsaturated hydraulic parameters. They observed strong temporal trends in  $K(\Psi)$  values which were a result of changes in the climatic conditions as well as tillage practices. They observed that reductions in the  $K(\Psi)$  values were most prominent in the pressure range varying between -0.04 m and -0.06 m. They also showed (using the  $t$ -test for analysis of variance) that temporal variations of  $K(\Psi)$  within soil water pressures of  $\Psi = -0.04$  to -0.06 m were statistically more prominent than their spatial variations. Logsdon and Jaynes, (1996) who conducted infiltration experiments in a cultivated field in Iowa observed strong temporal variability of  $K(\Psi = -0.15 \text{ m})$  during a period ranging from July 1991 to May 1992 matching four different agricultural operations and they asserted that this reflected the evolution of micropores with tillage. The  $K_{\text{sat}}$  values did not show consistent temporal variations but were more spatially correlated. The authors attributed this phenomenon to the influence of macropores which were unstable due to tillage, shrink/swell and root activities. Lin et al., (1998) observed that spatial variability of  $K(\Psi)$  values at low tension could be related to soil macropore distribution in vertisols and vertic integrades in Texas. They also noticed marked temporal variations of  $K(\Psi = -0.03 \text{ m})$  and  $K_{\text{sat}}$  values over a three month period between August and October. They attributed this to the shrink/swell characteristics of the clay due to the variations in precipitation during the measurement period. These limited past studies document the need for conducting more *in situ* experiments using tension infiltrometers for determining the saturated and unsaturated soil hydraulic parameters and address the impacts of their induced/natural spatio-temporal variations across different space and

time scales on various applications like agricultural activities, surface hydrology, land-atmosphere feedback and groundwater contamination etc.

In this study we focused on spatio-temporal dynamics of unsaturated hydraulic parameters of a Texas vertisol occurring naturally over a longer duration (across a 21 month period) at one field plot. The objectives of this study included: 1. to conduct infiltration experiments using tension infiltrometers on a 20 m x 16 m plot near College Station, TX and determine the steady state infiltration rate  $i_f$  [ $\text{ms}^{-1}$ ], saturated hydraulic conductivity  $K_{\text{sat}}$  [ $\text{ms}^{-1}$ ], unsaturated hydraulic conductivity  $K(\Psi)$  [ $\text{ms}^{-1}$ ] and matric flux potential  $\Phi(\Psi)$  [ $\text{ms}^{-2}$ ], 2. to ascertain the effect of varying infiltration disc diameters/ measurement support sizes on the estimation of  $i_f$  rates, 3. to estimate the spatial variability of  $i_f$  within the experimental plot, and 4. to determine temporal variability of  $i_f$  within the plot over a 21 month period ranging from May 2003 to January 2005.

### **Site description and methodology**

The experimental site (30°31'N / 96°21'W) was an abandoned agricultural plot (20 x 16 m) located on the Brazos river flood plain within Texas A&M University field station near College Station, TX (Fig. III-1). The plot had previously been used for growing cotton, corn and grain sorghum. In the recent years, the vegetation in the plot consisted of Bermuda grass, and Bunch grass. The plot contained ships clay (2% sand, 32% silt and 66% clay) characterized by very-fine, mixed, thermic Chromic Hapluderts (Lin, 1995). The soil was taxonomically classified as a vertisol. Fig. III-2 illustrates the vegetation at the plot and crack formations on the soil. Tension infiltrometers based on the design of Perroux and White (1988) were used to conduct the *in situ* infiltration

experiments. Before commencing the experiments, the ground was prepared by removing the grass cover. The site was gently cleaned with a brush and a thin layer of contact sand was placed to provide good contact between the soil surface and the tension infiltrometer discs.

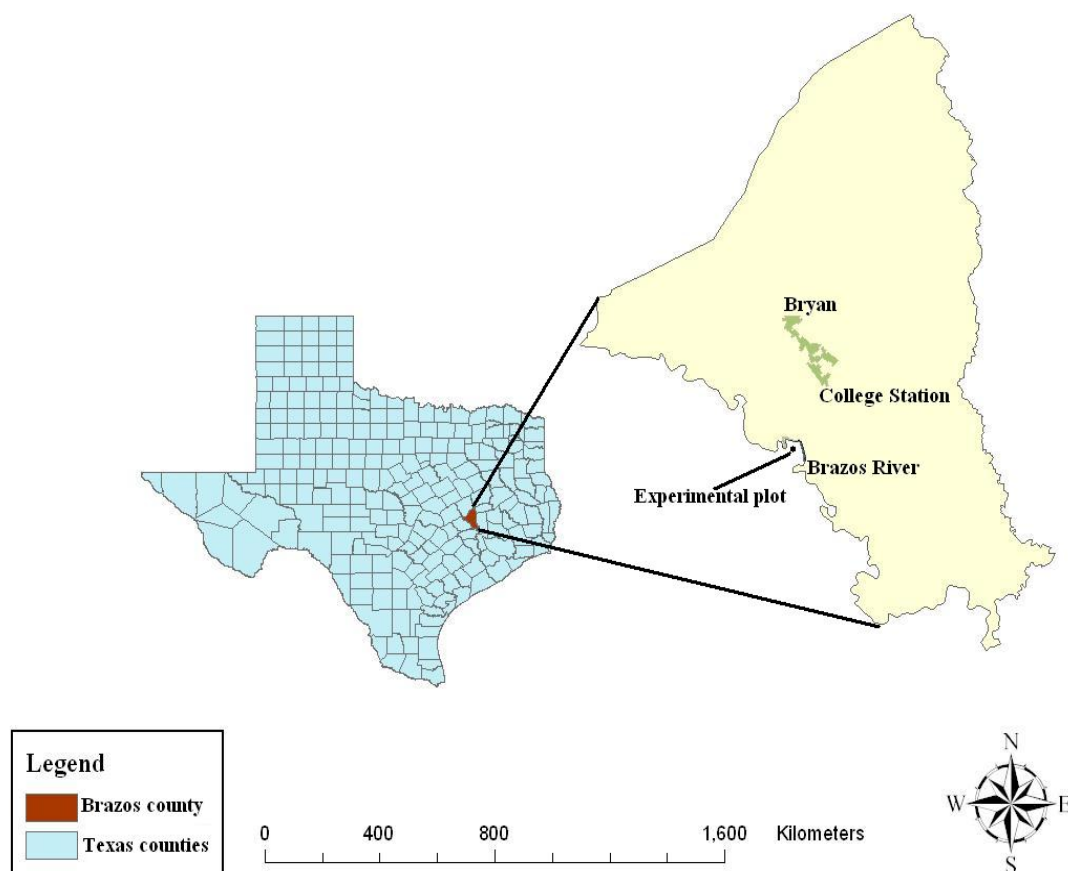


Fig. III-1. Location of experimental plot near College Station, TX.



Fig. III-2. Vegetation and surface cracks in soil within the experimental plot.

A metal ring was placed and inserted ( $\sim 1$ cm) to the ground around each disc (Fig. III-3). The infiltration experiments were conducted at 6 different soil water pressures ( $\Psi = -0.2\text{m}, -0.15\text{m}, -0.1\text{m}, -0.05\text{m}, -0.02\text{m}$  and  $0\text{m}$ ). The tension infiltrometer was pre-set to the first soil water pressure of  $-0.2\text{m}$ , the infiltration disc was placed above the contact sand and the infiltration experiments were carried out for the six different soil water pressures sequentially up to saturation ( $\Psi = 0\text{m}$ ). This type of ascending sequence of pressures was chosen over a descending sequence since the latter might cause air-entrapment leading to hysteresis (Reynolds and Elrick, 1991). Water in the supply tower of each infiltrometer was re-filled after an infiltration test at a particular soil water pressure. A pressure transducer was attached to the lower end of the supply tower of each infiltrometer to determine/monitor the flow rate by calibrating with water height (pressure head) during the experiment. Data was collected using Campbell scientific's datalogger (CR-10 X) using the PC208W version 3.3 (Campbell scientific, inc., Utah) software. The transducers were connected to the datalogger, which was programmed to record data at 30 second intervals. The antecedent volumetric water content of the soil at each location (within a meter from infiltrometer experiment) was measured using ML-2 (Dynamax<sup>®</sup>, Houston) theta probes. The experimental plot (20m X 16m) was divided into four sites (7m X 5m) as shown in Fig. III-4. The experiments were carried out on each site on a particular day. During each experiment, five tension infiltrometers with varying disc diameters ( $\delta = 0.24, 0.2, 0.17, 0.15, \text{ and } 0.1 \text{ m}$ ) were placed randomly in each site. Four experiments were conducted during a 12 day period in May 2003 and the data was used to determine the spatial variability of  $i_f$  rates within

the plot as well as the effect of varying disc diameters on the  $i_f$  rates. Subsequent to this short-duration (across 12 days) spatially extensive experiment and its findings, only two of the largest disc diameters (0.2 and 0.24m) were used to conduct follow up experiments at site 1 over a 21 month period to determine the nature of the temporal variability of  $i_f$  rates. Table III-1 lists the details of all the experiments carried out in the plot.



Fig. III-3. Infiltration disc placed on the soil. A thin layer of contact sand was applied for good contact between the disc and soil. The disc was surrounded by a metal disc to prevent any lateral flow.



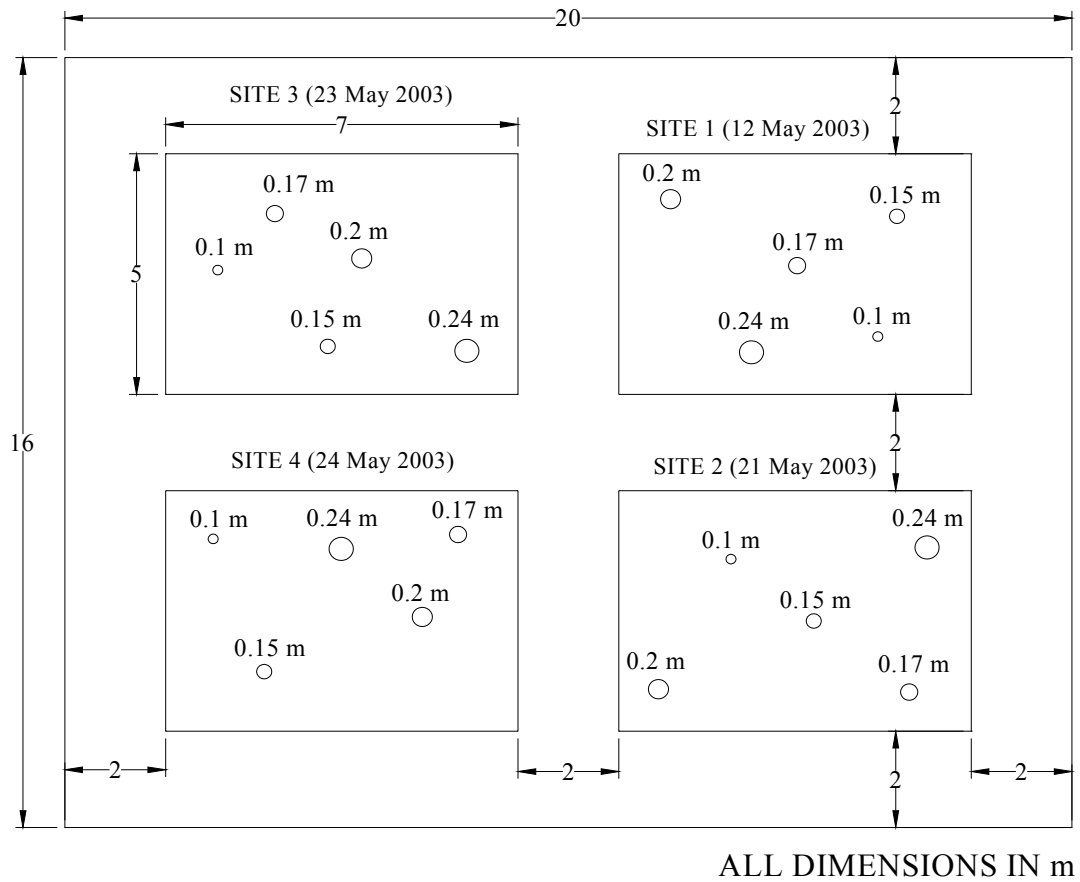


Fig. III-4. The 20 m x 16 m experimental plot divided into four (7 m x 5 m) sites with 2 m spacings from all sides. The circles in each site denote the different infiltration disc diameters used for the experiments. A typical experimental layout for May 2003 is illustrated.

Table III-1. Details of infiltration experiments over a 21 month period.

Date	Location	Tension infiltration disc diameter				
		0.1m	0.15m	0.17m	0.2m	0.24m
Number of discs used for each experiment						
12 May, 2003	Site 1	1	1	1	1	1
21 May, 2003	Site 2	1	1	1	1	1
23 May, 2003	Site 3	1	1	1	1	1
24 May, 2003	Site 4	1	1	1	1	1
24 June, 2003	Site 1	-	-	-	1	1
27 August, 2003	Site 1	-	-	-	2	2
16 March, 2004	Site 1	-	-	-	2	2
29 September, 2004	Site 1	-	-	-	2	2
22 October, 2004	Site 1	-	-	-	2	2
28 November, 2004	Site 1	-	-	-	2	2
28 December, 2004	Site 1	-	-	-	2	2
29 January, 2005	Site 1	-	-	-	2	2
					Total = 19	

### Data analysis

The calculation of the hydraulic parameters was based on the method given by Wooding (1968) and as adapted by Ankeny et al., (1991). This method has been chosen over other methods (White and Sully, 1987; Smettem and Clothier, 1989; Reynolds and Elrick, 1991; Logsdon and Jaynes, 1993; and Jarvis and Messing, 1995) because of its mathematical simplicity and convenient *in situ* measurement techniques. Wooding's relationship for unconfined steady-state water infiltration into soil from a circular pond of radius  $r$  [m] is given by

$$Q = \pi r^2 K + 4r\Phi \quad \text{[III-1]}$$

In the above equation,  $Q$  [ $m^3s^{-1}$ ] is the steady-state infiltrating flux,  $K$  [ $ms^{-1}$ ] is the field saturated hydraulic conductivity and  $\Phi$  [ $m^2s^{-1}$ ] is the matric flux potential given by Gardner, (1958). Measurements conducted at two potentials  $\Psi_1$  and  $\Psi_2$  and using the same radius for the infiltration disc gives the following two equations:

$$Q(\Psi_1) = \pi r^2 K(\Psi_1) + 4r\Phi(\Psi_1) \quad [III-2]$$

$$Q(\Psi_2) = \pi r^2 K(\Psi_2) + 4r\Phi(\Psi_2) \quad [III-3]$$

The data obtained from the datalogger was used to plot graphs of cumulative infiltration over time for each infiltration experiment at varying pressures. The steady state infiltration rate ( $i_f$ ) is obtained from the slope of the plot of cumulative infiltration vs. time. Thereafter, the steady state infiltration flux is obtained by multiplying the cross sectional area of the infiltration disk with the steady state infiltration rate.

$$Q(\Psi) = \pi r^2 i_f \quad [III-4]$$

Assuming a constant ( $K(\Psi)/\Phi(\Psi) = A$ ) ratio between the pressure range  $\Psi_1$  and  $\Psi_2$ , equations [III-2] and [III-3] can be re-written as:

$$Q(\Psi_1) = \left( \pi r^2 + \frac{4r}{A} \right) K(\Psi_1) \quad [III-5]$$

$$Q(\Psi_2) = \left( \pi r^2 + \frac{4r}{A} \right) K(\Psi_2) \quad [III-6]$$

Dividing [III-5] by [III-6], we get

$$K(\Psi_1) = Q(\Psi_1)/Q(\Psi_2) * K(\Psi_2) \quad [III-7]$$

Ankeny et al., (1991) also obtained an equation based on a numerical approximation, which is given by

$$[K(\Psi_1) - K(\Psi_2)]/A = \Delta\Psi [K(\Psi_1) + K(\Psi_2)]/2 \quad [III-8]$$

Substituting [III-7] in [III-8], and re-arranging, we get

$$A = 2[Q(\Psi_1) - Q(\Psi_2)] / \Delta\Psi [Q(\Psi_1) + Q(\Psi_2)] \quad \text{[III-9]}$$

Finally, we substitute [III-9] in [III-6] to obtain the value of  $K(\Psi_2)$  and then substitute this value in [III-7] to obtain the value of  $K(\Psi_1)$ . The values of  $K(\Psi)$  are then substituted in equations [III-2] and [III-3] to obtain the values of  $\Phi(\Psi)$ . Since 5 different disc diameters were used for this study, the above mentioned parameters were calculated for each disc diameter or measurement support. The parameters were also calculated separately for each site within the experimental plot.

The  $i_f$  values were used to determine the spatio-temporal variations as well as effect of varying disc diameters. A one way analysis of variance (ANOVA) test (Ott and Longnecker, 2001) was conducted to compare means using the different  $i_f$  values using a significance level  $\alpha = 0.5$ . The 'null hypothesis' for each ANOVA test was that the means for each group were equal. The decision of acceptance or rejection of the null hypothesis was based on the  $F_{\text{statistic}}$  and significance level ('p' values) for each test. The null hypothesis was rejected if the  $F_{\text{statistic}}$  value exceeded the cutoff value from the charts or if the 'p' value was lower than  $\alpha$ . Fig. III-5 illustrates the flow chart that was adapted for running the ANOVA test. Since five different disc diameters were used on each of the four sites during the 12-day period, there were 20 different  $i_f$ . Since each infiltration experiment was conducted in a descending sequence of 6 different soil water pressures, the ANOVA test was run separately for each pressure group for each of the 20 infiltration experiments. For determining the effect of varying disc diameters, the  $i_f$  values were divided into five groups of varying diameters (0.24, 0.2, 0.17, 0.15 and 0.1

m). Since the  $i_f$  values within each pressure group were not normally distributed, the  $\log_{10}$  transformed values were considered for the test to satisfy the condition of 'normality'. For the spatial variability analysis,  $i_f$  values were divided into 4 groups based on each site within the plot. The ANOVA test was run separately for each pressure group and the log-transformed values of the  $i_f$ .

It is essential to point out that the statistical power of both the ANOVA tests mentioned above is low because the number of data points ( $n = 4$  for investigating the effect of varying diameters and  $n = 5$  for the spatial variations) was very low (as there were only 4 experiments conducted at different sites within the plot in May, 2003). Since the experiments were repeated on site 1 using the 0.2 and 0.24 m diameter discs, a third ANOVA test was conducted to investigate the effect of varying diameters (0.2 and 0.24 m) on the soil hydraulic responses over a longer (21-month) period. In this case, there were 19 experiments ( $n = 19$ ) conducted during the 21-month period for each of the disc diameters. The ANOVA test was conducted separately for each soil water pressure group. Log-transformed values of  $i_f$  were used. The data set for the -0.05 m pressure group did not exhibit normality even after the log transformation and hence excluded from the test.

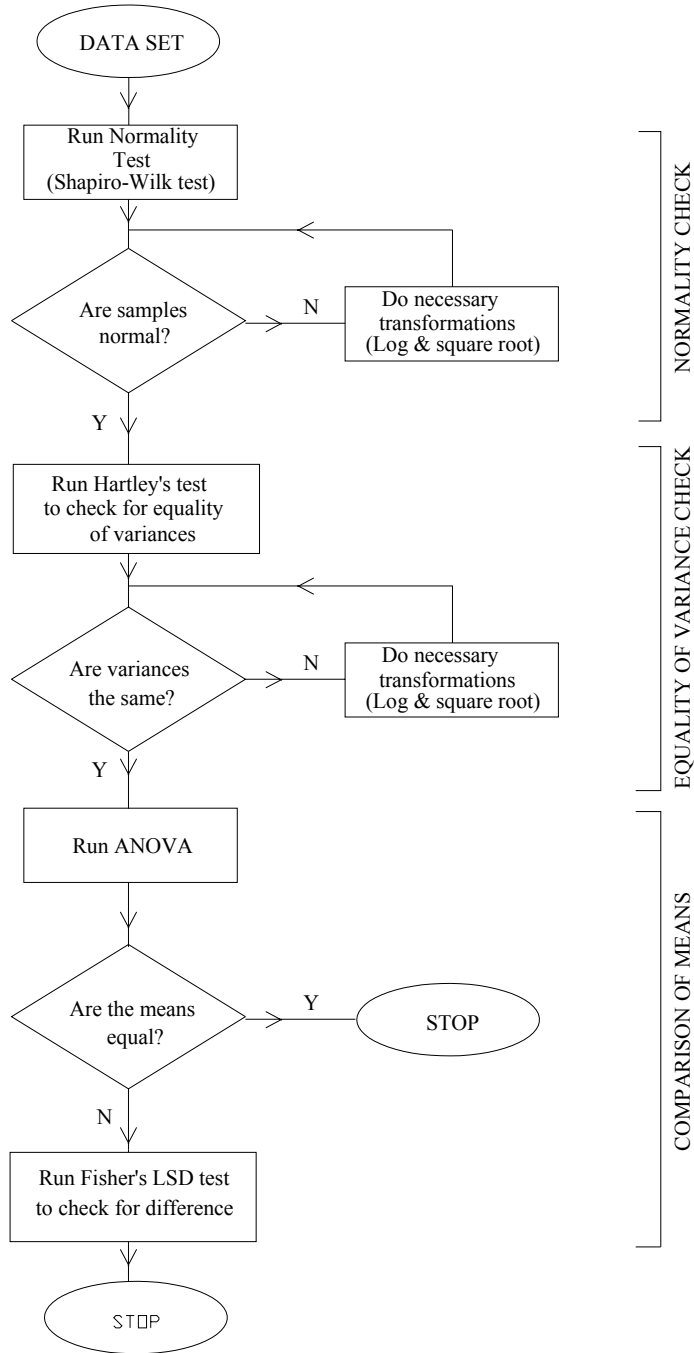


Fig. III-5. Flow chart adapted for running the one way analysis of variance (ANOVA) test.

## Results and discussions

Box plots of steady state infiltration rates ( $i_f$ ) for different disc diameters at 6 varying pressures are illustrated in Fig. III-6. Each box plot shows data from the 4 experiments that were conducted (one on each site) within the plot during the 12 day period in May 2003. It can be seen that the  $i_f$  increases as  $\Psi$  increases from -0.1 to 0 m. It is also seen that the values and variations of  $i_f$  are comparable at the pressure range  $\Psi = -0.2$  to -0.1m. The  $i_f$  rates show a sharp increase from  $\Psi = -0.05$ m to saturation (0 m). It is also evident that the variability of  $i_f$  rates is maximum at  $\Psi = -0.02$  and 0 m. This behavior can be attributed to the spatial variation of macropores and grass roots that act as preferential flow paths at pressures close to saturation (Hillel, 1980). Thus, the large variations in Fig. III-6 indicated that the sub-surface water flow at the plot was mostly driven by gravity through preferential flow paths at pressures close to saturation (Mohanty et al., 1997, Lin et al., 1997).

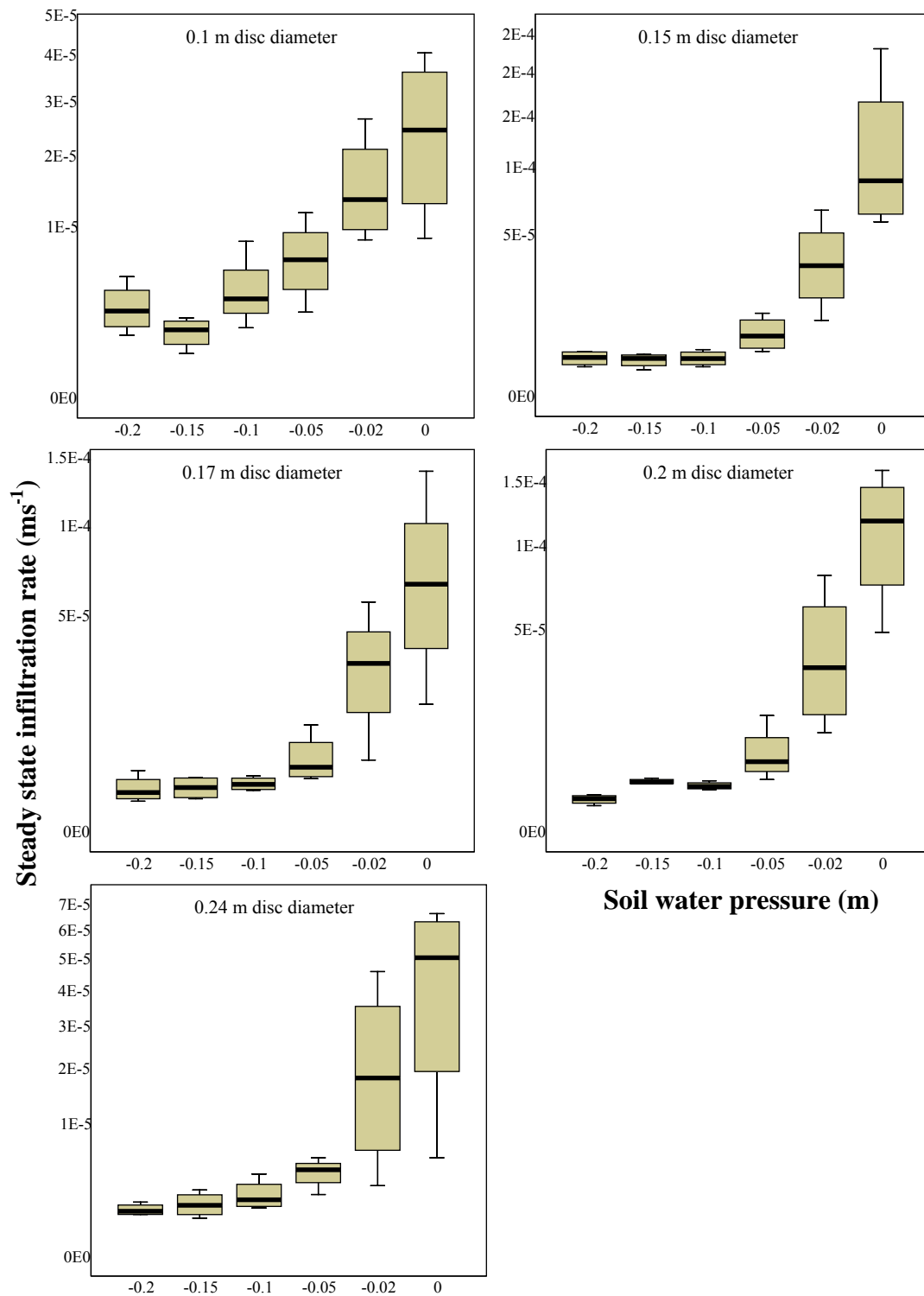


Fig. III-6. Box plots of steady state infiltration rates ( $i_f$ ) at different pressures for varying disc diameters.



Table III-2 shows the results of the ANOVA test for estimating spatial variability of  $i_f$  within the experimental plot. The  $F_{\text{statistic}}$  values were lower than the cutoff values from the charts and the significance level ('p' values) were higher than  $\alpha$  for each ANOVA test in a particular pressure range. Thus the null hypothesis (which stated that the means were equal) cannot be rejected which indicated that the means of the  $i_f$  values from each of the four sites within the experimental plot were equal. This indicated that for a particular soil water pressure, the soil hydraulic responses were similar throughout the experimental plot. This could be explained by the fact that hydraulic parameters estimated using the infiltrometers encompass the representative elementary volume (REV) of the soil (based on the support size/area under the disc diameter) and not specific flow paths like macropores and root channels (Mohanty et al., 1997). Hence, this lumped approach eliminates the individual effects of specific preferential flow paths resulting in homogeneous hydraulic characteristics throughout the field. This allowed us to conduct the subsequent infiltration experiments for determining the temporal variability at only one location, namely site 1.

Table. III-2. Results of one way analysis of variance (ANOVA) test for comparing the means of  $\text{Log } i_f$  values between four sites within the plot. Each soil water pressure range has been classified as a separate group for the comparison. 'df' denotes degrees of freedom, 'F' denotes the statistic value and 'Sig' denotes the significance 'p' value for the test for  $\alpha=0.5$ .

Variable		Sum of Squares	df	Mean Square	F	Sig.
Log $i_f$ ( $\Psi=-0.20$ )	Between Groups	0.072	3	0.024	0.418	0.742
	Within Groups	0.916	16	0.057		
	Total	0.988	19			
Log $i_f$ ( $\Psi=-0.15$ )	Between Groups	0.121	3	0.040	0.833	0.495
	Within Groups	0.774	16	0.048		
	Total	0.895	19			
Log $i_f$ ( $\Psi=-0.10$ )	Between Groups	0.023	3	0.008	0.185	0.905
	Within Groups	0.667	16	0.042		
	Total	0.690	19			
Log $i_f$ ( $\Psi=-0.05$ )	Between Groups	0.177	3	0.059	0.967	0.432
	Within Groups	0.974	16	0.061		
	Total	1.151	19			
Log $i_f$ ( $\Psi=-0.02$ )	Between Groups	0.402	3	0.134	0.931	0.449
	Within Groups	2.301	16	0.144		
	Total	2.702	19			
Log $i_f$ ( $\Psi=0$ )	Between Groups	0.115	3	0.038	0.192	0.901
	Within Groups	3.205	16	0.200		
	Total	3.320	19			

Table III-3. shows the results of the ANOVA test for determining the effect of disc diameters on  $i_f$ . Since the  $F_{\text{statistic}}$  values were lower than the cutoff values from the charts and the significance level ('p' values) were higher than  $\alpha$  for each ANOVA test in a particular pressure range, the null hypothesis (which stated that the means of  $i_f$  from

varying disc diameters were equal) cannot be rejected. This indicated that for a particular soil water pressure and under the specified experimental conditions, the soil hydraulic responses did not depend on the size of the infiltration disc. This also highlighted the fact the representative elementary volumes (REV's) of the soil (based on the area under the disc diameters) did not affect the soil hydraulic responses.

Table III-3. Results of one way analysis of variance (ANOVA) test for comparing the means of  $\text{Log } i_f$  values between varying disc diameters within the plot. Each soil water pressure range has been classified as a separate group for the comparison. ( $\alpha = 0.5$ ).

Variable		Sum of Squares	df	Mean Square	F	Sig.
Log $i_f$ ( $\Psi = -0.20$ )	Between Groups	0.426	4	0.107	2.848	0.061
	Within Groups	0.561	15	0.037		
	Total	0.988	19			
Log $i_f$ ( $\Psi = -0.15$ )	Between Groups	0.346	4	0.087	2.366	0.100
	Within Groups	0.549	15	0.037		
	Total	0.895	19			
Log $i_f$ ( $\Psi = -0.10$ )	Between Groups	0.133	4	0.033	0.899	0.489
	Within Groups	0.556	15	0.037		
	Total	0.690	19			
Log $i_f$ ( $\Psi = -0.05$ )	Between Groups	0.174	4	0.043	0.667	0.625
	Within Groups	0.977	15	0.065		
	Total	1.151	19			
Log $i_f$ ( $\Psi = -0.02$ )	Between Groups	0.460	4	0.115	0.770	0.561
	Within Groups	2.242	15	0.149		
	Total	2.702	19			
Log $i_f$ ( $\Psi = 0$ )	Between Groups	1.486	4	0.372	3.038	0.051
	Within Groups	1.834	15	0.122		
	Total	3.320	19			

Table III-4. shows the results of the ANOVA test for investigating the effect of two varying disc diameters on  $i_f$  during a 21 month period. The  $F_{\text{statistic}}$  and p values for all pressures groups except zero indicate that the disc diameters do not affect the  $i_f$ . For the zero pressure group, the  $F_{\text{statistic}}$  is higher than the cutoff value from the table and the p value is lower than  $\alpha$  which indicates that the means for  $i_f$  are significantly different for the two diameters used. This highlights the fact that variations in disc diameters affect soil hydraulic responses only at saturation and that it can be observed over a longer time frame due to alterations in pore features (e.g., buried or open to atmosphere) because of change in natural conditions at the field site. This variation is a result of the heterogeneity of the soil due to the presence of macropores/roots which are active at pressures close to saturation. This effect was negligible when the experiments were conducted during a 12 day period, probably because the soil properties (in other words pore spaces) did not change much during the short span of the experimentation period. Therefore, it can be concluded that variations in disc diameters encompassing different macroporosity influence temporal soil hydraulic properties at saturation.

Table III-4. Results of one way analysis of variance (ANOVA) test for comparing the means of  $i_f$  values between 0.2 and 0.24 m disc diameters. Each soil water pressure range has been classified as a separate group.

Variable		Sum of Squares	df	Mean Square	F	Sig.
$i_f(\Psi=-0.20)$	Between					
	Groups	6.5E-15	1	6.5E-15	0.013	0.909
	Within Groups	1.8E-11	36	5.0E-13		
	Total	1.8E-11	37			
$i_f(\Psi=-0.15)$	Between					
	Groups	5.7E-13	1	5.7E-13	0.769	0.386
	Within Groups	2.7E-11	36	7.5E-13		
	Total	2.7E-11	37			
$i_f(\Psi=-0.10)$	Between					
	Groups	1.2E-13	1	1.2E-13	0.209	0.650
	Within Groups	2.1E-11	36	5.9E-13		
	Total	2.1E-11	37			
$i_f(\Psi=-0.02)$	Between					
	Groups	2.6E-09	1	2.6E-09	1.424	0.241
	Within Groups	6.7E-08	36	1.9E-09		
	Total	7.0E-08	37			
$i_f(\Psi=0)$	Between					
	Groups	1.7E-08	1	1.7E-08	8.557†	0.006†
	Within Groups	6.9E-08	36	1.9E-09		
	Total	8.6E-08	37			

† Significant at  $\alpha = 0.5$

Note that in this test, Log values have not been considered since the  $i_f$  values demonstrated normality.

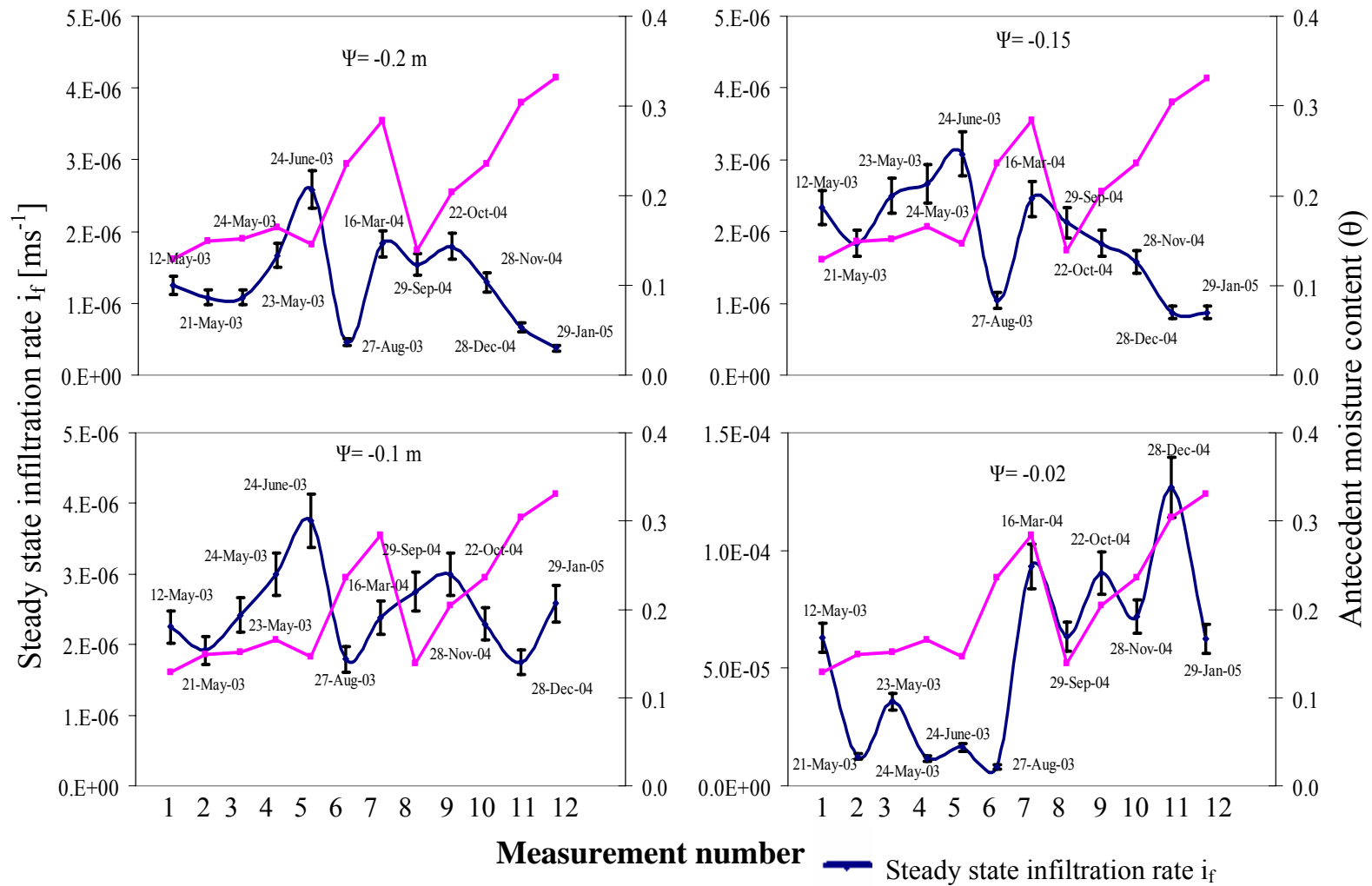


Fig.III-7. Temporal variability of  $i_f$  [ $\text{ms}^{-1}$ ] and antecedent moisture content  $\theta$  at varying pressures.

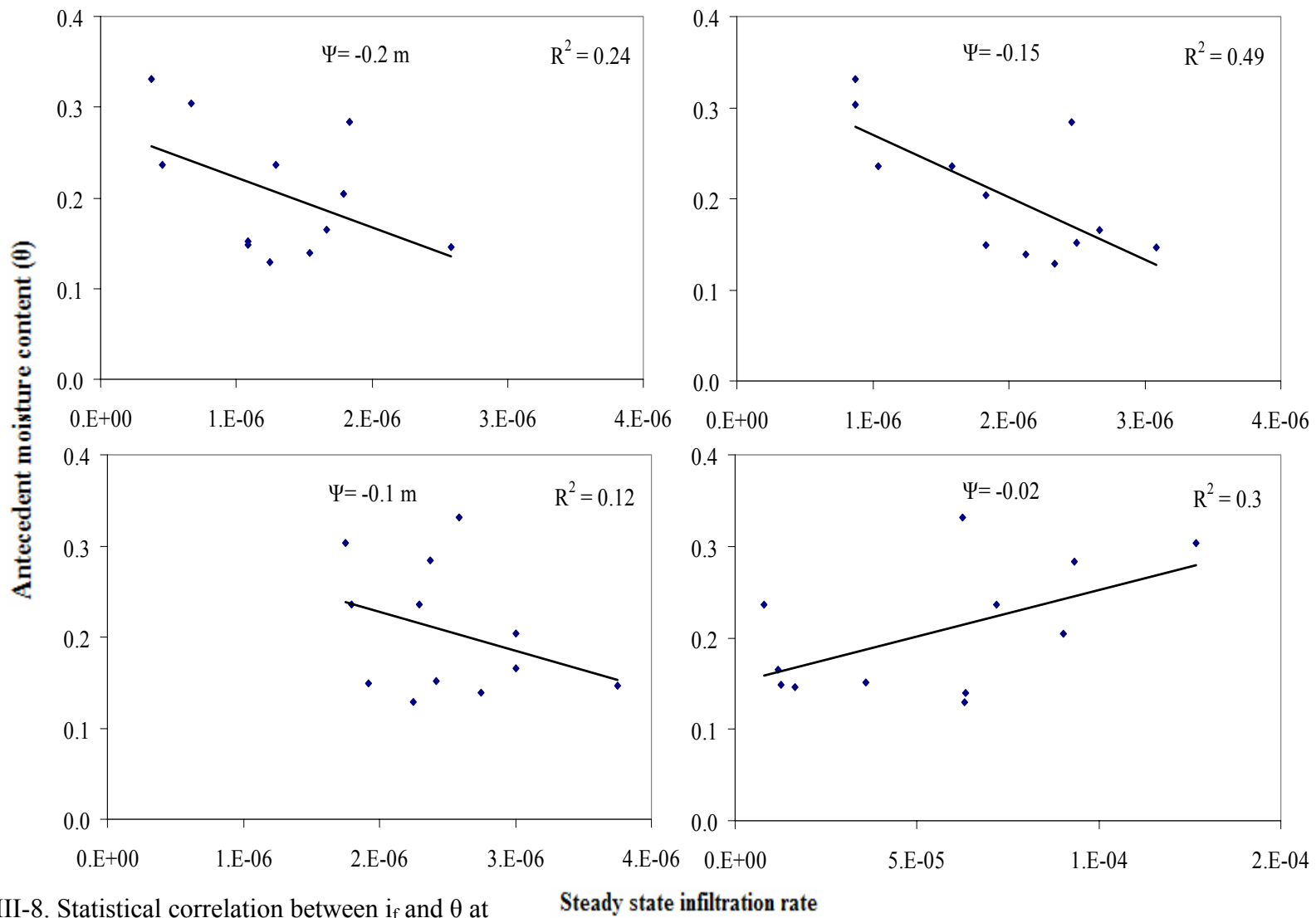


Fig. III-8. Statistical correlation between  $i_f$  and  $\theta$  at  $\Psi = -0.2, -0.15, -0.1$  and  $-0.02$  m.

Fig. III-7 shows the temporal variations of  $i_f$  and  $\theta$  from 12 May 2003 until 29 January 2005. The average  $i_f$  of both 0.2 and 0.24 m disc diameters are represented in the graphs together with 10% error bars. The average values were considered as the means of the 0.2 and 0.24 m diameters were statistically similar, based on the ANOVA test. The -0.05m pressure group was not considered since it was excluded in the ANOVA test. In addition, the zero pressure group was not included since the means for the two different disc diameters were significantly different. Although, the  $i_f$  values demonstrated strong seasonal variations at the given pressures ( $\Psi=0.2, 0.15, 0.1$  and  $0.02$  m), it was difficult to identify a common seasonal trend among  $i_f$  rates at different pressures as their behavior was different at different pressures. In addition, the  $i_f$  did not have any relationship with antecedent moisture content. This was further highlighted by observing the low correlation between  $i_f$  at different pressures and antecedent moisture content (Fig. III-8) during the 21-month period. Fig. III-9 (a) illustrates the temporal variations at saturation of  $i_f$  when a 0.2 m disc diameter was used and Fig. III-9 (b) shows the same when a 0.24 m disc diameter was used. The seasonal pattern of  $i_f$  between the two disc diameters was very dissimilar which strengthened the results of the ANOVA test, suggesting that at saturation, variations in infiltration disc diameters influenced  $i_f$  values.



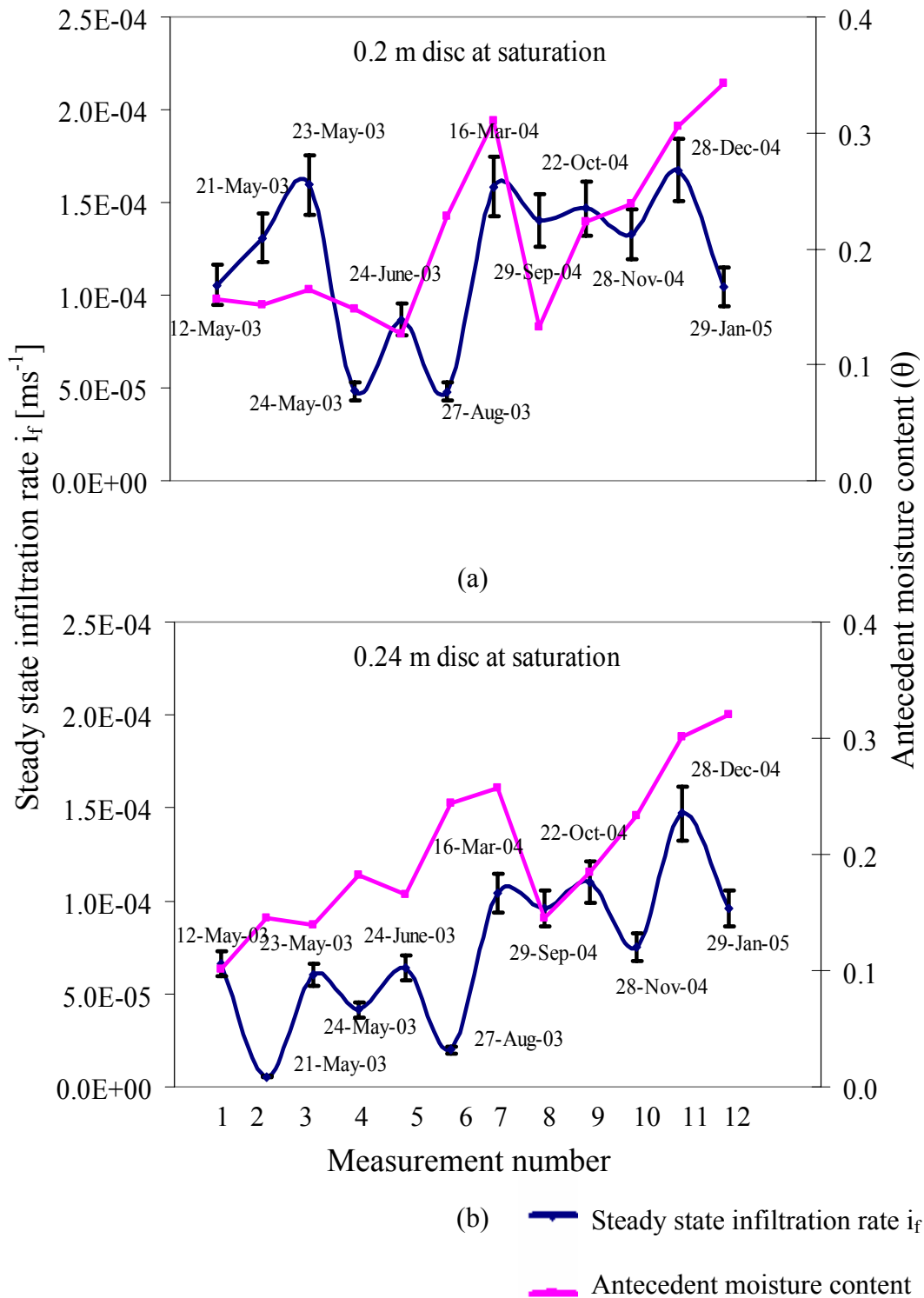
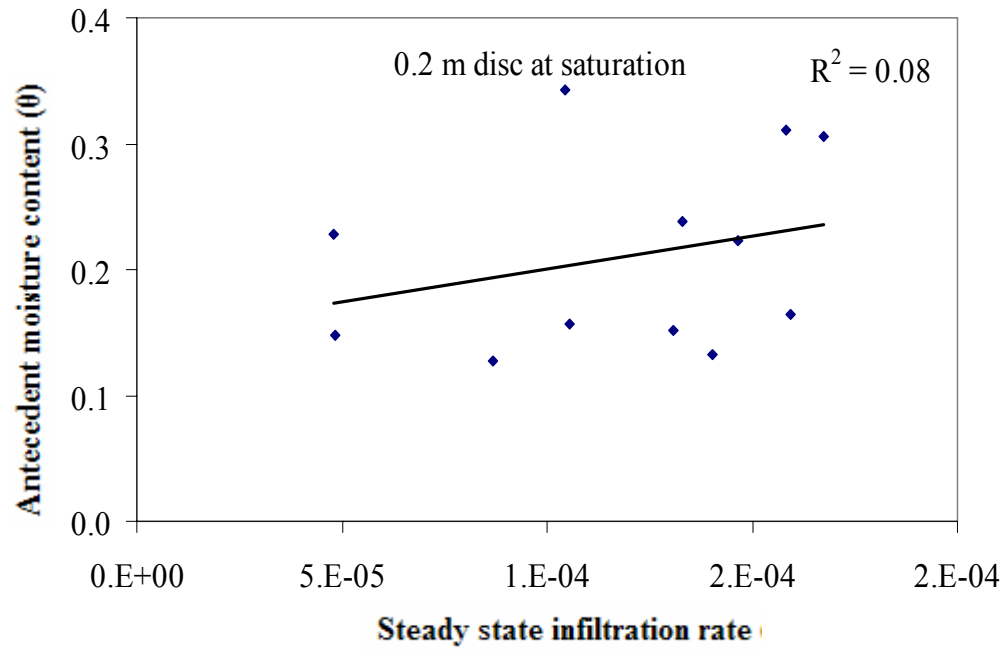
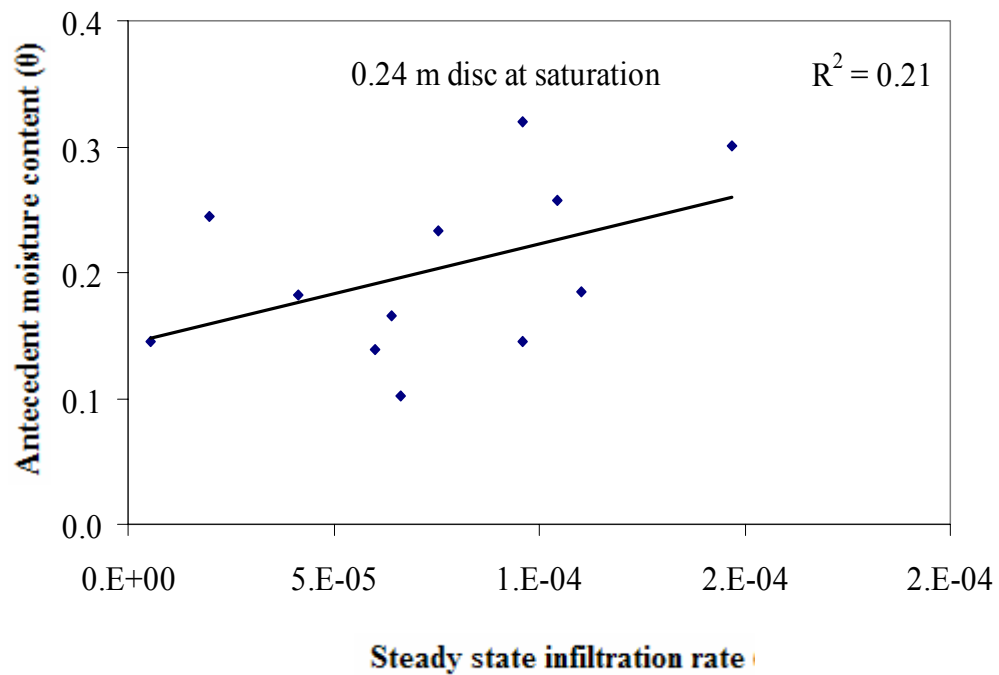


Fig. III- 9. Temporal variability of  $i_f$  and  $\theta$  at saturation for 0.2 and 0.24 m disc diameters.



(a)



(b)

Fig. III-10. Statistical correlation between  $i_f$  and  $\theta$  at saturation for 0.2 and 0.24 m disc diameters.

The  $i_f$  values did not show any significant relationship with  $\theta$ , and this was demonstrated by the low correlation between the  $i_f$  values for both disc diameters and  $\theta$  at saturation (Fig.III-10 (a) and (b)). These graphs provide us with valuable insights about the temporal variations of soil parameters based on natural environmental conditions. Combining the correlation results from Fig. III-8 and Fig. III-10, it was seen that the  $i_f$  values were inversely proportional to antecedent moisture content except at  $\Psi=-0.02$  m. Although, this behavior was similar to the shrink/swell characteristics of vertisols, the correlation coefficients were too low to be of any statistical significance. Hence, it can be concluded that soil within the plot did not exhibit sufficient shrink/swell characteristics. Table III-5. lists the unsaturated hydraulic parameters for site 1 for different disc diameters at varying pressures. These values would be effective in predicting the rate of water flow and contaminant transport at different scales. Furthermore, temporal variation of soil hydraulic conductivity due to natural conditions will bring unprecedented insight to soil-atmosphere-vegetation transfer (SVAT) modeling leading to better climate change predictions.

Table III-5. Soil hydraulic parameters of five different infiltration disc diameters at six soil water pressures during the 12 day period.

$\psi$	0.1m disc diameter			$\psi$	0.15m disc diameter		
	$i_f$	$K(\psi)$	$\Phi(\psi)$		$i_f$	$K(\psi)$	$\Phi(\psi)$
[m]	[ $ms^{-1}$ ]	[ $ms^{-1}$ ]	[ $m^2s^{-1}$ ]	[m]	[ $ms^{-1}$ ]	[ $ms^{-1}$ ]	[ $m^2s^{-1}$ ]
0	8.67E-06	5.54E-05	-1.84E-06	0	5.80E-05	4.64E-05	6.82E-07
-0.02	1.62E-05	5.41E-05	-1.49E-06	-0.02	1.10E-05	8.00E-06	1.76E-07
-0.05	1.17E-05	2.78E-06	3.49E-07	-0.05	3.83E-06	2.01E-06	1.07E-07
-0.1	8.83E-06	3.03E-06	2.28E-07	-0.1	2.17E-06	-4.28E-07	1.53E-07
-0.15	1.83E-06	-1.98E-06	1.50E-07	-0.15	3.17E-06	-1.58E-06	2.80E-07
-0.2	5.00E-06	-1.34E-05	7.21E-07	-0.2	3.67E-06	-7.63E-07	2.61E-07

$\psi$	0.17m disc diameter			$\psi$	0.20m disc diameter		
	$i_f$	$K(\psi)$	$\Phi(\psi)$		$i_f$	$K(\psi)$	$\Phi(\psi)$
[m]	[ $ms^{-1}$ ]	[ $ms^{-1}$ ]	[ $m^2s^{-1}$ ]	[m]	[ $ms^{-1}$ ]	[ $ms^{-1}$ ]	[ $m^2s^{-1}$ ]
0	1.39E-04	1.02E-04	2.42E-06	0	1.06E-04	5.46E-05	4.00E-06
-0.02	5.63E-05	4.29E-05	8.95E-07	-0.02	8.02E-05	5.18E-05	2.23E-06
-0.05	5.50E-06	3.43E-06	1.38E-07	-0.05	1.65E-05	1.20E-05	3.53E-07
-0.1	2.83E-06	5.36E-07	1.53E-07	-0.1	3.17E-06	7.82E-07	1.87E-07
-0.15	3.00E-06	3.98E-07	1.74E-07	-0.15	3.50E-06	6.48E-07	2.24E-07
-0.2	2.00E-06	6.96E-07	8.70E-08	-0.2	1.50E-06	8.35E-07	5.22E-08

$\psi$	0.24m disc diameter		
	$i_f$	$K(\psi)$	$\Phi(\psi)$
[m]	[ $ms^{-1}$ ]	[ $ms^{-1}$ ]	[ $m^2s^{-1}$ ]
0	6.63E-05	4.20E-05	2.30E-06
-0.02	4.58E-05	3.36E-05	1.16E-06
-0.05	5.50E-06	4.20E-06	1.22E-07
-0.1	1.33E-06	5.98E-07	6.92E-08
-0.15	1.17E-06	2.48E-07	8.65E-08
-0.2	1.00E-06	2.25E-07	7.30E-08

## Conclusions

The infiltration experiments demonstrated that infiltration in this region occurred in a bi-modal fashion consisting of preferential flow and matrix flow. The preferential/bypass flow occurred at soil water pressures ranging from  $\Psi = -0.05$  to  $0$  m and matrix flow occurred at  $\Psi = -0.2$  to  $-0.1$  m. Preferential flow was characterized by high  $i_f$  values and matrix flow was characterized by low  $i_f$  values. The macropores/roots resulted in gravity-dominated infiltration of water at pressures ranging from  $-0.05$  m to  $0$  m which caused substantial variability of the  $i_f$  at these pressures as compared to the higher negative soil water pressures. The effect of these preferential flow was absent at larger soil water pressures ( $-0.2$  m to  $-0.1$  m). The experimental plot of  $20$  m x  $16$  m demonstrated homogeneity of steady state infiltration rates based on the one way analysis of variance (ANOVA) test during the 12 day period in May 2003. Also, during this 12 day period, the variations of infiltration disc diameters had no effect on the soil hydraulic responses at soil water pressures  $\Psi = -0.2, -0.15, -0.1, -0.05, -0.02$  and  $0$  m. However, the effect of difference in diameter was observed when two different diameters ( $0.2$  and  $0.24$  m) were used to compare the  $i_f$  values for a 21 month period. It was observed (based on the ANOVA test) that the means of  $i_f$  values were significantly different between the two diameters only at saturation ( $\Psi = 0$ ). This could be attributed to the effects of macropores/roots present within the soil that become active at pressures close to saturation. Interestingly, the ANOVA test conducted to compare the effect of varying diameters during the 12-day period resulted in similar means of  $i_f$  for all disc diameters even at saturation. This would indicate that the macropore/root activity which

caused variations in soil hydraulic responses between different disc diameters was prominent only at saturation over a long duration of time. Although, we observed strong seasonal variations of  $i_f$  from May 2003 to January 2005, the  $i_f$  values were not significantly influenced by changes in the antecedent moisture contents of the soil, suggesting that the soil within the experimental plot did not exhibit sufficient shrink/swell properties. Based on the nature and methodology of the infiltration experiments conducted, it can be concluded that the hydraulic properties of the soil at the field site were not dependent on the antecedent moisture conditions, as measured using theta probes. Alternate methods of measuring soil moisture content and conducting infiltration experiments on a regular basis on the plot might provide better insights about the relationships between soil hydraulic parameters and antecedent soil moisture contents. Such long-term temporal variations in soil hydraulic properties will help improve the land-atmosphere feedback and long-term climate predictions using General Circulation Models (GCM's).

## CHAPTER IV

### GENERAL CONCLUSIONS

This study deals with process of infiltration of water at two contrasting hydrologic scenarios in Texas. Although, the two experiments were conducted at two completely different environmental settings, they are intrinsically very similar because they both highlight the importance of preferential/bypass flow that influences the process of infiltration. The experiments conducted at Honey creek illustrated that sub-surface flow occurred in a tri-modal manner. Within a karst environment dominated by juniper roots, the water essentially flowed through the large conduits, planar limestone fractures and the soil matrix. The flow path as well as the flow times of each type of flow was different. While the conduit flow occurred within 2-3 hours as turbulent flow from the start of a rainfall simulation through the large sized fractures, the fracture flow occurred as a combination of relatively slower flow from the small sized fractures and drips from the root tips within the trench face. The flow through the soil matrix usually reached the trench face after 25-30 hours from the start of the rainfall simulation (as registered by the TDR probes). The detailed characterization of this rapid bypass flow would eventually provide valuable insights about the recharge rates to the Edwards Aquifer besides determining the groundwater contamination processes. The HYDRUS-2D model simulated sub-surface flow characteristics like exchange processes and difference between conduit and preferential flow that was observed at the trench face during

experiments. Besides providing detailed hydrologic characterization of various geologic layers as observed at the trench face, it illustrated the role played by fractures/roots in proliferating vertical preferential flow.

The infiltration experiments conducted at the agricultural field using tension infiltrometers demonstrated the ability of macropores/roots to become active agents of preferential flow paths at soil water pressures close to saturation ( $\Psi = -0.05$  to  $0$  m). The steady state infiltration rates of the vertisol increased exponentially as the infiltration experiments were conducted in a descending sequence of soil water pressures, reaching a maximum at saturation. Analogous to the previous experiment, the process of infiltration occurred in a bi-modal fashion consisting of matrix flow (which occurred at suctions  $\Psi = -0.2$  to  $-0.1$  m) and bypass/preferential flow which occurred at  $\Psi = -0.05$  to  $0$  m. The steady state infiltration rates showed strong seasonal variations over a 21 month period based on natural environmental conditions. Thus, the natural and environmental conditions like biological activities (worm holes, root decay etc), ecology and geology influence the mechanism of preferential flow. At the Edwards Plateau, the juniper roots and limestone fractures were the main agents of preferential flow, whereas at the agricultural field, the macropores and grass/shrub roots were responsible for bypass flow.



## REFERENCES

- Ankeny M.D., M. Ahmed, T.C. Kaspar, and R. Horton. 1991. Simple field method for determining unsaturated hydraulic conductivity. *Soil. Sci. Soc. Am. J.* 55:467-470.
- Archer, S. 1994. Woody plant encroachment into southwestern grasslands and savannas: Rates, patterns and proximate causes. *In* M. Vavra, W. A. Laycock, and R. D. Pieper, (eds). *Ecological implications of livestock herbivory in the West*. Society for Range Management, Denver, Colo. 13-68.
- ASTM, American Society for Testing and Materials. 1961. Methods for grain-size analysis of soils. *ASTM Standards* 1961. 4:1271-1283.
- Barrett, M.E., and R.J. Charbeneau. 1997. A parsimonious model for simulating flow in a karst aquifer. *Journal of Hydrology*. 196:47-65.
- Cassel, D.K., and L.A. Nelson. 1985. Spatial and temporal variability of soil physical properties. *Soil Tillage Res.* 5:5-17.
- Clothier, B.E., and I. White. 1981. Measurement of sorptivity and soil water diffusivity in the field. *Soil. Sci. Soc. Am. J.* 45:241-245.
- DiCarlo, D.A., T.W.J. Bauters, C.J.G. Darnault, T.S. Steenhuis, and J.Y. Parlange. 1999. Lateral expansion of preferential flow paths in sands. *Water Resour. Res.* 35:427-434.
- Dugas, W.A., and R.A. Hicks. 1998. Effect of removal of *Juniperus ashei* on evapotranspiration and runoff in the Seco Creek watershed. *Water Resour. Res.* 34:1499-1506.
- Edwards Aquifer Bibliography. 2003. Available at [www.edwardsaquifer.org](http://www.edwardsaquifer.org). Accessed on August, 2004.
- Flint, L.E. 2003. Physical and hydraulic properties of volcanic rocks from Yucca Mountain, Nevada. *Water Resour. Res.* 39:5:1119.
- Ford D.C., and P.W. Williams. 1989. *Karst geomorphology and hydrology*. University Press, Cambridge, Great Britain.
- Gardner, W.R. 1958. Some steady-state solutions of the unsaturated moisture flow equation with applications to evaporation from a water table. *Soil Science*. 85:228-232.

- Greene, E.A., A.M. Shapiro, and J.M. Carter. 1999. Hydrogeologic characterization of the Minnelusa and Madison aquifers near Spearfish, South Dakota. US Geological Survey., Water Resour. Inv. Rept . 98:4156-4164.
- Hillel, D. 1980. Fundamentals of soil physics. Academic Press, Toronto.
- Jackson, R.B., H.J. Schenk, E.G. Jobbagy, J. Canadell, G.D. Colello, R.E. Dickinson, C.B. Field, P. Friedlingstein, M. Heimann, K. Hibbard, D.W. Kicklighter, A. Kleidon, R.P. Neilson, W.J. Parton, O.E. Sala, and M.T. Sykes. 2000. Belowground consequences of vegetation change and their treatment in models. *Ecol. Appl.* 10:470-483.
- Jarvis N.J., and I. Messing. 1995. Near-saturated hydraulic conductivity in soils of contrasting texture measured by tension infiltrometers. *Soil. Sci. Soc. Am. J.* 59:27-34.
- Jaynes, D.B., and D.J. Hunsaker. 1989. Spatial and temporal variability of water content and infiltration on a flood irrigated field. *Transactions of the ASAE.* 32:1229-1238.
- Kaufmann, G. 2003. A model comparison of karst aquifer evolution for different matrix-flow formulations. *J. Hydrol.* 283:281-289.
- Keeler, R.R., and Y.K. Zhang. 1997. Modeling of groundwater flow in a fractured-karst aquifer in the Big Springs Basin, Iowa. *Geol. Soc. Am., Abs. Programs.* 29(4):25.
- Kuniansky, E.L., L. Fahlquist, and A.F. Ardis. 2001. Travel times along selected flow paths of the Edwards aquifer, Central Texas. U.S. Geological Survey Water-Resources Investigations Report. 01- 4011:69-77.
- Lin H.S. 1995. Hydraulic properties and macropore flow of water in relation to soil morphology. Ph.D. dissertation. Texas A&M University. Available at <https://txspace.tamu.edu>
- Lin, H.S., K.J. McInnes, L.P. Wilding, and C.T. Hallmark. 1996. Effective porosity and flow rate with infiltration at low tension into a well-structured subsoil. *Transactions of the ASAE.* 39(1):131-133.
- Lin, H.S., K.J. McInnes, L.P. Wilding, and C.T. Hallmark. 1997. Low tension water flow in structured soils. *Can. J. Soil Sci.* 77:649-654.

- Lin, H.S., K.J. McInnes, L.P. Wilding, and C.T. Hallmark. 1998. Macroporosity and initial moisture effects on infiltration rates in vertisols and vertic intergrades. *Soil Science*. 163:2-8
- Loaiciga H.A., D.R. Maidment., and J.B. Valdes. 2000. Climate-change impacts in a regional karst aquifer, Texas, USA. *Journal of Hydrology*. 227:173-194.
- Logsdon, S.D., and D.B. Jaynes. 1993. Methodology for determining hydraulic conductivity with tension infiltrometers. *Soil. Sci. Soc. Am. J.* 57:1426-1431.
- Logsdon, S.D., and D.B. Jaynes. 1996. Spatial variability of hydraulic conductivity in a cultivated field at different times. *Soil. Sci. Soc. Am. J.* 60:703-709.
- Martin, J.B., and E.J. Sreaton. 2001. Exchange of matrix and conduit water with examples from the Floridian aquifer. U.S. Geological Survey Karst Interest Group Proceedings, Water-Resources Investigations Report. 01-4011:38-44.
- Messing, I., and N.J. Jarvis. 1993. Temporal variation in the hydraulic conductivity of a tilled clay soil as measured by tension infiltrometers. *J. of Soil Science*. 44:11-24.
- Mohanty, B.P., M.D. Ankeny, R. Horton, and R.S. Kanwar. 1994 a. Spatial analysis of hydraulic conductivity measured using disc infiltrometers. *Water Resour. Res.* 30(9):2489-2498.
- Mohanty, B.P., R.S. Kanwar, and C.J. Everts. 1994 b. Comparison of saturated hydraulic conductivity measurement methods for a glacial-till soil. *Soil. Sci. Soc. Am. J.* 58:672-677.
- Mohanty B.P., R.S. Bowman, J.M.H. Hendrickx, and M.T. van Genuchten. 1997. New piecewise-continuous hydraulic functions for modeling preferential flow in an intermittent flood-irrigated field. *Water Resour. Res.* 33(9):2049-2063.
- Mohanty B.P., T.H. Skaggs and M.T. van Genuchten. 1998. Impact of saturated hydraulic conductivity on the prediction of tile flow. *Soil Sci. Soc. Am. J.* 62:1522-1529.
- Mohanty, B.P. 1999. Scaling hydraulic properties of a macroporous soil. *Water Resour. Res.* 35(6):1927-1931.
- Mualem, Y. 1976. A new model for predicting the hydraulic conductivity of unsaturated porous media. *Water Resour. Res.* 12(3):513-522.

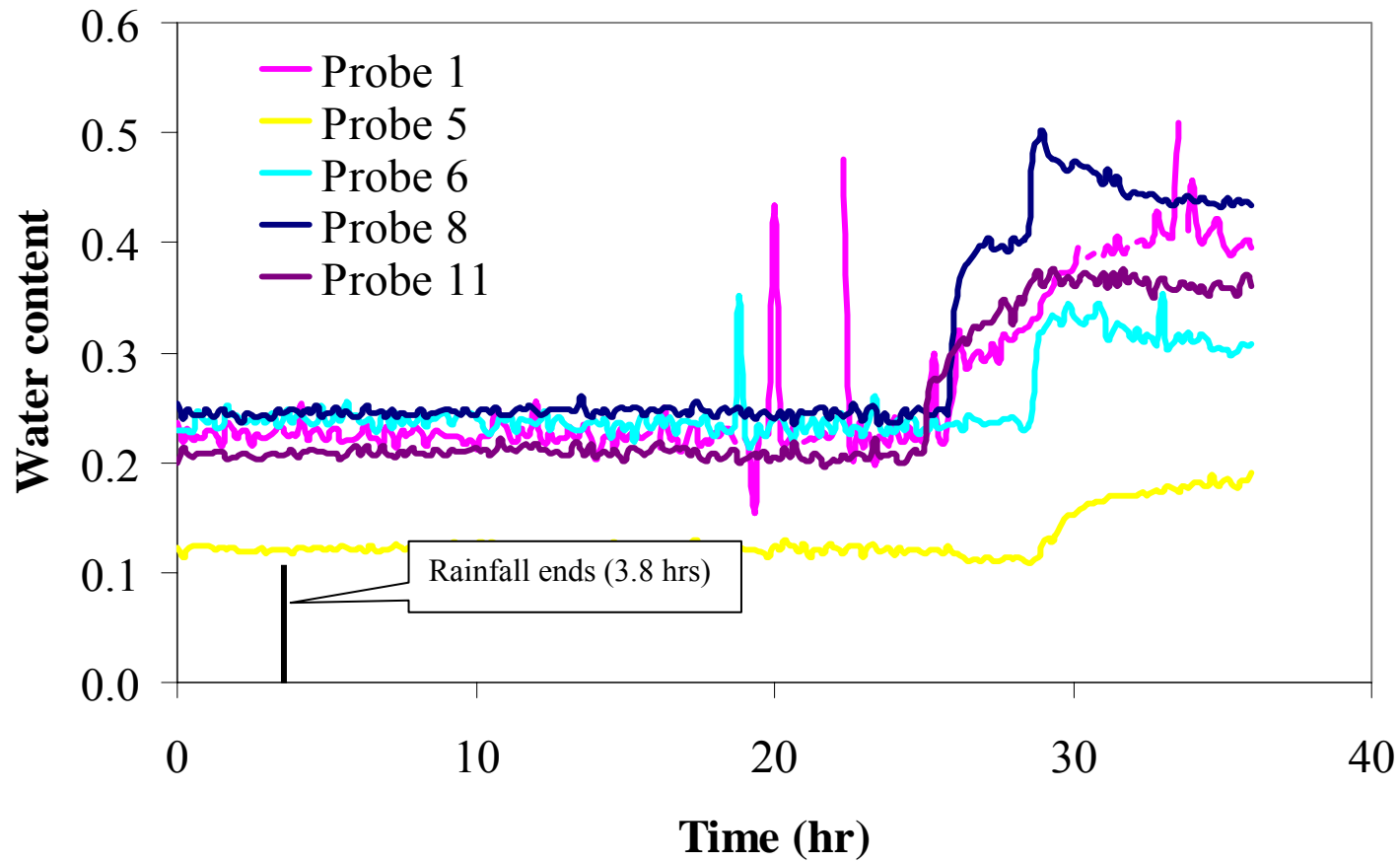
- Ott, L., R.L. Ott, and M.T. Longnecker. 2001. An introduction to statistical methods and data analysis. 5 edition. Duxbury Press, California.
- Perroux, K.M., and I. White. 1988. Designs for disc permeameters. *Soil. Sci. Soc. Am. J.* 52:1205-1215.
- Reynolds, W.D., and D.E. Elrick. 1991. Determination of hydraulic conductivity using a tension infiltrometer. *Soil. Sci. Soc. Am. J.* 55:633-639.
- Richardson, C.W., E. Burnett, and R.W. Bovey. 1979. Hydrologic effects of brush control on Texas rangelands. *Transactions of the ASAE.* 22;315-319.
- Scanlon, B.R., R.E. Mace, M.E. Barrett, and B. Smith. 2003. Can we simulate regional groundwater flow in a karst system using equivalent porous media models? Case study, Barton Springs Edwards aquifer, USA. *Journal of Hydrology.* 276:137-158.
- Shouse P.J., and B.P. Mohanty. 1998. Scaling of near-saturated hydraulic conductivity measured using disc infiltrometers. *Water Resour. Res.* 34(5)1195-1205.
- Simunek, J., M. Sejna, and M. Th. van Genuchten. 1999. The HYDRUS – 2D software package for simulating the two-dimensional movement of water, heat and multiple solutes in a variably saturated media. Version 2.0 U.S Salinity Lab. USDA, ARS, Riverside , California.
- Smettem, K.R.J, and B.E. Clothier. 1989. Measuring unsaturated sorptivity and hydraulic conductivity using multiple disc permeameters. *J. Soil. Sci.* 40:563-568.
- Spangler, L.E. 2002. Use of dye tracing to determine conduit flow paths within source-protection areas of karst spring and wells in the Bear River Range, Northern Utah. U.S. Geological Survey Karst Interest Group Proceedings, Water-Resources Investigations Report. 02-4174.
- Starr, J.L. 1990. Spatial and temporal variation of ponded infiltration. *Soil. Sci. Soc. Am.* J. 54:629-636.
- Teutsch, G. 1993. An extended double-porosity concept as a practical modeling approach for a karstified terrain. *Intl. Assoc. Hyd. Sci. Publ.* 207:281-292.
- Topp, G.C., J.L. Davis, and A.P. Annan. 1980. Electromagnetic determination of soil water content: Measurements in coaxial transmission lines. *Water Resour. Res.* 16(1):574-588.

- US Environmental Protection Agency and U.S. Geological Survey, Water Resources Division. 1998. Application of dye-tracing techniques for determining solute- transport characteristics of ground water in Karst terrains. Available at [www.karstwaters.org](http://www.karstwaters.org)
- van Genuchten, M.T. 1980. A closed-form equation for predicting the hydraulic conductivity of unsaturated soils. *Soil. Sci. Soc. Am. J.* 44:892-898.
- White, I., and M.J. Sully. 1987. Macroscopic and microscopic capillary length and time scales from field infiltration. *Water Resour. Res.* 23:1514-1522.
- White, I., and M.J. Sully. 1988. Field characteristics of the macroscopic capillary lengths or alpha parameter. Paper presented at International Conference and Workshop on the Validation of flow and transport models for the unsaturated zone. New Mexico State Univ., Las Cruces, New Mexico.
- White W.B. 1998. *Geomorphology and hydrology of Karst terrains*. Oxford University Press, New York.
- White W.B. 2002. Karst hydrology: Recent developments and open questions. *Engineering Geology.* 65:85-105.
- Wilcox, B.P. 2002. Shrub control and streamflow on rangelands: A process based viewpoint. *J. Range Manage.* 55:318-326.
- Wooding, R.A. 1968. Steady infiltration from a shallow circular pond. *Water Resour. Res.* 4:1259-1273.
- Wright, H.A., F.M. Churchill, and W.C. Stevens. 1976. Effect of prescribed burning on sediment, water yield, and water quality from dozed juniper lands in central Texas. *J. Range Manage.* 29:294-298.

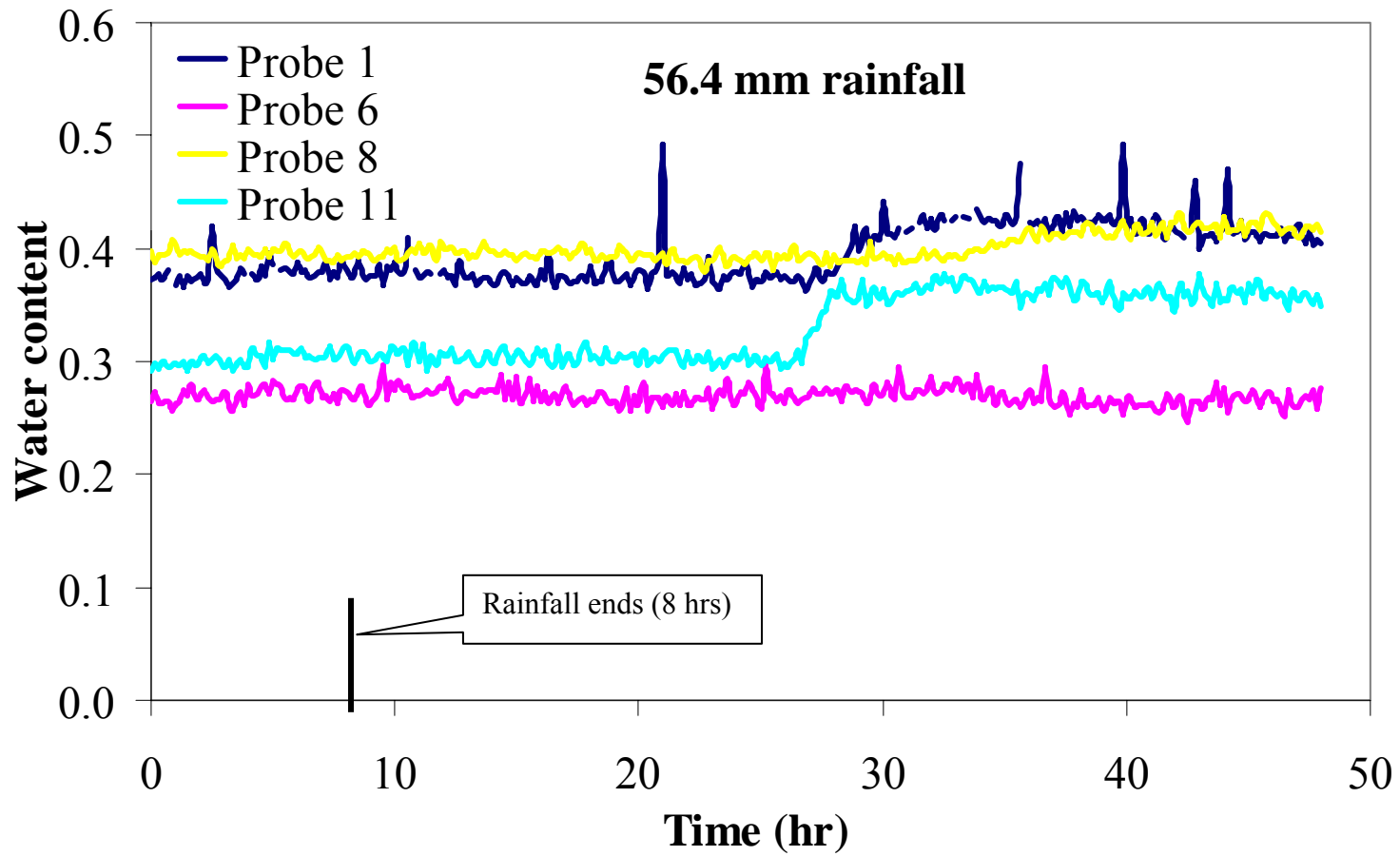
## APPENDIX A

### TDR RESPONSES FOR VARIOUS SIMULATIONS

The following pages contain graphs which illustrate the TDR probe response times for various simulation events. The total amount of rainfall that was applied during each simulation event is mentioned in each of the graphs. Different colors have been used to differentiate between different TDR probes. Fig. II-3 (a) shows the locations of the TDR probes for simulation events 1 to 5. The probe locations were changed to better monitor the flow processes. The new locations of the TDR probes for simulation 6 and the two dye-tracer studies is shown in Fig. II-3 (b). The X axis shows response time and starts from the beginning of the first run of each simulation. Each graph also shows the time rainfall simulation ended from the start of the first run. Refer to Table II-2 for details of each simulation event. The Y axis shows the volumetric water content as recorded by the TDR probes.

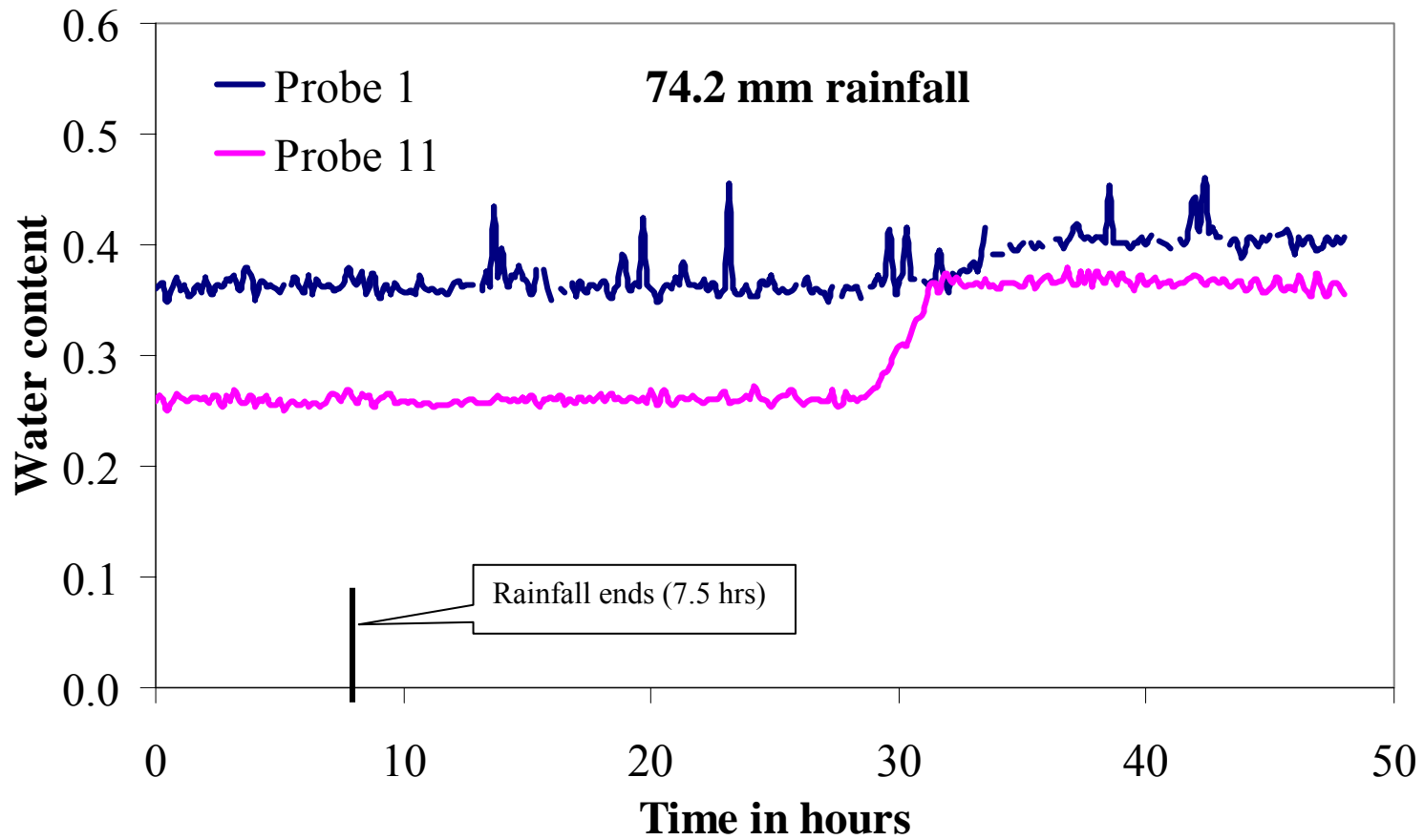


A-1. Response times of various TDR probes for Simulation 1. (Total rainfall amount = 170.2 mm)

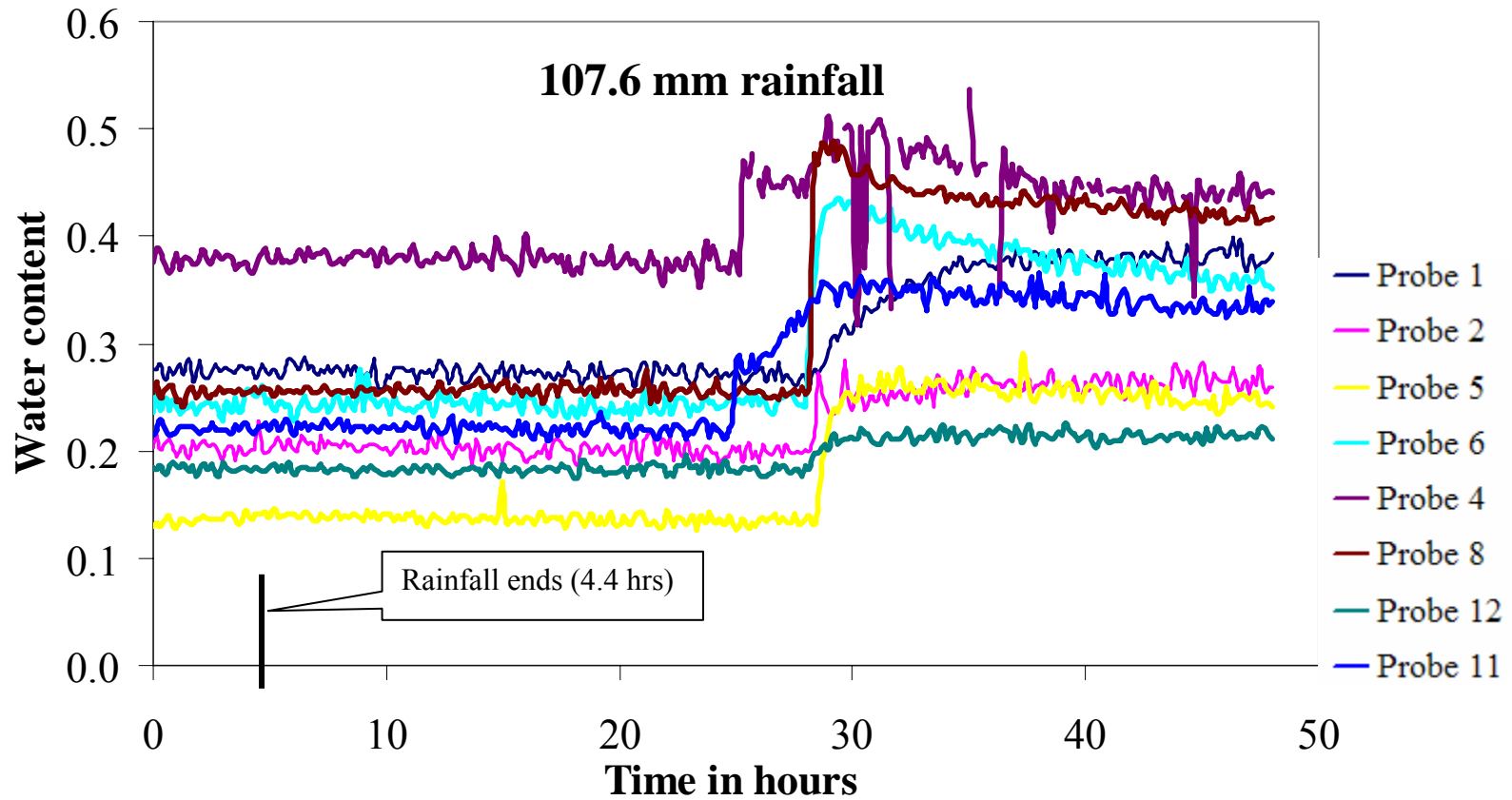


A-2. Response times of various TDR probes for Simulation 2. (Total rainfall amount = 56.4 mm)

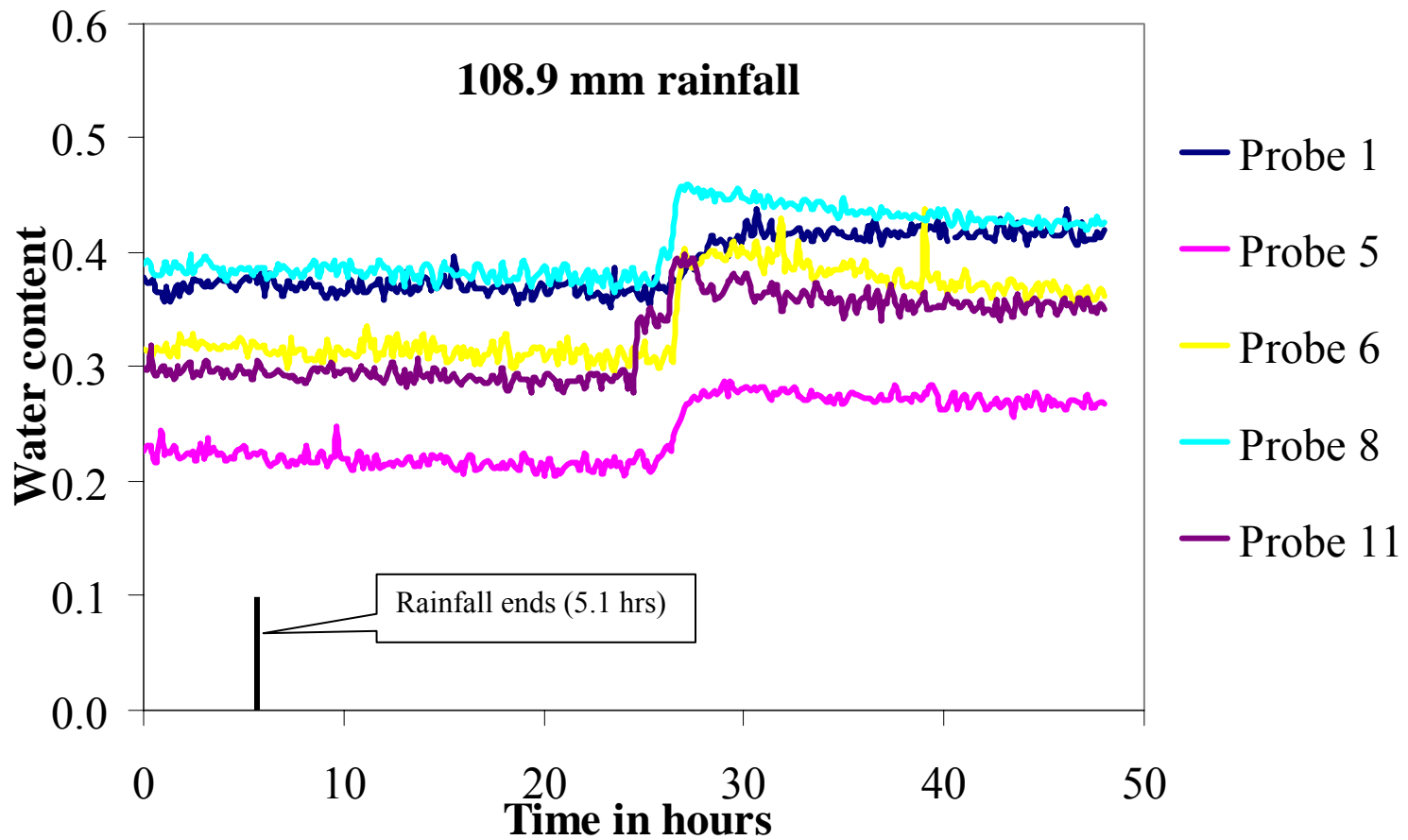




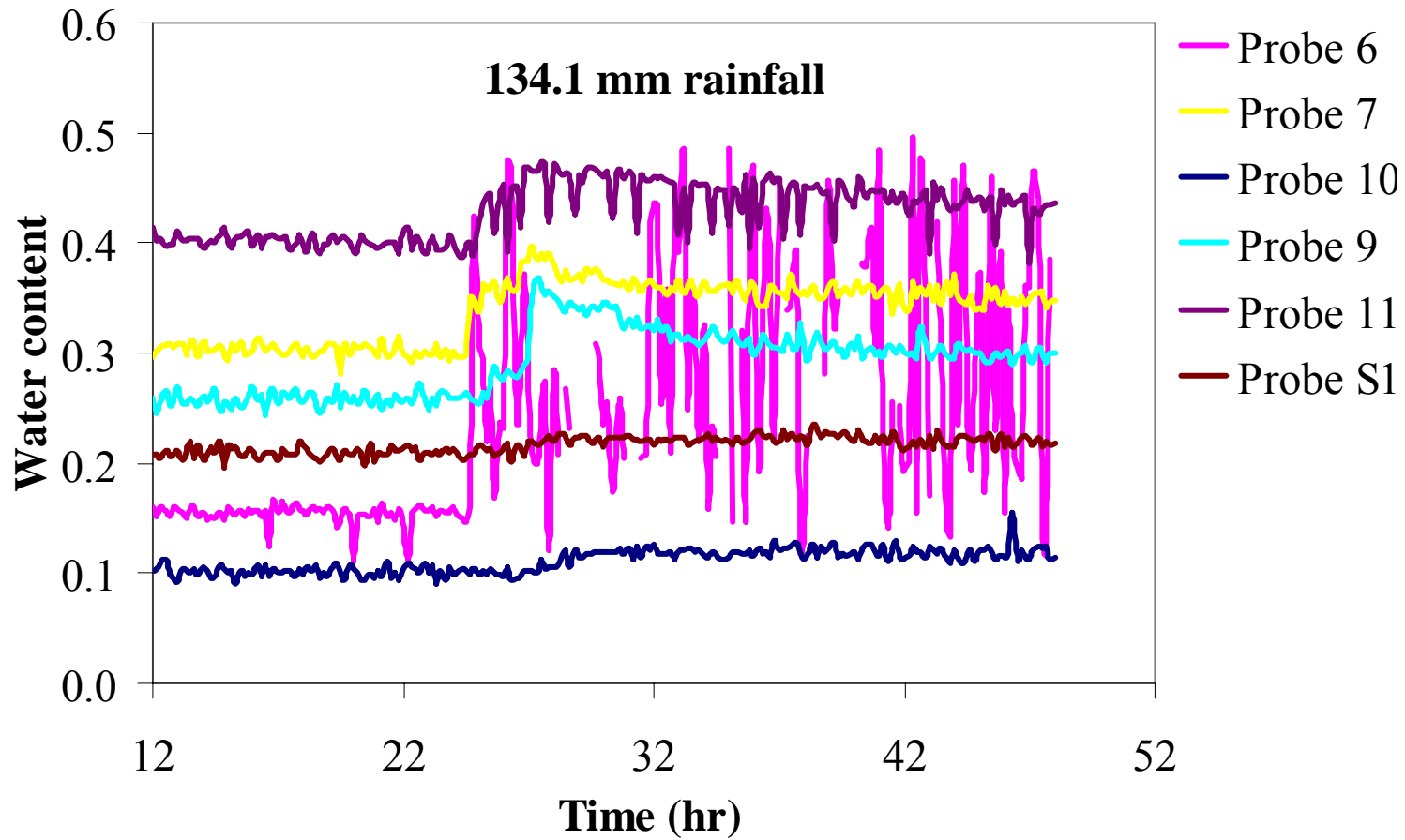
A-3. Response times of various TDR probes for Simulation 3. (Total rainfall amount = 74.2 mm)



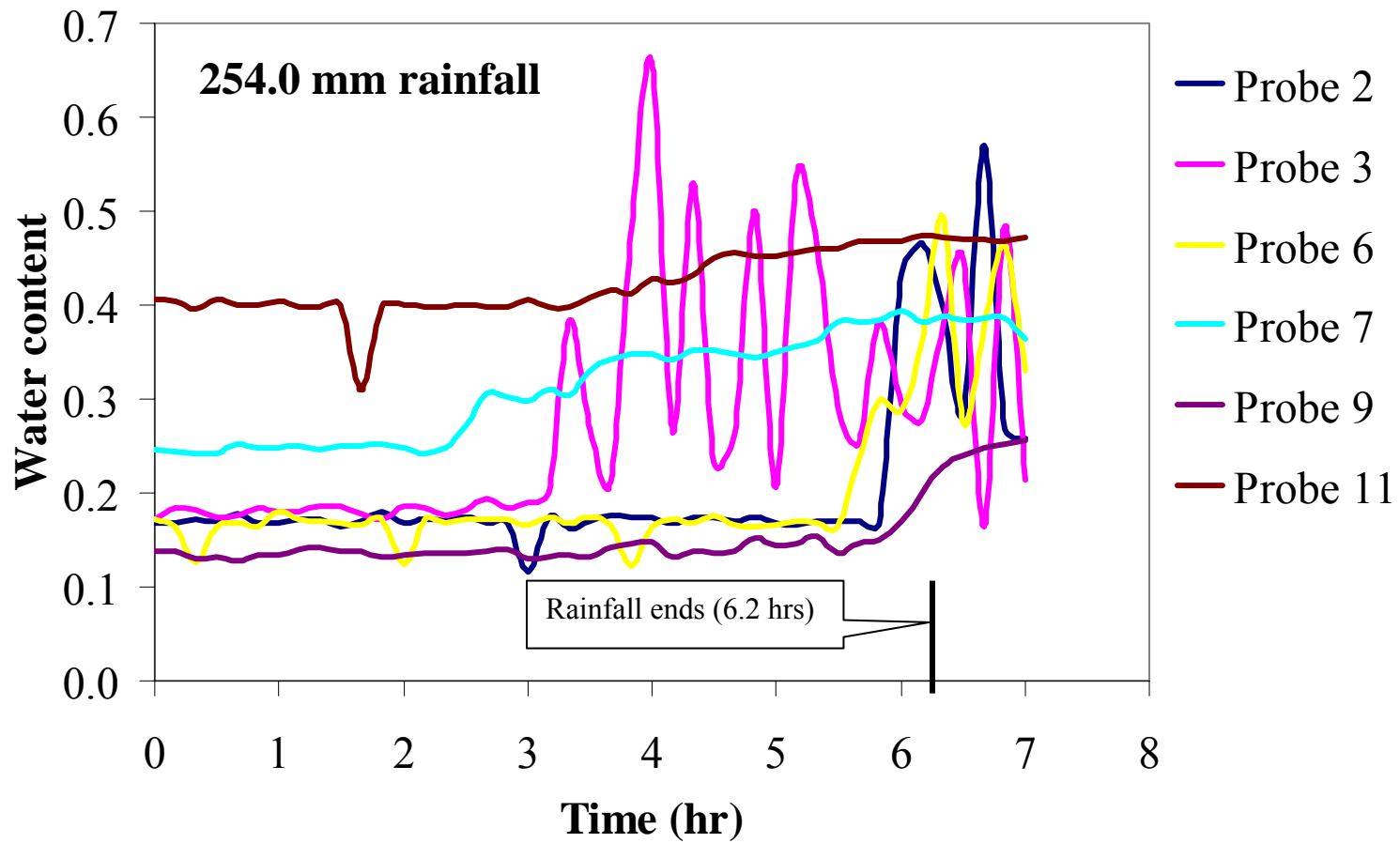
A-4. Response times of various TDR probes for Simulation 4. (Total rainfall amount = 107.6 mm)



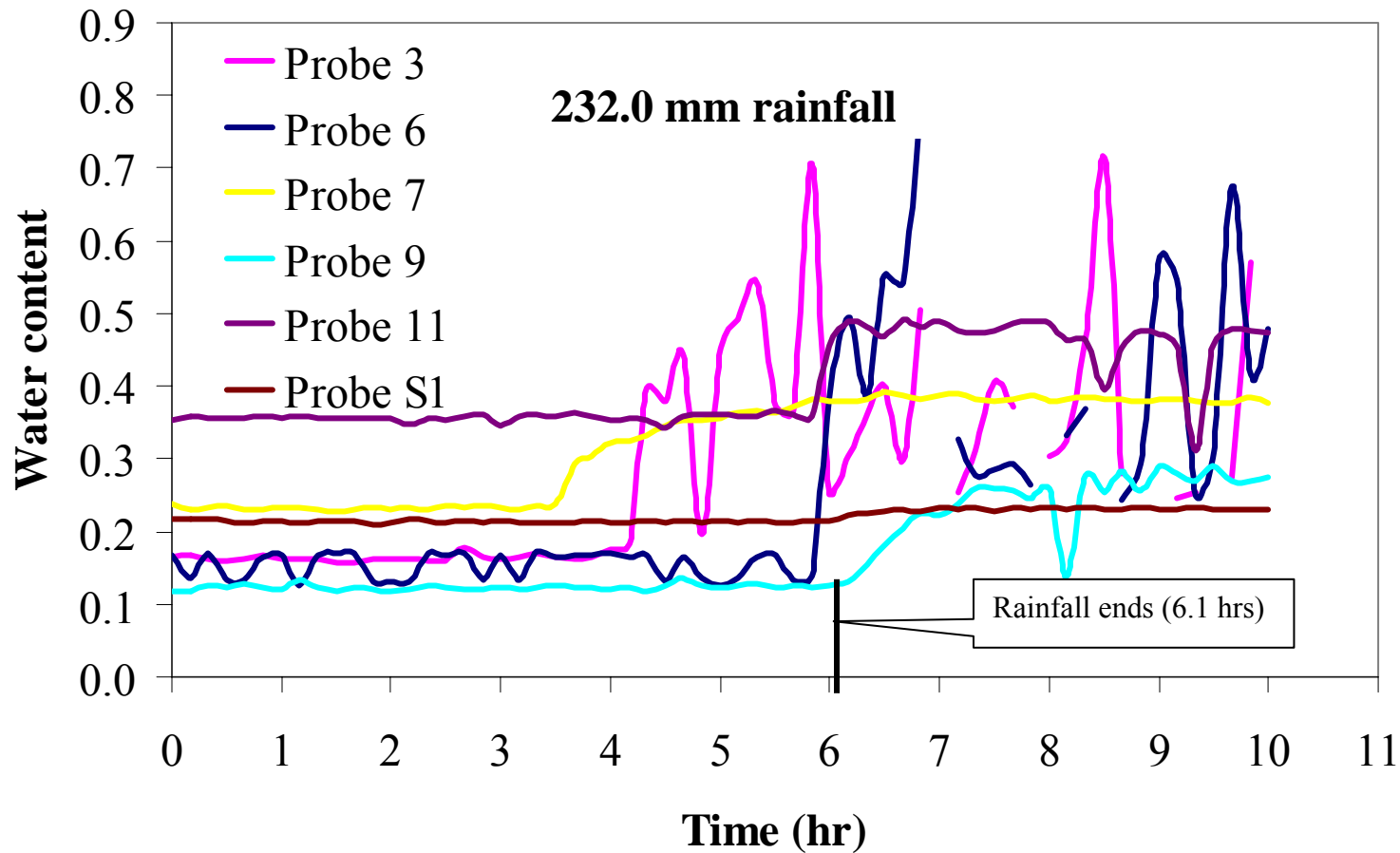
A-5. Response times of various TDR probes for Simulation 5. (Total rainfall amount = 108.9mm)



A-6. Response times of various TDR probes for Simulation 6. (Total rainfall amount = 134.1 mm). Note that we did not have data from the start of simulation 6 due to technical errors during experimentation. Rainfall ended 5.4 hours from start of first run.



A-7. Response times of various TDR probes for first Dye-tracer test. (Total rainfall amount = 254.0 mm)



A-8. Response times of various TDR probes for second Dye-tracer test. (Total rainfall amount = 232.0 mm)

## APPENDIX B

## WATER BALANCE CALCULATIONS USING MODEL

Given below are the detailed water balance calculations for both modeling domains (with and without fractures) for a 7 hour period.

## Water balance calculations for model with fractures

Total inflow = 1.160 m<sup>2</sup>

Total seepage face flux = 0.465 m<sup>2</sup>

Total deep drainage flux = 0.401 m<sup>2</sup>

Total volume of water retained in system = 0.226 m<sup>2</sup>

Layer	$\theta_f$	$\theta_i$	$\Delta\theta$	Area [m <sup>2</sup> ]	Water retained [m <sup>2</sup> ]
Litter/clay	0.539	0.501	0.038	1.160	0.044
Conduit	0.338	0.183	0.155	0.486	0.075
Upper limestone	0.161	0.153	0.008	3.260	0.026
Lower limestone/Marl	0.169	0.153	0.016	3.490	0.056
Lower clay	0.469	0.438	0.031	0.801	0.025
				Total =	0.226

Total outflow = 1.092 m<sup>2</sup>

Total water balance error = 5.86%

## Water balance calculations for model without fractures

Total inflow = 1.160 m<sup>2</sup>

Total seepage face flux = 0.490 m<sup>2</sup>

Total deep drainage flux = 0.327 m<sup>2</sup>

Total volume of water retained in system = 0.225 m<sup>2</sup>

Layer	$\theta_f$	$\theta_i$	$\Delta\theta$	Area [m <sup>2</sup> ]	Water retained [m <sup>2</sup> ]
Litter/clay	0.572	0.487	0.085	1.160	0.099
Upper limestone	0.166	0.153	0.013	3.600	0.047
Lower limestone/Marl	0.168	0.153	0.015	3.640	0.055
Lower clay	0.469	0.438	0.031	0.800	0.025
Total =					0.225

Total outflow = 1.042 m<sup>2</sup>

Total water balance error = 10.17%



## VITA

Surajit Dasgupta, son of Amitabha and Pronoti Dasgupta, was born in Calcutta on May 01, 1976. After graduating from St. James' School, Calcutta in 1994, he obtained a Bachelor's degree in Mechanical Engineering at Bapuji Institute of Engineering & Technology in Karnataka, India in 1998. Thereafter, he worked as a Project Engineer in a steel fabrication firm, Global International in Oman for a period of three years. He enrolled in graduate school at Texas A&M University, College Station in the fall 2002 and has been working since then as a graduate research assistant in the Department of Biological & Agricultural Engineering. He has also served as a teaching assistant in the Department of Rangeland Ecology & Management. His permanent address is: 47/2A Nabanaritala First Bye Lane, Howrah, Kolkata, India.